General Disclaimer

One or more of the Following Statements may affect this Document

- This document has been reproduced from the best copy furnished by the organizational source. It is being released in the interest of making available as much information as possible.

- This document may contain data, which exceeds the sheet parameters. It was furnished in this condition by the organizational source and is the best copy available.

- This document may contain tone-on-tone or color graphs, charts and/or pictures, which have been reproduced in black and white.

- This document is paginated as submitted by the original source.

- Portions of this document are not fully legible due to the historical nature of some of the material. However, it is the best reproduction available from the original submission.

NASA

Technical Memorandum 85078

Geodynamics Branch
Research Report - 1982

Edited by W. D. Kahn and S. C. Cohen

SEPTEMBER 1983

NOV 1983
RECEIVED
NASA STI FACILITY
ACCESS DEPT.

National Aeronautics and
Space Administration

Goddard Space Flight Center
Greenbelt, Maryland 20771

GEODYNAMICS BRANCH RESEARCH REPORT — 1982

Edited by

W. D. Kahn
S. C. Cohen

September 1983

GODDARD SPACE FLIGHT CENTER
Greenbelt, Maryland 20771

GEODYNAMICS BRANCH

CODE 921

LIST OF RESEARCHERS

David E. Smith, Branch Head
Ph.D., 1966, University of London, Satellite Geodesy
Beatrice S. Boccucci, Secretary

Demosthenes C. Christodoulidis, Ph.D. 1976, Ohio State University, Satellite Geodesy
Steven C. Cohen, Ph.D. 1973, University of Maryland, Physics
Theodore L. Felsentreger, M.A., 1961, University of Maryland, Mathematics
Werner D. Kahn, M.S., 1955, University of Illinois, Mathematics
Ronald Kolenkiewicz, M.S., 1965, Catholic University , Space Science and Applied Physics
William B. Krabill, B.S., 1968, Salisbury State College, Mathematics
Francis J. Lerch, M.S., 1950, University of Delaware, Mathematics
Han-Shou Liu, Ph.D., 1963, Cornell University, Physics
James G. Marsh, M.S., 1963, West Virginia University, Physics
David C. McAdoo, Ph.D., 1976, Cornell University, Geophysics
Patrick H. McClain, M.S., 1959, Howard University, Mathematics
Barbara H. Putney, B.S., 1960, Brooklyn College, Mathematics
David P. Rubincam, Ph.D., 1973, University of Maryland, Physics
Braulio V. Sanchez, Ph.D., 1975, University of Texas, Aerospace Engineering
Frederick G. Schamann, B.S., 1967, City College of New York, Mathematics
Jean E. Welker, M.A., 1980, University of Maryland, Physical Geography/ History
George H. Wyatt, B.S., 1962, North Carolina State College, Mathematics

Resident Research Associates

Benjamin F. Chao, Ph.D., 1981, University of California (San Diego), Earth Sciences
Richard S. Gross, Ph.D., 1982, University of Colorado, Geophysics

CONTENTS

CONTENTS (Continued)

INTRODUCTION

This report is the first annual summary of the research program of the Geodynamics Branch. The branch is located within the Earth Survey Applications Division of the Applications Directorate of the Goddard Space Flight Center. The research activities of the branch staff cover a broad spectrum of geoscience disciplines including space geodesy, geopotential field modeling, tectonophysics, and dynamic oceanography. The NASA programs which are supported by the work described in this document include the Geodynamics and Ocean Programs, the Crustal Dynamics Project, the proposed Ocean Topography Experiment (TOPEX), and Geopotential Research Mission (GRM). The reports highlight the investigations conducted by the Geodynamics Branch Staff during calendar year 1982. The individual papers are grouped into chapters on Crustal Movements, Global Earth Dynamics, Gravity Field Model Development, Sea Surface Topography, and Advanced Studies. Further information on the activities of the branch or the particular research effort described here can be obtained through the Branch Office or from the individual staff members.

CHAPTER 1

CRUSTAL MOVEMENTS

OVERVIEW

Studies of crustal movements are devoted to the interrelated goals of determining tectonic plate motions, understanding their driving forces and the nature of plate interactions, and predicting the occurrence of earthquakes. The analysis of global and regional scale crustal movements provide information on seafloor spreading and continental drift, the creation and destruction of crustal material, and the structure, rheology, and dynamics of the earth's interior. Crustal deformation in seismically active zones provide information on strain accumulation and release, the state of stress in the earth's crust, and the mechanisms responsible for earthquakes. The work of the Geodynamics Branch includes activities in both the Crustal Dynamics Project which involves space geodetic observations and in the Geodynamics Research Program which involves basic studies into the dynamic processes of the earth.

This section of the Geodynamics Branch report includes papers on the measurement of crustal movements, modeling of earthquake related crustal deformations, modeling of sublithospheric stress fields, and the development of satellite tracking facilities for space geodetic measurements. The four reports are summarized as follows: 1) The first report is devoted to observations of crustal movements using satellite laser ranging measurements to the Lageos satellite. Repeated determination of the distances between observing sites on the North American, Australian, Pacific and South American Plates are being used to determine both relative plate motion and intraplate rigidity. 2) The second report focuses on the modeling of crustal deformation subsequent to an earthquake. The analyses is based on the physics of stress redistribution with time and distance from the seismic event and yields information on the rheology and structure of the earth's interior. 3) In the third report, the sublithospheric stress field in the Baikal-Stanovoy region of Siberia is derived from an analysis of the satellite determined gravity field. The computed stress field is interpreted in terms of the regional seismicity, and geologic structure and the phenomenon of gravity sliding of seismotectonic blocks. 4) The fourth report describes data confirming the successful conversion of the lunar laser ranging system of the University of Hawaii at Maui into a system capable of tracking near-earth satellites. The site is being used in measurements of tectonic plate motion involving the Pacific Plate.

Contributors to this section are: D.C. Christodoulidis, S.C. Cohen, R. Kolenkiewicz, H.S. Liu and D.E. Smith.

GLOBAL GEOTECTONICS FROM SATELLITE LASER RANGING

Demosthenes C. Christodoulidis
and
David E. Smith

OBJECTIVE

The detection of global geodynamics and tectonic processes through the use of satellite laser ranging data.

BACKGROUND

The accuracy with which tectonic plate velocity vectors can be computed increases with the repetition rate of the measurements and accuracy in the measurement of interplate distances and heights. As a result, a fair amount of GSFC activity has been devoted to increasing the temporal resolution and precision of baseline and height determinations for laser instruments deployed surrounding tectonic plate boundaries.

RECENT ACCOMPLISHMENTS

Dynamic reduction of Satellite Laser Ranging (SLR) provides a unique tool for the precise positioning of a point on the Earth's surface in three dimensions. The sensitivity of the SLR data requires that, for a well conditioned solution, the longitude of one of the tracking stations be constrained to an a priori value. The vertical components of the stations, however, through the tracking geometry provided by the global network and the accurate knowledge of orbital dynamics, are uniquely related to the center-of-mass of the earth.

The Lageos laser data for the period May 1976 to April 1982 have been analyzed for the determination of sets of annual station locations and earth orientation and force model parameters. The results of this analysis, referred to as SL5, are approaching the useful accuracies required by geophysics. The annual height variations for eight base stations, spread over four tectonic plates are shown in Fig. 1. Station positions determined from data collected prior to 1979 are of inferior accuracy due to the poorer quality, quantity and distribution of the data. The three sigma formal errors of these heights are between 2 and 5 cm. Inspection of the heights versus their sigmas shows that, for most of the cases, the variations are insignificant, with the exceptions being Maui, Hawaii and Yarragadee, Australia. The horizontal positions of the stations have an accuracy of better than 2 cm which has permitted preliminary comparisons of SLR tectonic plate motions with those estimated by Minster and Jordan (1974, 1978). These comparisons are discussed below.

SIGNIFICANCE

The change in the SLR chord lengths, free from height variations give the horizontal component of the velocity vectors between the tectonic plates. These ellipsoidal chords interconnect the projections of the tracking station positions onto the reference ellipsoid. As such, they may be compared directly with the horizontal changes suggested by Minster and Jordan. The Lageos data analyzed was collected from 1979 through 1981. In order to increase the sample size, the chords were averged per tectonic plate. The computed inter-plate deformations are shown in Figure 2. The heavy lines connect the geographic barycenter of the sites where more than one site was available per plate. For the purpose of comparisons the same per plate averaging was applied to the Minster and Jordan rates which are shown in Figure 2 also. The agreement between the two independent sets is within one sigma of the laser data (approximately $\pm$ 2 cm/yr) the exception being the Australia to S. American rate. It has to be kept in mind, however, that this chord crosses two plates (the Nazca plate and the Pacific plate) and therefore what we see is the result of the combination of movements from four plates. Furthermore, the Minster and Jordan rates reflect average movements over millions-of-years whereas the SLR rates are 2 year averages. Although these results seem to be very encouraging indeed, much attention will be given to future higher quality laser results. These results will increase the length of the movement records for the laser sites and will thus enable the verification of the observed deformation rates.

FUTURE EMPHASIS

The results discused above are viewed as preliminary. Studies are now underway to better understand and evaluate the variation of the heights and chord lengths and to further improve their temporal resolution and accuracy over the entire history of the Lageos mission. Improvements in the current data reduction approach include the incorporation of the Wahr nutation series, the development and use of a Lageos tidal model and Lageos' tidal displacement Love numbers, and the description of the site displacement due to ocean loading via an available model. Studies are also underway to better model and understand the along-track acceleration of the spacecraft, as well as forces due to the earth's albedo. Preliminary error analyses indicate that the incorporation of improvements along with better control of the overall systems performance could decrease the average positional uncertainty by about 25 percent.

REFERENCES

Minster, J.B., T.H. Jordan, P. Molnar, and E. Haines, "Numerical Modeling of Instantaneous Plate Tectonics," Geophys. J. of the Royal Astron. Soc., 36, 541-576, 1974.

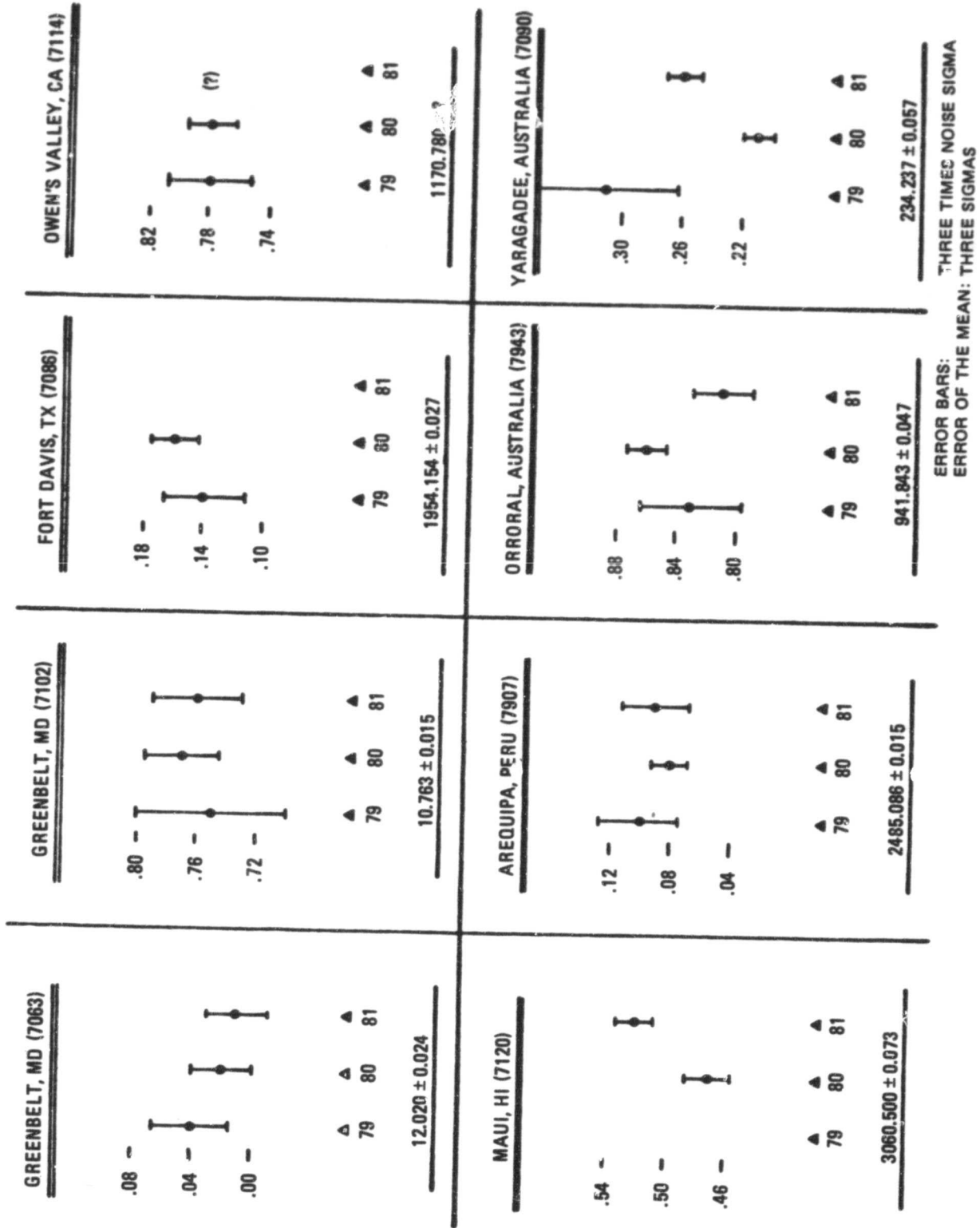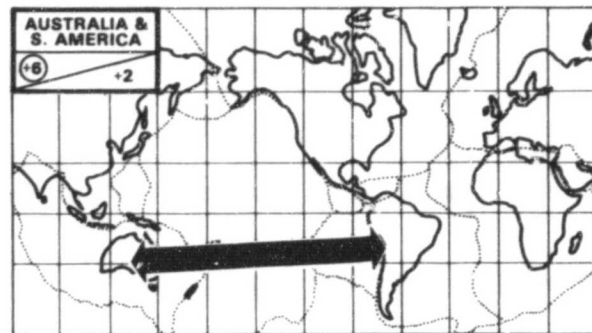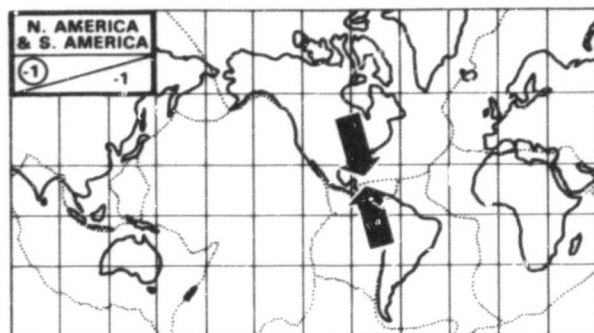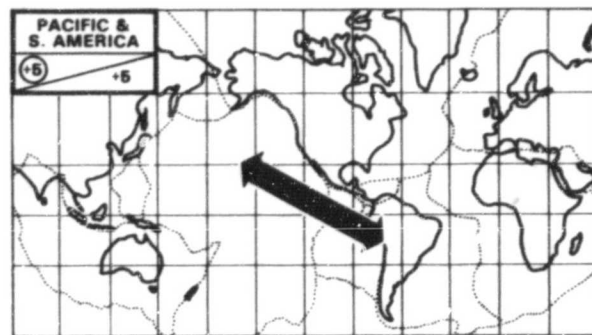Minster, J.B. and T.H. Jordan, "Present-Day Plate Motions, J. Geophys. Res., 83 (B11), 5331-5354, 1978.
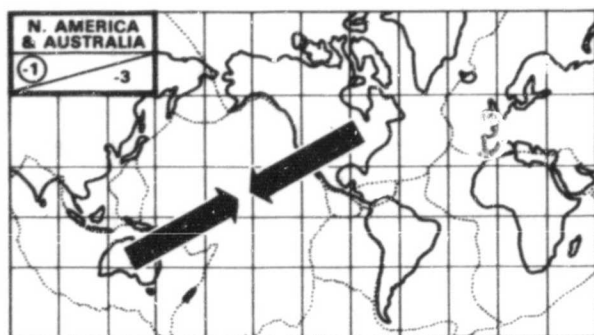
Figure 1. Variation in Annual Heights (m)

Inter-plate Deformations Observed by SLR. Averaged Ellipsoidal Chord Rates vs. Rates Given by Minster & Jordan (cm/yr.)

CRUSTAL DEFORMATION DURING THE EARTHQUAKE CYCLE

Steven C. Cohen

OBJECTIVES

The purpose of this work is to develop an understanding of how the earth's surface deforms during the cycle of stress accumulation and release along major faults. The major research thrusts are the development of numerical models of the spatial and temporal patterns of crustal displacements and strains and the determination of numerical values of the geophysical parameters that describe the earth's rheology and structure.

BACKGROUND

Vertical and horizontal crustal deformations are common characteristics of the earth in zones of active seismicity. Certain temporal and spatial patterns of crustal deformation evolve as the earth passes through successive stages of the earthquake cycle: strain accumulation, preseismic movement, earthquake rupture, and postseismic rebound. The patterns that develop depend on the interaction of the various forces responsible for driving earthquakes and tectonic plate movements, the rheology and structure of the earth, and the fault geometry. The research reported herein involves the development of numerical models that replicate the patterns of deformation of surface near- and far-field features. The computer simulations of an earthquake cycle are fit to observed geodetic data to determine key physical parameters of the earth. The specific models that are discussed in this report involve postseismic deformation due to viscoelastic flow in subcrustal layers of the earth. The flow is activated by the coseismic stress field established by an earthquake. As the viscoelastic creep advances in the subcrustal layers coupling to the crust results in surface deformation.

RECENT ACCOMPLISHMENTS AND SIGNIFICANCE

A finite element computer code has been used to study postseismic rebound on strike-slip and dip-slip faults. A multilayered viscoelastic rheological structure for the earth has been used. In this model the earth's lithosphere is divided into two layers. The upper layer is elastic and contains within it a fault that pentrates through all or only a part of the layer. Below this layer is a viscoelastic lower lithosphere represented by a standard linear solid rheology. This representation of the lower lithosphere permits modeling the following deviatoric behavior: elastic deformation coseismic to the earthquake fault slip, viscoelastic rebound subsequent to the earthquake, and permanent elastic support of stress with a shear modulus reduced from the instantaneous coseismic value. Below the lithosphere lies an asthenospheric layer represented by a Maxwell viscoelastic

fluid. The relaxation time of the Maxwell fluid is significantly less than that of the overlying linear solid due to the expected thermal enhancement of creep processes at depth.

For strike-slip faults the model predicts that postseismic deformations increase as the ratio of fault depth to elastic lithosphere thickness increases. The effects of partial relaxation of the lower lithosphere are to increase the magnitude of the postseismic displacements and strains and to extend the duration of postseismic straining. In addition, the graded decreasing viscosity profile with depth retards the lateral growth of the zone of significant postseismic restressing. In general the effects of asthenosphere flow are significant if the asthenosphere depth is less than about 3 fault depths from its surface and the viscosity is on the order of 10^{20} poise. The partial relaxation of the lower lithosphere is significant if the relaxation time is not much more than an order of magnitude greater than that of the asthenosphere and if the fractional change in the effective shear modulus with time is greater than about 1/4.

The dominant effect in the postseismic rebound from dip-slip event is subsidence centered over the fault and uplift in the intermediate or far-field region. Over a wide range of dip angles the magnitude of the subsidence is greatest when the fault extends through one-half the lithosphere. For greater or lesser fault depths the subsidence is reduced; it becomes uplift when nearly all the lithosphere is penetrated. The width of the subsidence zone is controlled primarily by the depth of the top of the asthenosphere and secondarily by the depth of the lower lithosphere. The influence of relaxation of the lower lithosphere on the surface deformation is much less than that for the strike-slip case. Rather the deformation due to asthenosphere relaxation dominates the early postseismic vertical displacement pattern and continues to develop over times long compared to the Maxwell time. This viscoelastic model has been compared to geodetic data obtain in 1900, 1934, and 1974 following the 1896 Riku-u, Japan earthquake (see Figure 1). The deduced value of total lithosphere thickness of about 40 km and asthenosphere viscosity of 5×10^{19} poise are moderately constrained. The thickness and viscosity of the lower lithosphere of 20 km and 1×10^{21} poise respectively fit the data but are poorly constrained.

FUTURE EMPHASIS

The modeling effort will be extended in the future to include strain accumulation during the interseismic phase of the earthquake cycle. It will be possible to model both the deformation due to a single earthquake cycle or to a sequence of recurring events. The finite element computer code will provide a general purpose modeling capability that will permit undertaking numerical experiments using different physical assumptions. The deformations that are due to lateral and vertical variations in rheological structure will be deduced. Numerical experiments will be performed to test the resolvability of different models of crustal deformation. The analysis will focus on how the surface deformations are influenced by: 1. a thin channel asthenosphere; 2. a subsurface low viscosity inclusion; 3. lithospheric thinning in a fault zone, and 4. elastic creep.

REFERENCES

Cohen, S.C., "A Multilayer Model of Time Dependent Deformation Following an Earthquake on a Strike-Slip Fault," J. Geophys. Res., 87, 5404-5421, 1982.

Cohen, S.C., "Postseismic Deformation Due to Subcrustal Viscoelastic Relaxation Following Dip-Slip Earthquakes," GSFC TM 84005, September 1982; submitted for publication.

Cohen, S.C., "Discussion of Models of Postseismic Rebound," EOS, 63, 429, 1982.
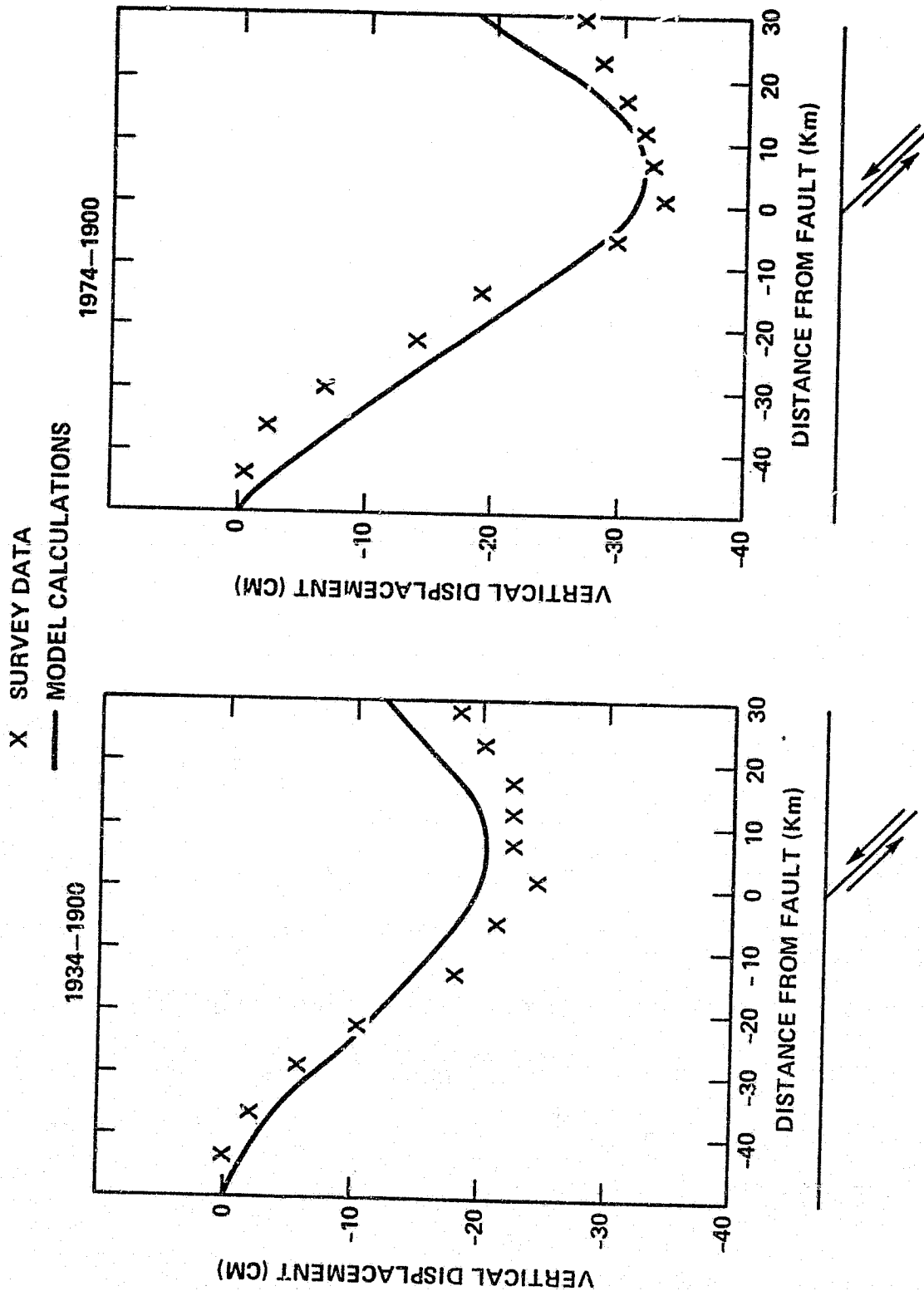
Figure 1. Comparison of leveling data and model calculations for postseismic rebound to 1896 Riku-u Japan earthquake: (a) 1934–1900 data; (b) 1974–1900 data. Survey results use a 3-point smoothing to data of Thatcher, et al. (1980). Model parameters are coseismic slip = 2 m, fault depth = 0–15 km; dip angle = 45°; asthenosphere depth = 40 km; asthenosphere viscosity = 5 x 10^{19} poise, lower lithosphere depth = 20 km, lower lithosphere viscosity = 1 x 10^{21} poise.

GRAVITY SLIDING: CRUSTAL DEFORMATION AND SEISMOTECTONIC BLOCK MOVEMENTS IN SIBERIA

Han-Shou Liu

OBJECTIVE

Geodynamics seeks to ascertain the causes of crustal deformation and its fundamental connection with geophysical and seismological features.   The objective of this study is to develop a genetic model which may account for the Baikal rift system and the associated seismotectonic block movements of Stanovoy Range in Siberia.

BACKGROUND

The knowledge of the seismic activity and tectonic structure of the Baikal-Stanovoy region in Siberia obtained by the Russian geoscientists is profound.   It provides geological and geophysical facts to test whether the solutions of the focal mechanisms for earthquakes, the distribution of orogenic activity, recent crustal block movements and upper mantle structure in this region can be integrated within a single Space Geodynamics Program.

The program for satellite measurements of the earth's gravity offers a variety of models to interpret the interior of the earth. Among the various interpretations, the sub-lithospheric stress field serves as an intraplate character which corresponds to the state of gravity sliding. In this study, the analysis of the Goddard Gravity Field Model is used in determining the horizontal projections of lithospheric sliding under the Baikal-Stanovoy region. This study involves a search for mutual agreement over large areas of the geopotential field with respect to seismic stresses.

RECENT ACCOMPLISHMENTS

The gravity sliding forces can be inferred from satellite gravity data. We have obtained stresses at 1,000 grid points in Siberia caused by gravity sliding. The results have determined a seismic gap and recognized two types of stress conditions in the structure of the Baikal-Stanovoy seismic belt.   The method developed for identifying stress zones from satellite gravity data makes it possible to direct the search for the mechanisms of earthquakes and rifts toward these stress structures. An interdisciplinary investigation of the stress pattern reveals an anomalous mantle beneath the Baikal Rift System.

SIGNIFICANCE

The stresses as shown in Figure 1 are comprised of several consistent stress patterns including the remarkable tensional stress field under the Baikal rift zone and the North-South compression in the Stanovoy Range region. By analyzing the satellite stress fields in conjunction with tectonic and seismological structures in Siberia, we have obtained the following significant results:

1. Seismicity and seismic gap: All the strong earthquakes in Siberia are concentrated within the Baikal-Stanovoy Seismic Belt (Figure 2) which includes the Baikal rift zone and extends eastward as far as the sea of Okhotsk. Around 118°-120°E there is a seismic gap where earthquake foci are absent. The western segment coincides with the Baikal rift zone in which strucures are under extension. The eastern segment of the belt is located between 120°E and the Okhotsk Sea coast. Within its limites, Baikal-type grabens disappear completely and the uplifted topography here points to compression rather than extension. The stress pattern, as inferred from satellite gravity data, is in good agreement with these seismological features. The most likely point of no strain along the Baikal-Stanovoy seismic belt is calculated to lie at 56°N 116°E (Figure 1), which lies at the position of the aforementioned seismic "gap."

2. The computed point of no strain (56°N 116°E), or seismic gap, coincides almost exactly with the position of the pole of rotation between the Eurasian and Amurian plates. This result suggests that gravity sliding may be the main cause for seismotectonic block movements.

3. Figure 1 shows an anomalous lens of upwelling mantle rocks under the rift zone which may be verified by seismic or magnetotelluric probing.

4. Mechanism for Baikal rift system - Gravity sliding in this region, as inferred from satellie gravity data, has provided a mechanism for continental rifting. It has been shown that rift evolution in continents is driven by the inexorable dissipation of thermal energy from the mantle and the concomitant upward transport of the asthenosphere. It may be probable to state that the crustal tension causing the Baikal rifting was originated by either the suction force acting on overriding plates at trenches or the collision force between the Indian and Eurasian plate along the Himalayan frontal thrust.

FUTURE EMPHASIS

Satellite capabilites for gravity measurements have been extended so rapidly in the past few years that there has not been time to bring them fully to bear on the interesting fundamental problems for which they seem so well suited. By applying the same method, the author plans to investigate gravity sliding in Europe. The gravity sliding stresses in the European crust will be obtained form satellite gravity data. The stress calcualtions will provide a real challenge to the best geophysical theories, and seismological observations.

REFERENCES
Liu, H.S., 1982. Geodynamics of the Baikal-Stanovoy Seismic Belt, _Physics of the Earth and Planetary Interiors_, Vol. 31, 77-82.
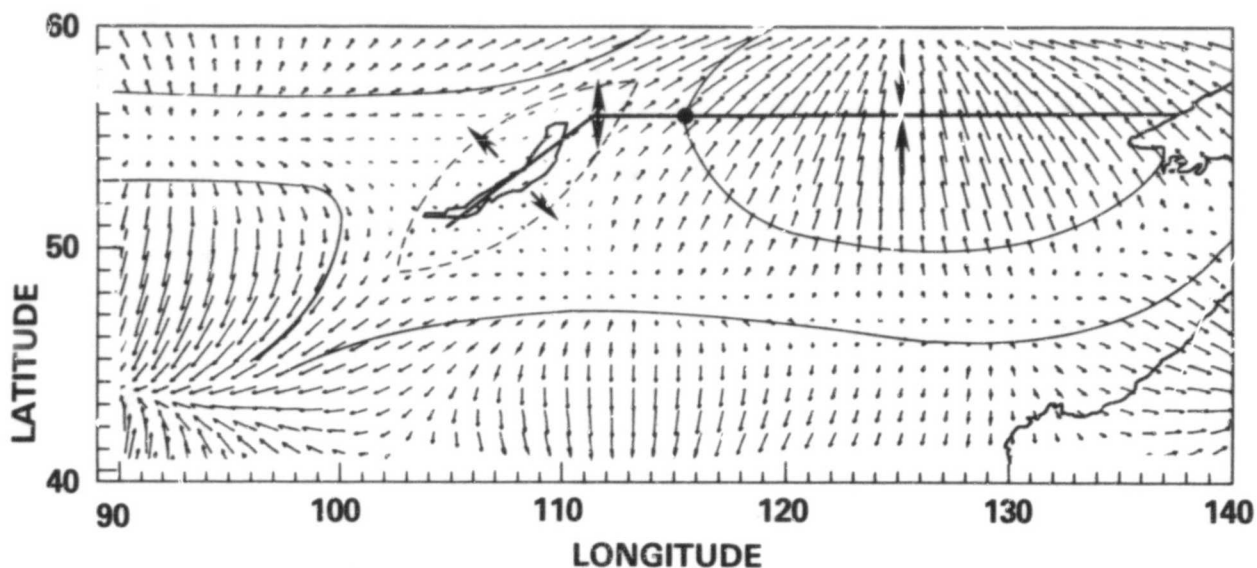
Figure 1. Subcrustal stresses beneath the Baikal-Stanovoy region as inferred from satellite gravity data. The stress pattern is consistent with the anomalous lens of upwelling mantle rocks under the Baikal rift region and the associated crustal compression of the Stanovoy Range.
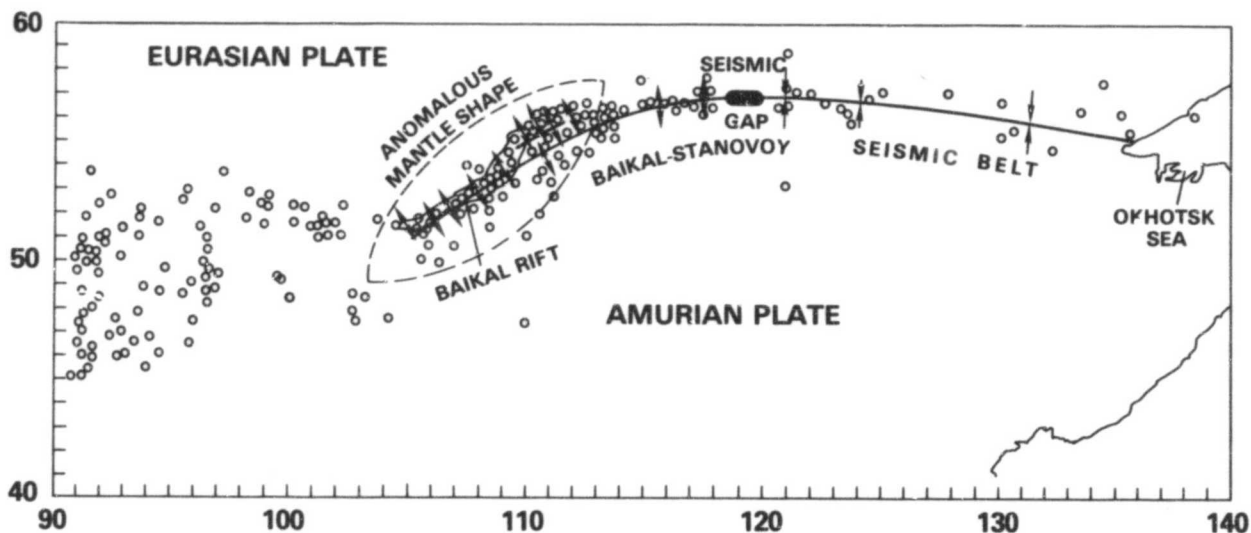

Figure 2. Seismicity and stress orientations of earthquake foci along the Baikal-Stanovoy seismic belt.

THE VERIFICATION OF THE LURE SYSTEM AS A SATELLITE LASER RANGING STATION

Ronald Kolenkiewicz

OBJECTIVE

The objective is to qualify the LURE (Lunar Ranging Experiment) laser ranging system of the University of Hawaii located on Maui, Hawaii to verify that it is suitable to be used as a near-earth satellite system. This enables it to join the NASA laser ranging network and thus contribute to the Crustal Dynamics Project.

BACKGROUND

In the past the LURE system was designed exclusively for laser ranging to the moon. NASA was in need of a Satellite Laser Ranging (SLR) system on the Pacific Plate in order to perform Global Studies for the Crustal Dynamics Project. These studies include monitoring of tectonic plate motion as well as polar motion and earth rotation. The LURE system was modified to enable it to track near-earth satellites. In order to verify the ability of the LURE system to accomplish this goal, a SLR system, MOBLAS I was collocated in the vicinity of the LURE laser.

These collocated systems tracked the BE-C, Starlette, and LAGEOS satellites to demonstrate that the LURE system gave the same ranging information as MOBLAS 1. These tests were conducted during September through November 1981.

RESULTS

The laser ranging data from the two collocated laser systems (LURE and MOBLAS I) was analyzed by selecting simultaneous passes of data to the same satellite. The residuals to an orbit calculated to these data based, upon the known survey position of the sites, were analyzed for relative range and timing biases. Figure 1 shows the laser range residuals from collocated lasers, about an orbit. The average residual for each station is determined. These averages are then differenced to give the mean residual difference for that pass. Figure 2 shows these mean residual differences plotted for the 36 satellite passes analyzed. Initial results indicated there was a relative bias of 5 cm between the stations. Allowing for one station to move to a new position relative to the other removed this bias.

A survey confirmed these analyses by showing the original position of MOBLAS I was in error by 6.8 cm in latitude and 3.8 cm in longitude and the calibration board distance was in error by 1.1 cm.

When the corrected position was used in the anlaysis the measurments made by both systems were in agreement with each other by less than 1 millimeter.

Figure 2 presents the results of this experiment. The mean residual difference for the 36 passes analyzed are seen to be spread between plus and minus 4 cm with an average of zero and a sigma of 2.4 cm.

CONCLUSIONS

The LURE system is capable of satellite laser ranging at the centimeter level, and SLR systems can detect survey errors at the centimeter level. This implies that relative site positions can be measured at the centimeter level providing tectonic and earth orientation measurements of value to the Crustal Dynamics Project investigators.

REFERENCES

"Collocation Test Plan for MOBLAS I and LURE Observatory Laser Ranging Systems at Mt. Haleakala," STDN Report No. 410.2, Goddard Space Flight Center, December 1980.

Kolenkiewicz, R., M. Torrence, and D. Edge, "Orbital Analysis for Several Collocated SAtellite Ranging Systems," presented at Fourth Annual Conference on the NASA Geodynamics Program, Goddard Space Flight Center, January 26-29, 1982.

Torrence, M. and R. Kolenkiewicz, "Collocations of Satellite Laser Ranging Stations," EOS, Vol. 62, No. 45, November 10, 1981, p. 480.
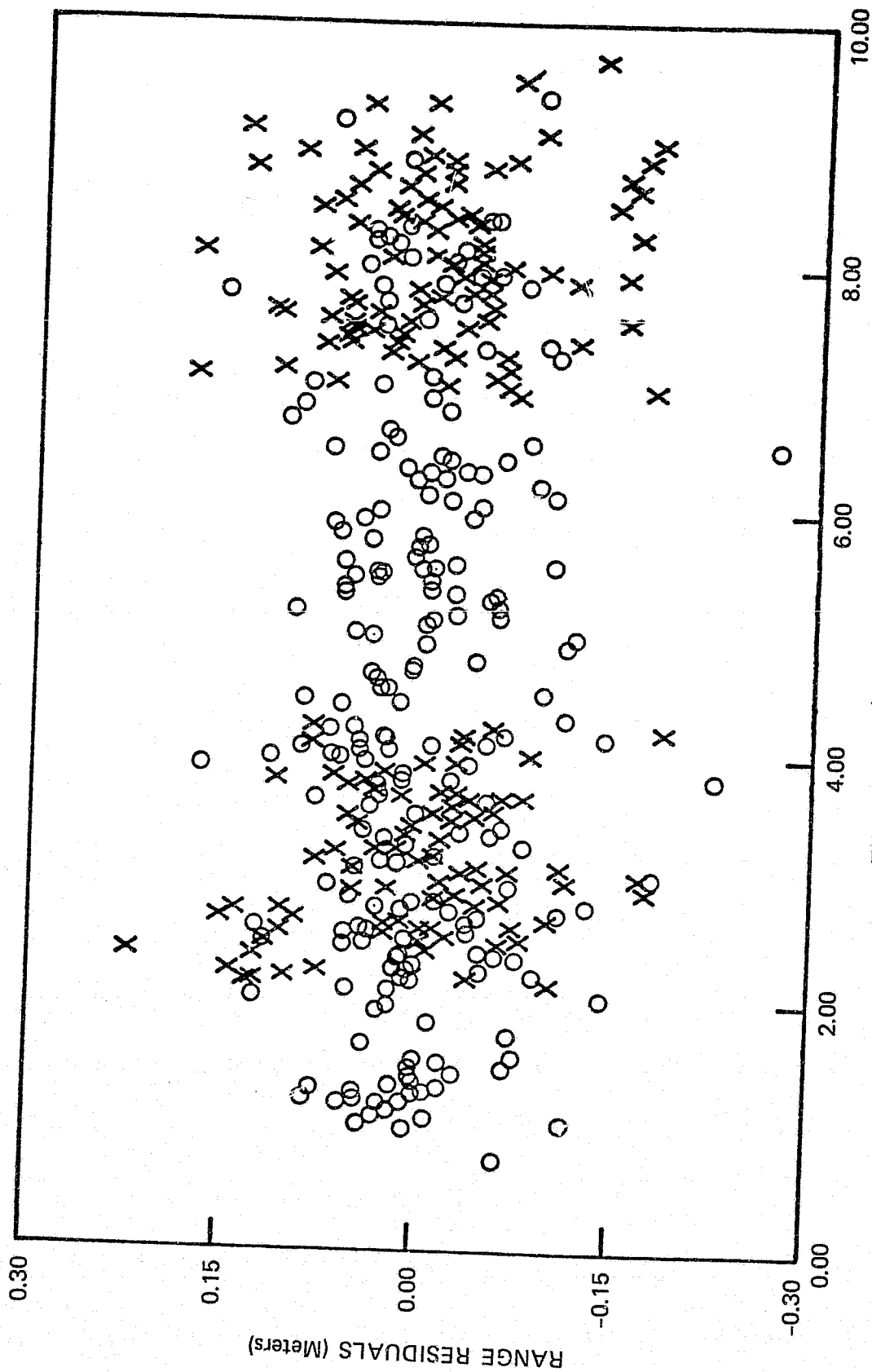
Figure 1. Laser Collocation

TIME FROM START OF PASS (Minutes)

RANGE RESIDUALS (Meters)
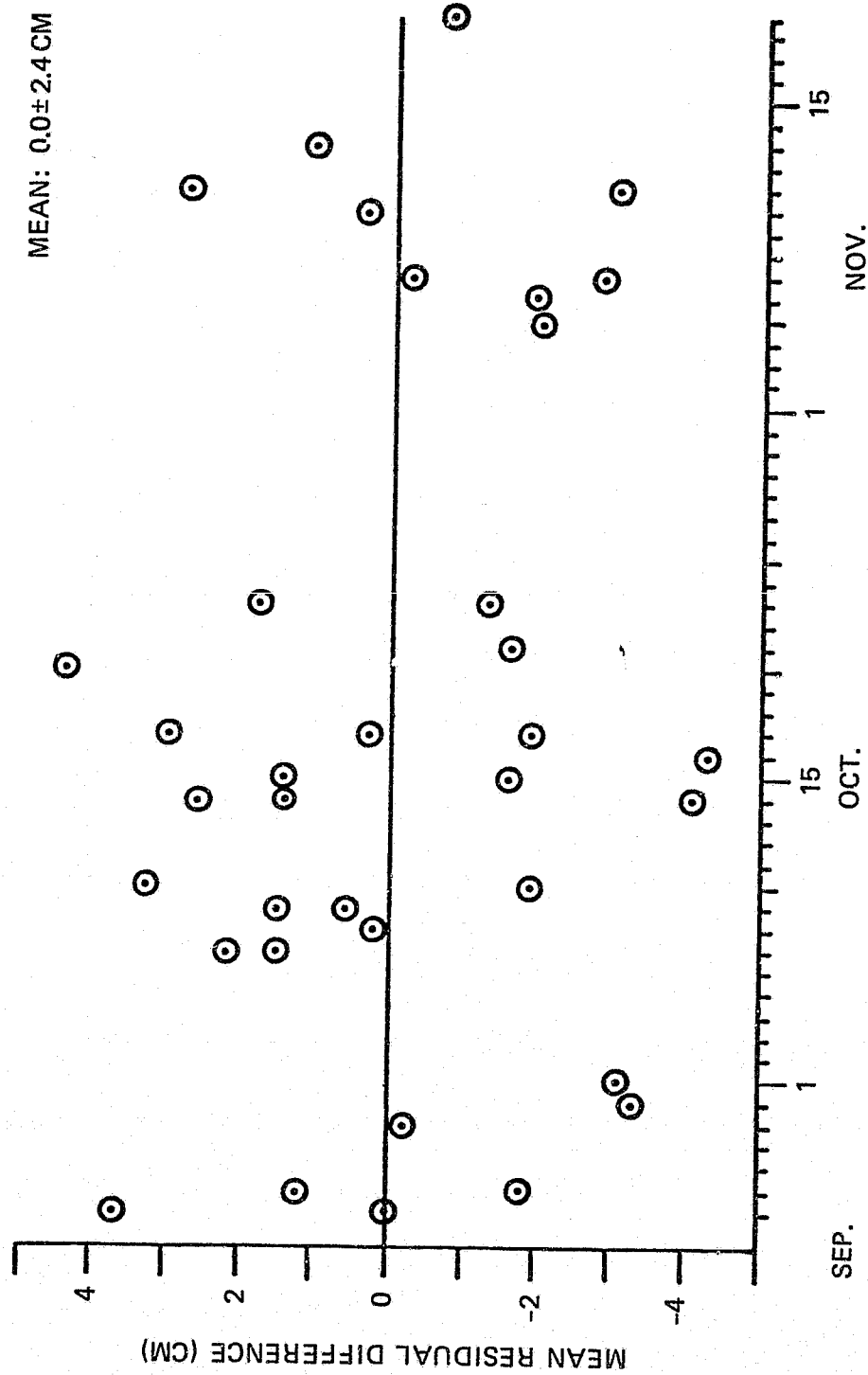
Figure 2. Collocation Results (HOLLAS – MOBLAS–1)

CHAPTER 2

GLOBAL EARTH DYNAMICS

OVERVIEW

Studies of global earth dynamics are devoted to improving the understanding of the origin of motions of the whole Earth and determining the structure and mechanical properties of the Earth's interior. The techniques employed in such studies are as varied as the studies themselves. They range from the determination or changes in satellite orbits, to spectrum analyses of polar motion data, to the inversion of gravity field representations. The reports in this chapter summarize as follows five research activities underway in the Geodynamics Branch during 1982:

1) The first report focuses on the determination of the effective viscosity of the lower mantle using observed accelerations in the node of Lageos' orbit. The results are discussed in terms constraints on the allowed modes for mantle convection.

2) The second report is the first of two papers on polar motion. Data from both the International Latitude Service and observations of Lageos have been analyzed to determine both the annual and Chandler Wobble component of polar motion. For both of these terms the frequencies, amplitudes, phases, and Q's of the signal have been determined.

3) Continuing the study of polar motion, the next report discusses the development of a matched filter to improve the signal recovery from a noisy time seris. This filter is being used to determine the frequency and Q of the Chandler Wobble.

4) The fourth paper describes the use of gravity data in an information theory based inference scheme to determine the lateral density distribution of the Earth.

5) Finally, a comparison is presented on length-of-day determinations from atmospheric wind data and from Lageos observations. The correlation between the 2-day sets argues that changes in the zonal winds are a major contributor to length-of-day changes.

Contributors to this chapter are B.F. Chao, D.C. Christodoulidis, R. Gross, D. Rubincam, D.E. Smith, and George Wyatt.

POSTGLACIAL REBOUND OBSERVED BY LAGEOS AND THE EFFECTIVE VISCOSITY OF THE LOWER MANTLE

David P. Rubincam

OBJECTIVE

The objective of this work is to infer the effective viscosity of the lower mantle from observations of the node of Lageos' orbit.

BACKGROUND

The Lageos satellite was launched in May 1976 for the purpose of studying crustal motion, plate motion, polar motion, and earth rotation (Smith and Dunn, 1980). Five years worth of laser ranging data reveal an acceleration in the node of Lageos' orbit which is not currently modeled in the GEODYN orbit determination computer program (see Fig. 1). Its value is $\ddot{\Omega} = -8.1 \pm 1.8) \times 10^{-8}$ arcseconds day^{-2}; hence the rate at which the node is progressing along the equator ($\dot{\Omega} = 0.343$ degrees day^{-1}) is becoming smaller.

An obvious geophysical interpretation of the data is to assume that the earth's equatorial bulge is getting smaller. Since the rate $\dot{\Omega}$ is proportional to the J_2 term in the spherical harmonic expansion of the earth's gravitational potential, the observed $\ddot{\Omega} = (8.1 \pm 1.8) \times 10^{-8}$ arcseconds day^{-2} implies that J_2 is changing at the rate of $\dot{J}_2 = (-8.2 \pm 1.8) \times 10^{-19}$ s^{-1}.

RECENT ACCOMPLISHMENTS

A complete description of the work summarized here may be found in Rubincam (1983). Briefly, the observed J_2 cannot be due to the tidal deceleration of the earth and the subsequent relaxation of the earth; it is a factor of 40 too small. Also, the long-period 18.6 year ocean tide does not appear to be the cause, since it woud have to be far from equilibrium.

The acceleration of the node does appear to be due to the postglacial rebound of the earth. During the Quaternary Ice Age the weight of the ice caps in the polar regions squashed the earth into a more elliptical shape; it is now relaxing and thus decreasing J_2. The magnitude of J_2 is controlled in part by the effective viscosity of the mantle. Hence the observed J_2 places constraints on earth structure.

Wu and Peltier's (1982) L1 and L2 earth models plus an assumed ice cap history were used to compute J_2 values to compare with the observed value. The L1 model has a 120 km-thick lithosphere, a 10^{21} Pa s mantle, and an inviscid core. The L2 model is the same as the L1, except that the effective viscosity of the lower mantle (below 671 km depth) is 10^{22} Pa s. The resulting J_2 values were -9.8×10^{-19} s^{-1} for the L1 model and -32.0×10^{-19} s^{-1} for the L2 model. Clearly the L1 model is closer to the observed value of $(-8.1 \pm 1.8) \times 10^{-19}$ s^{-1} and is preferred to the L2 model.

SIGNIFICANCE

The results indicate that the effective viscosity of the mantle must be a fairly uniform 10^{21} Pa s. In other words, there is no great difference between the effective viscosities of the upper and lower mantle. Hence any objection to whole mantle convection based on such a difference apparently cannot be invoked.

FUTURE EMPHASIS

The behavior of the node of Lageos' orbit will be monitored in the future to see whether it still conforms to that predicted by postglacial rebound. Also, other possible causes for the acceleration of the node will be investigated.

REFERENCES

Rubincam, D.P., Postglacial Rebound Observed by Lageos and the Effective Viscosity of the Lower Mantle, NASA/GSFC TM 84982, Goddard Space Flight Center, Greenbelt, MD, February 1983.

Smith, D.E., and P.J. Dunn, Long Term Evolution of the Lageos Orbit, Geophys. Res. Lett., 7, 437-440, 1980.

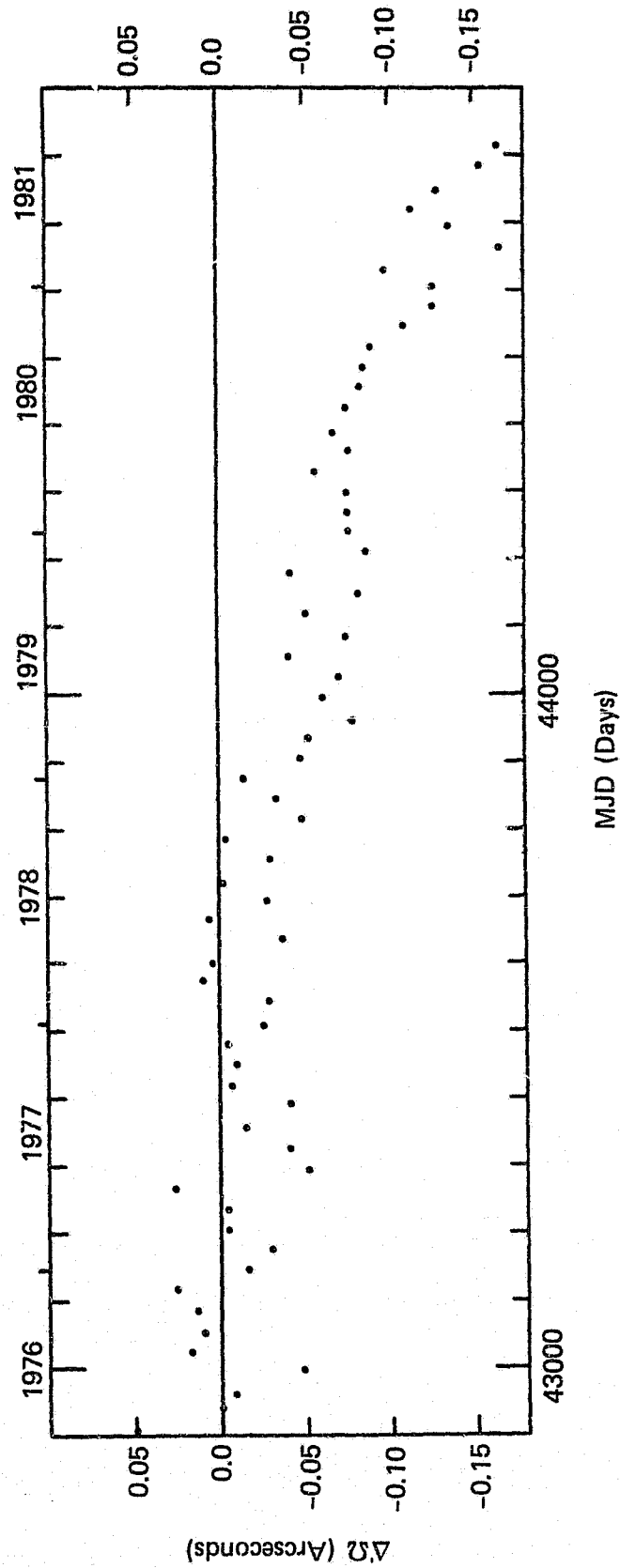Wu, P., and W.R. Peltier, Viscous Gravitational Relaxation, Geophys. J.R. Astr. Soc., 70, 435-485, 1982.

Figure 1. Plot of the residuals in the node, presumably due to postglacial rebound.

DYNAMICS OF THE EARTH'S POLAR MOTION

B. Fong Chao

OBJECTIVE

To analyze polar motion data obtained by geodetic techniques including classical astrometry and satellite laser ranging, and to compare the observations with the atmospheric and seismic excitation functions.

BACKGROUND

The Earth's rotational axis does not remain fixed relative to the body of the Earth. Instead, the interception of the axis with the surface of the Earth (i.e., the pole) traces out a quasi-periodic path about some mean position on a scale <10 meters. This motion is known as the polar motion of the Earth. The polar motion in principle consists of a number of components arising from various dynamical processes. The two major components are the annual wobble with a yearly period and the 14-month Chandler Wobble.

The annual wobble is a forced motion and the variations in atmospheric mass distribution have long been identified as the major cause for the annual wobble. Other mechanisms, such as ocean circulations, core-mantle coupling, solar winds and radiations, are believed to have minor effects on Earth's polar motion. Numerically, lacking any information that indicates otherwise, the annual wobble has been modeled as a pure sinusoid with a period of 365.25 days.

The Chandler wobble, on the other hand, ; the Earth's free motion corresponding to the Eulerian nutation of a rigid body. Its excitation sources have remained unidentified despite an ongoing effort over many decades. Two plausible candidates have been proposed: atmospheric and seismic excitations. However, as to date, both seeem to suffer from insufficient energy. Despite this difficulty (rightfully or not), the period and the Q of the Chandler Wobble have been estimated by means of various numerical techniques; and there has been no agreement on the structure of Chandler period(s) (whether it is single, multiple, or even time-variable), nor on the value of the Chandler Q (estimates range from from ~30 to ~1000, depending on data and techniques used).

RECENT ACCOMPLISHMENTS AND SIGNIFICANCE

Naturally, for our purposes (namely, the numerical modeling of polar motion using atmospheric and seismic excitation functions), the essential first step is to separate the annual and the Chandler wobbles into optimum numerical

representations--in the present case, complex harmonic functions of time. Thus, we completed a harmonic analysis of the following two sets of polar motion data: (1) monthly solutions by ILS (the International Latitude Service) using classical astrometry, spanning 80 years (1900-1979), and (2) 5-day solutions of LAGEOS (the Laser Geodynamics Satellite) using satellite laser ranging, spanning 5.7 years (1976.4-1982.1). The method used is the "Autoregressive (AR) method" (Chao and Gilbert 1980), devised to estimate the complex frequency (frequency and Q) and the complex amplitude (amplitude and phase) of each complex harmonic function in a time series. Tables 1 and 2 give the results for ILS data (Chao, 1983a). Major conclusions include (i) the annual wobble is stationary over the long period of time spanned by ILS observation, and (ii) the ILS data are consistent with a Chandler wobble model that consists of four components. Tables 3 and 4 give the LAGEOS results (Chao, 1983b). The multiple-component behavior of the Chandler wobble, if it exists, cannot be resolved due to the short record length. Note that the estimated annual periods are significantly shorter than the theoretical value 365.25 days (by 5-10 days) during 1976.4-1982.1. It should be pointed out that the observations in Table 3, including the anomalous periods, the decay in amplitudes, and the differences in amplitudes and phases, simply reflect the yearly behavior of the driving mechanism(s) of the annual wobble, and can and should be accounted for by the latter.

On the theoretical front, the problem of excitation of the Earth's (free) Chandler wobble by a transient, indigenous source (as exemplified by a seismic event whose duration is generally much shorter than the Chandler period) has been revisited (Chao 1983c), with particular emphasis on the compatibility in coordinate systems used for observations and for computations. It is found that the difference between the two types of coordinate systems is far from trivial. However, for most practical purposes, this discrepancy is small compared with the amplitude of the polar motion itself.

FUTURE EMPHASIS

The long ILS data set is ideal for statistical studies for the excitation of polar motion. One such study is a statistical analysis of the relationship between the polar motion and the occurrence of major earthquakes. Thus, correlation between the longitudes of over 1500 earthquakes (over the same period spanned by the ILS observation) and the phases of the pole position at the time of the events will be calculated in order to detect the existence of any possible cause-and-effect relation.

The high-density, accurate LAGEOS data, whose annual and Chandler wobbles having been separated and analyzed, can now be compared with the atmospheric

angular momentum data (also available since 1976, see Rosen & Salstein 1981). In particular, we can compute the polar motion that is caused by the atmospheric variations and subsequently conduct a wobble-by-wobble comparison. This presumably will account for the behavior of the annual wobble presented in Table 3, and determine how much of the Chandler wobble can be accounted for by the atmosphere and hence give clues to the importance of other excitation agents.

	Period (days)	Q	Amplitude (")	Phase (°)
ILS-X	365.20	-1480	0.0884	108
ILS-Y	365.10	1370	0.0840	10

Table 1. AR estimates for the ILS annual Wobble

Comp. No	Period (days)	Q	Amplitude (")	Phase (°)
I	406.45	1840	0.0267	216
II	426.00	711	0.1199	273
III	437.46	-189	0.0573	342
IV	452.73	180	0.0686	150

(a)

Comp. No.	Period (days)	Q	Amplitude (")	Phase (°)
I	406.85	-386	0.0170	132
II	426.15	703	0.1195	185
III	437.43	-184	0.0572	253
IV	452.39	320	0.0569	54

(b)

Table 2. AR estimates for the Chandler wobble from
(a) IIS-X   (b) ILS-Y.

	Period (days)	Q	Amplitude (")	Phase (°)
LAG-X	360.0	13.2	0.153	196
LAG-Y	354.9	8.7	0.182	80

Table 3. AR estimates for the LAGEOS annual wobble.

	Period (days)	Q	Amplitude (")	Phase (°)
LAG-X	434.2	22.5	0.188	319
LAG-Y	436.4	12.8	0.245	238

Table 4. AR estimates for the LAGEOS Chandler wobble

REFERENCES

Chao, B.F. and F. Gilbert, 1980. Autoregressive Estimation of Complex Eigenfrequencies in Low Frequency Seismic Spectra, Geophys. J. R. Astron. Soc., 63, 641-657.

Chao, B.F., 1983a. A Harmonic Analysis fo the Earth's Polar Motion Using ILS Data, submitted to J. Geophys. Res.

Chao, B.F., 1983b. Analysis of LAGEOS Polar Motion Data, in preparation.

Chao, B.F., 1983c. On Excitation of Earth's Free Wobble and Reference Frames, in preparation.

Rosen, R.D. and D.A. Salstein, 1981. Variations in Atmospheric Angular Momentum, ERT Technical Report A345-T1.

POLAR MOTION

Richard S. Gross

OBJECTIVES

The objective of this research effort is to study some of the outstanding problems in the field of polar motion such as the nature of the excitation mechanism of the Chandler wobble, the value of the period and Q of the Chandler wobble, the Markowitz wobble and the long term stability of the latitude observation stations.

BACKGROUND

In 1765 Euler predicted that any rigid body, including the earth, which is rotating about some axis which is not its principal moment of inertia axis will experience a wobble as it rotates. In 1891 Chandler was able to observe this wobble of the earth and since 1899 it has been observed and studied by the International Latitude Service (ILS) and, more recently, by many other organizations. This motion of the rotation pole about the principal moment of inertia axis is primarily composed of two components. The first has an annual period and is a forced motion of the pole commonly believed to be caused by meteorological events. The second is Euler's free nutation at a period of approximately 434 days and is now known as the Chandler wobble. However, the motion of the rotation pole also exhibits a long term drift in its mean position and there is some evidence that a component (called the Markowitz wobble after the person who proposed its existence) might exist having a period of roughly 24 years.

RECENT ACCOMPLISHMENTS

As a graduate student I used a damped least squares technique to obtain the polar motion along with station corrections from the homogeneous ILS latitude observations in order to obtain a polar motion data set at 19-day time intervals. This polar motion time series spans the years 1899-1979 and can be used to study the long term behavior of the motion of the pole. Since the solution technique took into account the individual station contributions via the station corrections we are also able to study the long term stability of the individual ILS latitude stations.

As our first use of this newly derived polar motion time series we will ascertain when the Chandler wobble is undergoing excitation by a technique based upon matched filters. A matched filter is the optimal linear filter that maximizes the signal to noise ratio in the output at some instant. This is desirable if we are trying to detect the onset time of some signal embedded in noise. The assumption is that our chances of detecting this signal will be increased if the signal to noise ratio is a maximum. For a time series consisting of a known signal $s(t)$ of amplitude A and arrival time t_0 embedded in noise $n(t)$:

$$x(t) = As(t-t_0) + n(t)$$

it can be shown (see, e.g., Robinson (1967)) that the desired filter in the frequency domain is simply $S*(\omega)$, the complex conjugate of the Fourier transform of the signal $s(t)$:

$$Y(\omega) = X(\omega)S*(\omega)$$

where $X(\omega)$ is the Fourier transform of the input signal $x(t)$ and $Y(\omega)$ is the Fourier transform of the output signal $y(t)$. It can be shown (see Gross (1982)) that if the signal $s(t)$ we are trying to detect is damped harmonic motion then the output signal $y(t)$ will exhibit a peak at the signal arrival time t_0 and it will decay exponentially from this peak value. In the case of the Chandler wobble which has a damping time of about 40 years this peak in the output will be rather broad. Of course, we would like the peak to be as delta like as possible. In fact we can form a narrower peak by using the filter:

$$Y(\omega) = X(\omega) \frac{S*(\omega)}{(||N(\omega)||^2 + ||S(\omega)||^2)^{1/2}}$$

where $N(\omega)$ is the Fourier transform of our estimate of the noise in the input time series. To illustrate the use of the above filter figure 1 shows the x-component of a synthetic time series we generated which consists of three signals embedded in noise. Figure 2 shows the amplitude of the time series resulting from applying the above filter (with N=0.1) to this input time series. As can be seen the output is peaked at the signal arrival times which are indicated by the dashed lines.

We are currently applying this noisy matched filter to various polar motion data sets. As an aid in interpreting the results we are also using it on many synthetic time series.

FUTURE EMPHASIS

We shall continue our investigations into the properties of the excitation process of the Chandler wobble as well as study other topics in the field of polar motion. In particular we will calculate the period and Q of the Chandler

wobble by assuming that it is the result of a white noise process exciting a resonant system. We will also study the Markowitz wobble as manifested in the data set derived by Gross (1982) and we will study the long term stability of the ILS latitude observation stations as indicated by their station corrections.

REFERENCES

Gross, R.S., "A Determination and Analysis of Polar Motion," Ph.D. Thesis, University of Colorado, 1982.

Robinson, E.A., "Statistical Communication and Detection," Griffin, London, 1967.
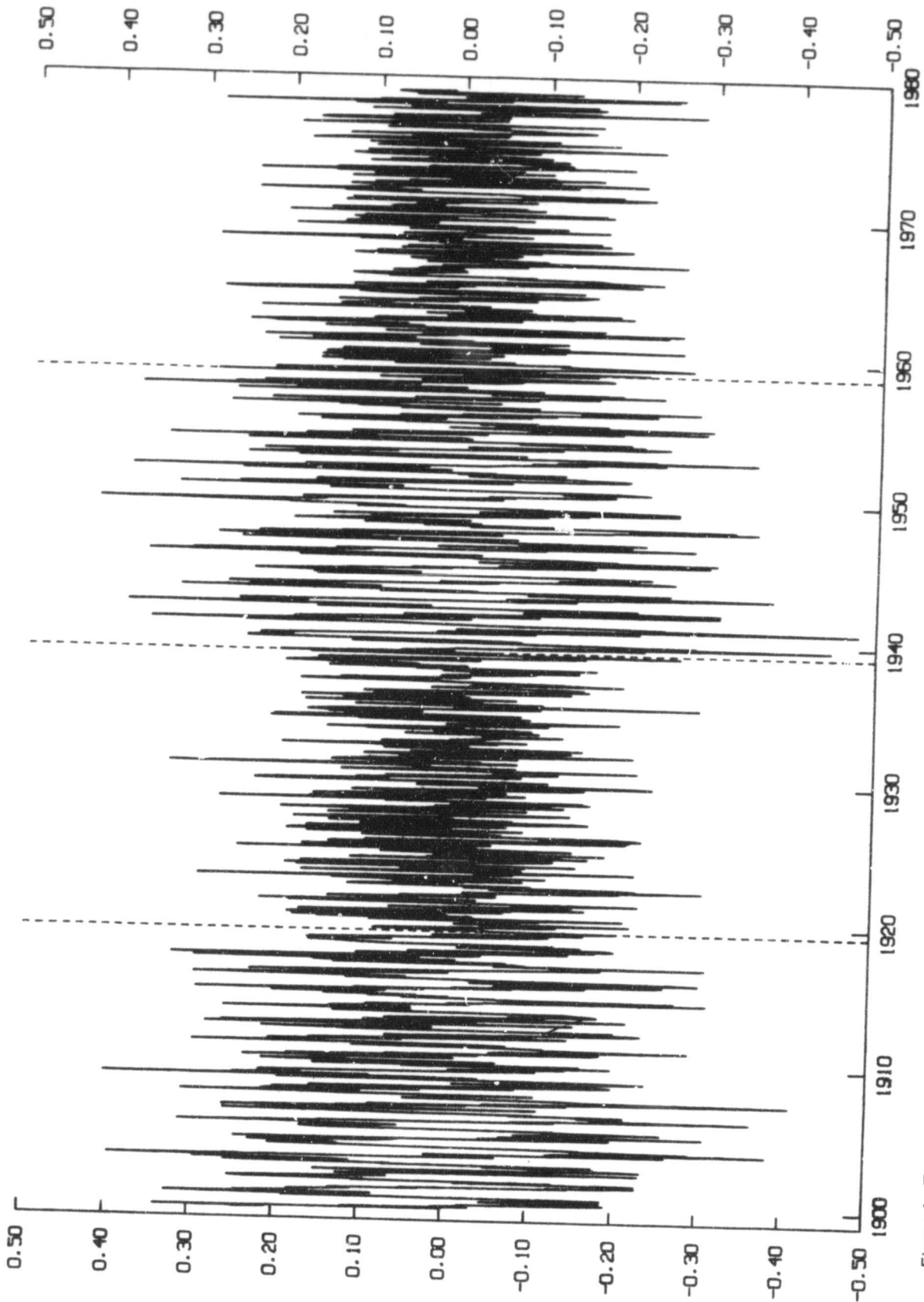
Figure 1. The x-component of a complex time series consisting of three damped harmonic signals (arriving at the times indicated by the dashed lines) embedded in gaussian white noise. The ordinate has units of arcseconds and the abscissa has units of time measured in years.
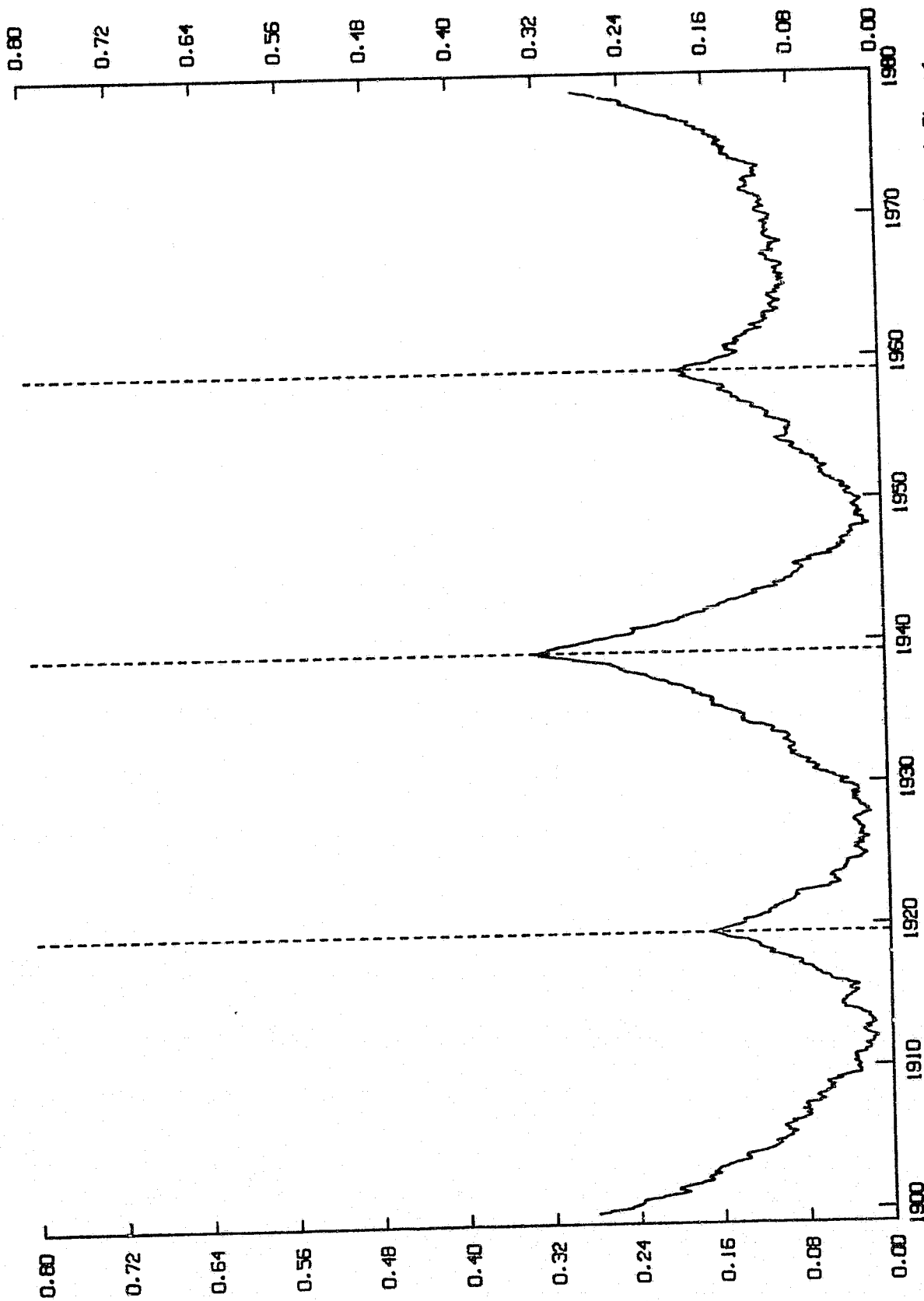
Figure 2. The amplitude of the result of applying the noisy matched filter to the complex time series whose x-component is shown in Figure 1. Note that the peaks in this figure are at the signal arrival times indicated by the dashed lines.

INFORMATION THEORY LATERAL DENSITY DISTRIBUTION

David P. Rubincam

OBJECTIVE

The objective of this work is to use information theory to infer the lateral density distribution inside the earth, using the external gravity field, crustal models, and an assumed radial density distribution as data.

BACKGROUND

The external gravity field gives information about the lateral density distribution inside the earth. However, it does not given enough information to determine the actual density distribution $\rho_I(\gamma,\theta,\lambda)$. The lateral density distribution must be inferred, not inverted from the data.

The inference technique used here is information theory better known as the Maximum Entropy Method (MEM). The rationale for using information theory is that it provides, in a certain sense the least prejudiced inference from the available data. In other words, it does not read more into the data than is actually there.

RECENT ACCOMPLISHMENTS

A complete description of the work summarized here may be found in Rubincam (1982). Briefly, a density distribution $\rho_I(\gamma,\theta,\lambda)$ is inferred from the the GEM 10B gravity field coefficients $C_{\ell m}$, $S_{\ell m}$ (complete to degree and and order 36) after subtracting off the coefficients of the hydrostatic bulge and an assumed crustal model. Two different models were used: one an isostatically compensated crust, and the other an uncompensated crust. Also the radial part of $\rho_I(\gamma,\theta,\lambda)$ is taken to be the Parametric Earth Model of Dziewonski et al. (1975).

The following results were obtained. The density anomalies generated by $\rho_I(\gamma,\theta,\lambda)$ tend to be spread throughout the mantle, but the largest anomalies occur near the top of the mantle. Typical density variations in the mantle are ±0.004 g cm^{-3} when the compensated crust is removed and ±0.04 g cm^{-3} when the uncompensated crust is removed. The lateral density variations across the equatorial plane are shown in Figs. 1 and 2 for compensated and uncompensated crusts removied, respectively.

SIGNIFICANCE

The $\rho_I(\gamma,\theta,\lambda)$ for either compensated or uncompensated crusts shows no obvious convection pattern in the mantle (such as organized convection cells). Hence mantle convection cannot be inferred from the gravity field data alone. Also, the information theory density distributions are quite different from the minimum elastic energy solution of Kaula (1963) and from the minimum elastic plus gravitational potential energy solution of Sanchez (1980).

FUTURE EMPHASIS

The extension of the information theory approach so as to include seismic data appears quite difficult. Hence no future work in this area is planned.

REFERENCES

Dziewonski, A.M., A.L. Hales, and E.R. Lapwood, Parametrically simple earth models consistent with geophysical data, Phys. Earth Planet. Interiors, 10, 12-48, 1975.

Kaula, W.M., Elastic models of the mantle corresponding to variations in the external gravity field, J. Geophys. Res., 68, 4967-4978, 1963.

Rubincam, D.P., Information theory lateral density distribution for earth inferred from global gravity field, J. Geophys. Res., 87, 5541-5552, 1982.

Sanchez, B.V., Lateral Density variations in elastic earth models from an extended minimum energy approach, NASA/GSFC TM 80742, Goddard Space Flight Center, Greenbelt, MD, June 1980.

Figure 1. Lateral density variation in the equatorial plane of the earth for the case of 30 km of compensated crust removed. Sea level is displaced from the earth's surface for clarity, and the rock-equivalent topography is greatly exaggerated. Anomalies in the core are not shown
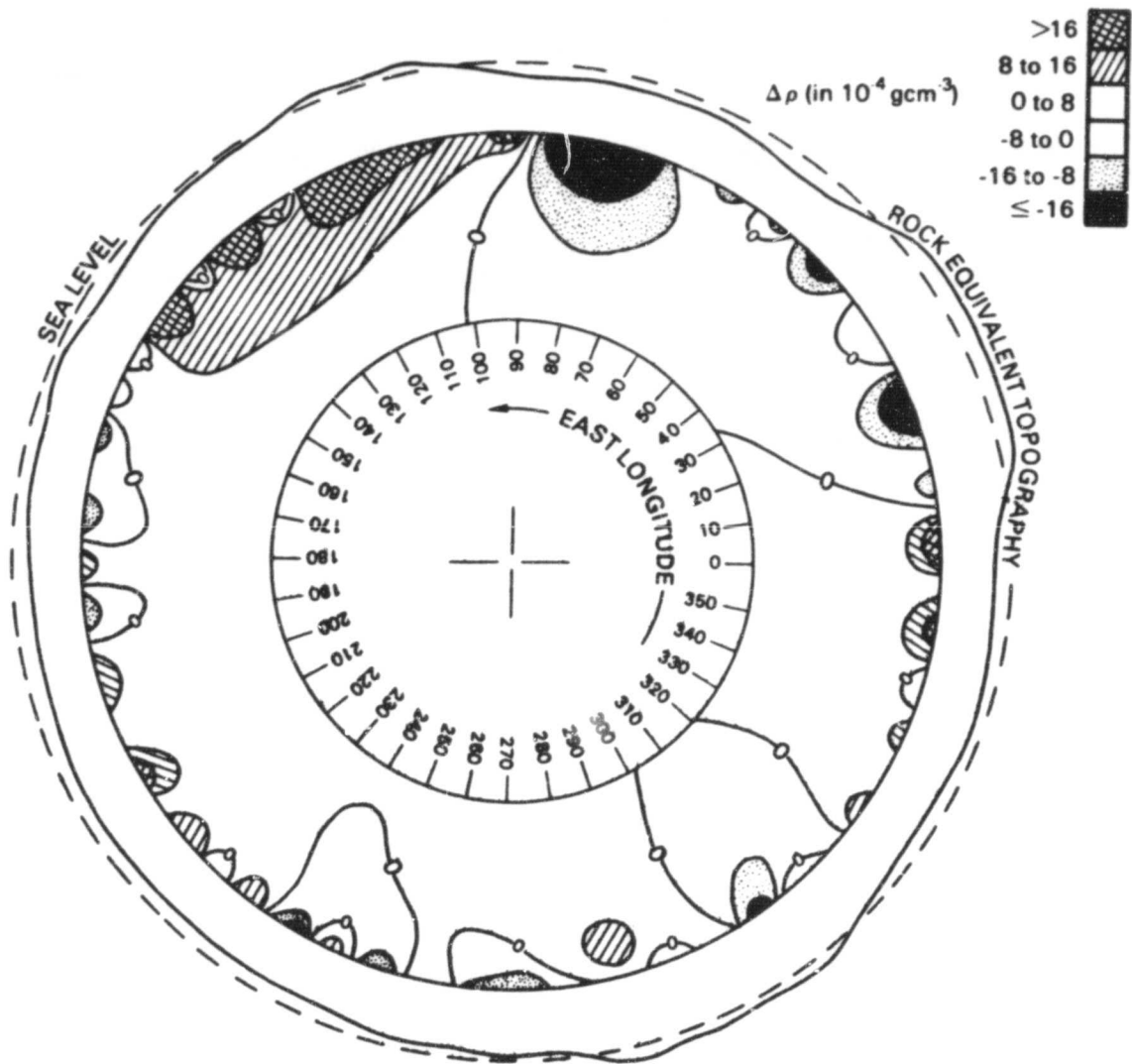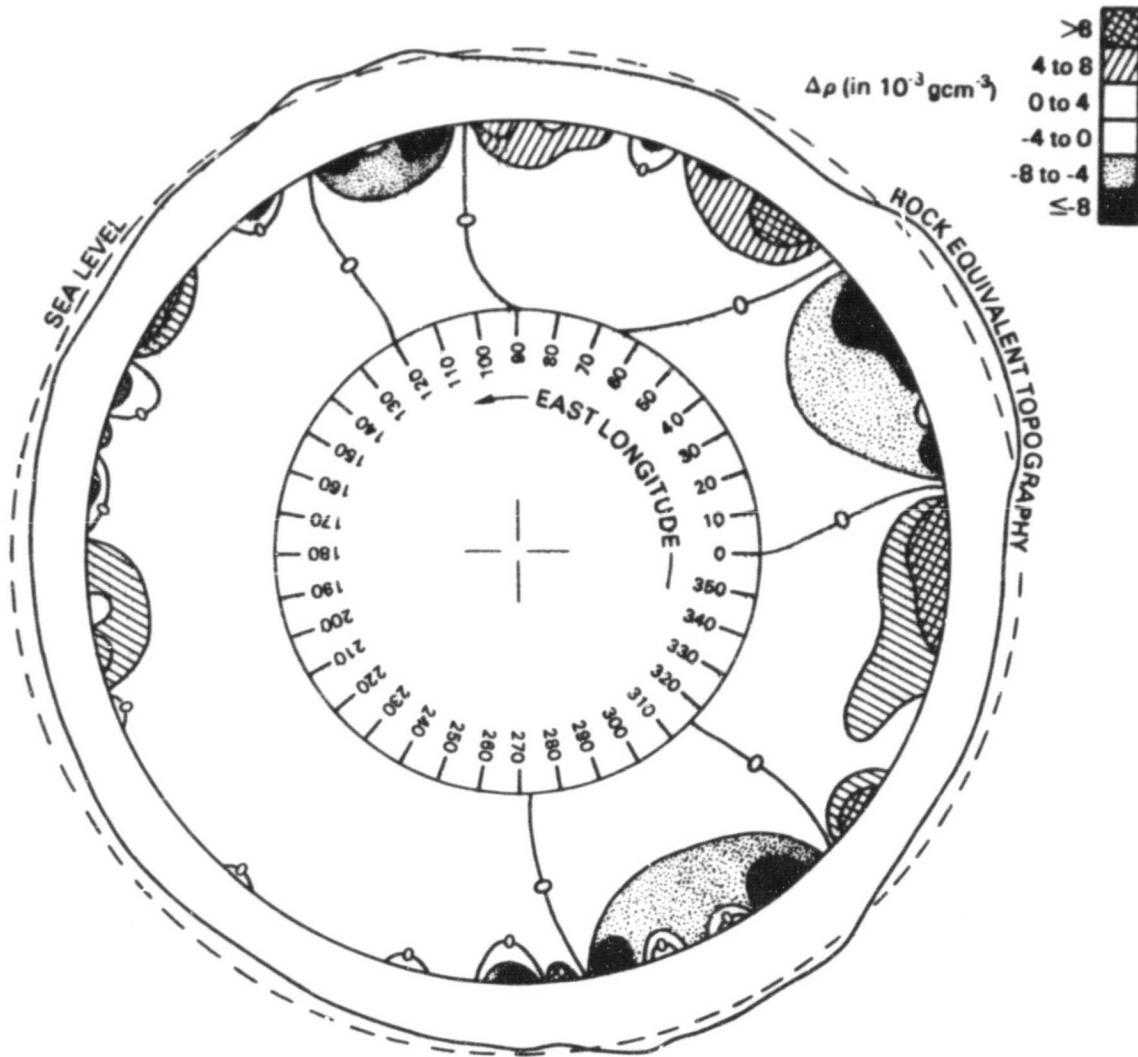
Figure 2. Lateral density variation in the equatorial plane of the earth for the case of 30 km of uncompensated crust removed. Sea level is displaced from the earth's surface for clarity, and the rock-equivalent topography is greatly exaggerated. Anomalies in the core are not shown.

ATMOSPHERICALLY INDUCED VARIATIONS IN THE LENGTH-OF-DAY DERIVED FROM LAGEOS

David E. Smith
Demosthenes C. Christodoulidis
George H. Wyatt

OBJECTIVE

A comparison is made of the length-of-day derived from Lageos with the length-of-day inferred from atmospheric wind data in order to determine the extent of the correlation, accuracies of the two data sets, and to better understand the causes of the changes in the earth's rotation rate.

BACKGROUND

Recently, global atmospheric wind data have been used to derive estimates for the angular momentum of the atmosphere (Rosen & Salstein, 1981) and, under the assumption of the conservation of angular momentum between the solid-earth and atmosphere, the resulting change in the rotation rate of the solid earth has been derived. In these computations the atmospheric zonal winds have been integrated from the surface (1000 mbars) to the 100 mbar level (i.e. 16 km) and averaged into latitude bands from which the angular momentum of the atmosphere has been derived every 12 hours since 1976. Considerable seasonal and short period (tens-of-days) variations are evident in this data set which has been compared with the actual changes in the earth's length-of-day derived from laser tracking of the Lageos spacecraft between May 1976 and July 1981.

RECENT ACCOMPLISHMENTS

The atmospheric angular momentum data was averaged to 5-day values so as to coincide in time with the Lageos length-of-day (LOD) values. The two data sets were analyzed using identical methods. A spectral analysis of the atmospherically inferred LOD for the whole 6-year period showed considerable power at a period of 1 year and a smaller, but significant, amount at 6 months. There appeared to be no secular trend or very long period evident in the data. The spectrum of the Lageos LOD showed greatest power at 6 months and almost the same at 1 year and significant power also at about 1166 days and 285 days. These latter periods are periods related to the tidal perturbations of the orbit by the K_1 and S_2 tides respectively and are not actual variations in the rotation rate of the earth. They were estimated and removed from the Lageos data set. The Lageos data set also showed a secular trend that indicated that the length-of-day was decreasing (earth was speeding up) at a rate of about 0.15 msecs/yr over the 6-year period. This trend is believed to be a result of changes within the earth's core and probably temporary in nature. Historical records of the earth's rotation rate show "decade length" changes that have generally been ascribed to core motions.

After removal of the secular trend and the tidal perturbations of the Lageos orbit (1166 days, 285 days) from the Lageos LOD data, the two data sets were compared. Figure 1 shows the atmospheric data superimposed on the Lageos data after the average value has been removed from each set. The correlation between the two "raw" data sets is 0.82 and the rms difference is 0.19 milliseconds. A major contributor to the rms difference is the very large noise present in the 1976 and 1977 Lageos LOD values. The best year, in terms of Lageos tracking, is 1980 when the correlation between the two LOD data sets is 0.90 and the rms difference in LOD values is 0.15 milliseconds.

The high degree of correlation between the two data sets is partly due to the strong annual and semi-annual periods in both data sets, and the rms difference between the curves is also greatly affected by the fact that each data set has different amplitudes for these terms. When the annual and semi-annual tems are removed from the data for the year 1980 the correlation falls to 0.67 (still very good) and the rms difference falls to 0.10 milliseconds. The decrease in rms can be almost completely explained by the removal of the power at 1 year and 1/2 year that appears in the single point rms. The true level of agreement between the atmospheric and Lageos data sets can be best seen in the year 1980 when a comparison of the two data sets is made after they have been weakly smoothed (so as to remove some of the measurement noise) and the annual and semi-annual terms removed. This comparison is shown in Fig. 2. The smoothing is achieved by a Gaussian weighting where the FWHM is about 8 days. The resulting rms difference is 0.069 milliseconds and the correlation is raised to 0.78.

CONCLUSIONS AND FUTURE EMPHASIS

Comparisons of the atmospheric and Lageos data sets strongly support the concept that most changes in the earth's length-of-day can be ascribed to changes in the earth's zonal winds. Good correlation appears to exist between the data sets for periods of about 10 days to more than a year. The disparity that appears in the amplitudes (0.17 msecs) at 1/2 year period is probably caused by winds not included in the atmospheric data, i.e., those above 100 mbars (Lambeck, 1980). At 1 year, the disparity (0.12 msecs) in amplitudes is probably associated with the lack of atmospheric data above 100 mbar but is also affected by the lack of consideration of variations in the angular momentum of the oceans (Eubanks, 1983).

Future work will try to explain the present differences and investigate other causes of change in the earth's length-of-day.

REFERENCES AND BIBLIOGRAPHY

Barnes, R.T. H., R. Hide, A.A. White and C.A. Wilson, "Atmospheric Angular Momentum Fluctuations, Length-of-Day Changes and Polar Motion," Proc. R. Sco. Lond. A387, 31-73, 1983.

Eubanks, T.M., J.A. Leppe, J.O. Dickey and P.S. Callahan, "A Spectral Analysis of the Earth's Angular Momentum Budget," J. Geophys. Res. (in press).

Hide, R., N.T. Birch, L.V. Morrison, D.J. Shea and A.A. White, "Atmospheric Angular Momentum Fluctuations and Changes in the Length of Day," Nature, Vol. 286, 10, July 1980.

Lambeck, K., The Earth's Variable Rotation: Geophysical Causes and Consequences, Cambridge University Press, 1980.

Lambeck, K., "Changes in Length-of-Day and Atmospheric Circulation," Nature, Vol. 286, 10 July 1980.

Langley, R.B., R.W. King, I.I. Shapiro, R.D. Rosen and D.A. Salstein, "Atmospheric Angular Momentum and the Length of Day: A Common Fluctuation with a Period Near 50 Days," Nature, Vol. 294, 24 December 1981.

Rosen, R.D. and D.A. Salstein, "Variations in Atmosperic Angular Momentum 1 January 1976 - 31 December 1980," ERT Technical Report A345-T1, June 1981.

Rosen, R.D. and D.A. Salstein, "Variations in Atmospheric Angular Momentum and the Length of Day," ERT Technical Report A345-T2, October 1982.

Rosen, R.D., and D.A. Salstein, "Variations in Atmospheric Angular Momentum on Global and Regional scales and the Length of Day," J. Geophys. Res. (in press), 1983.
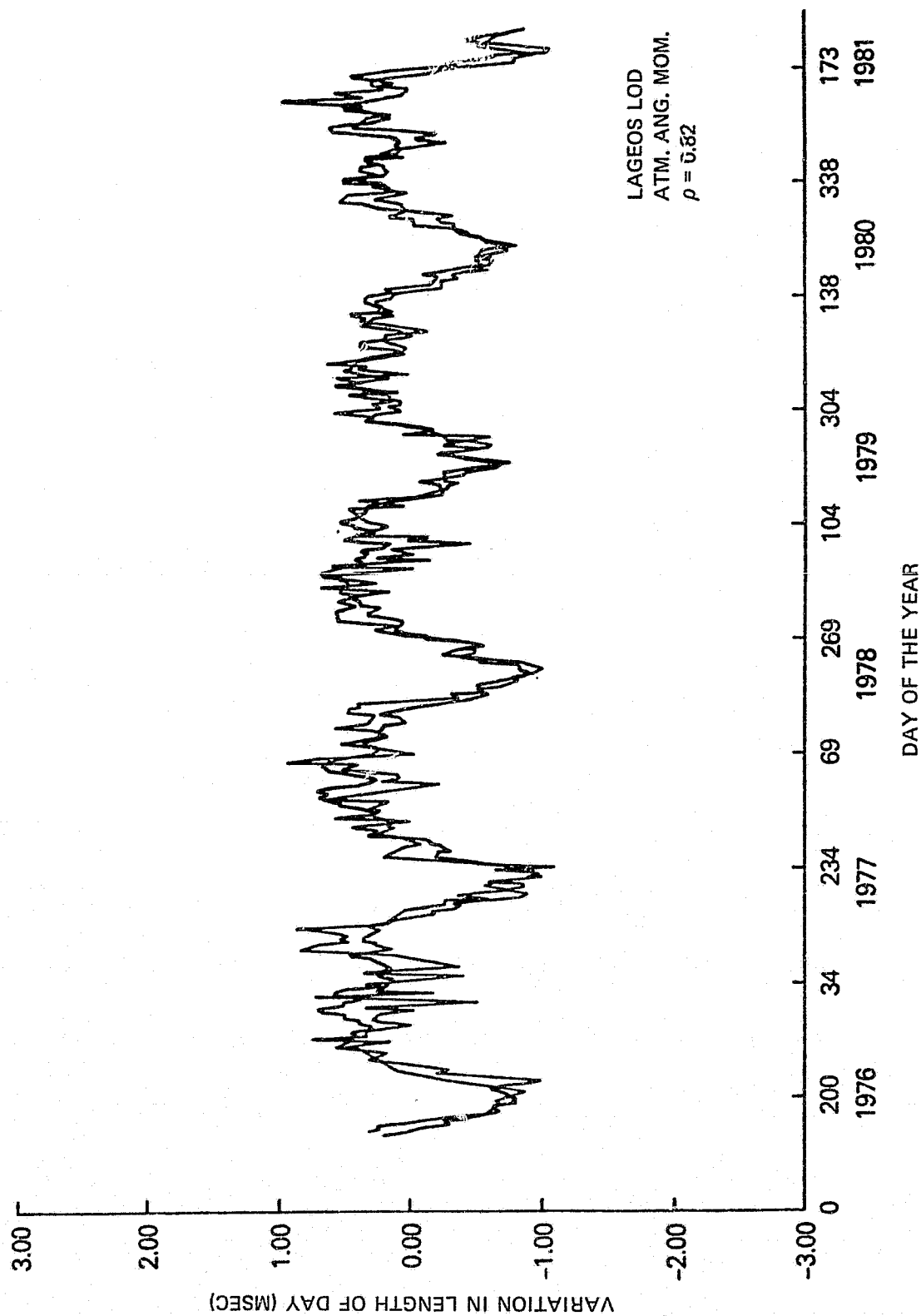
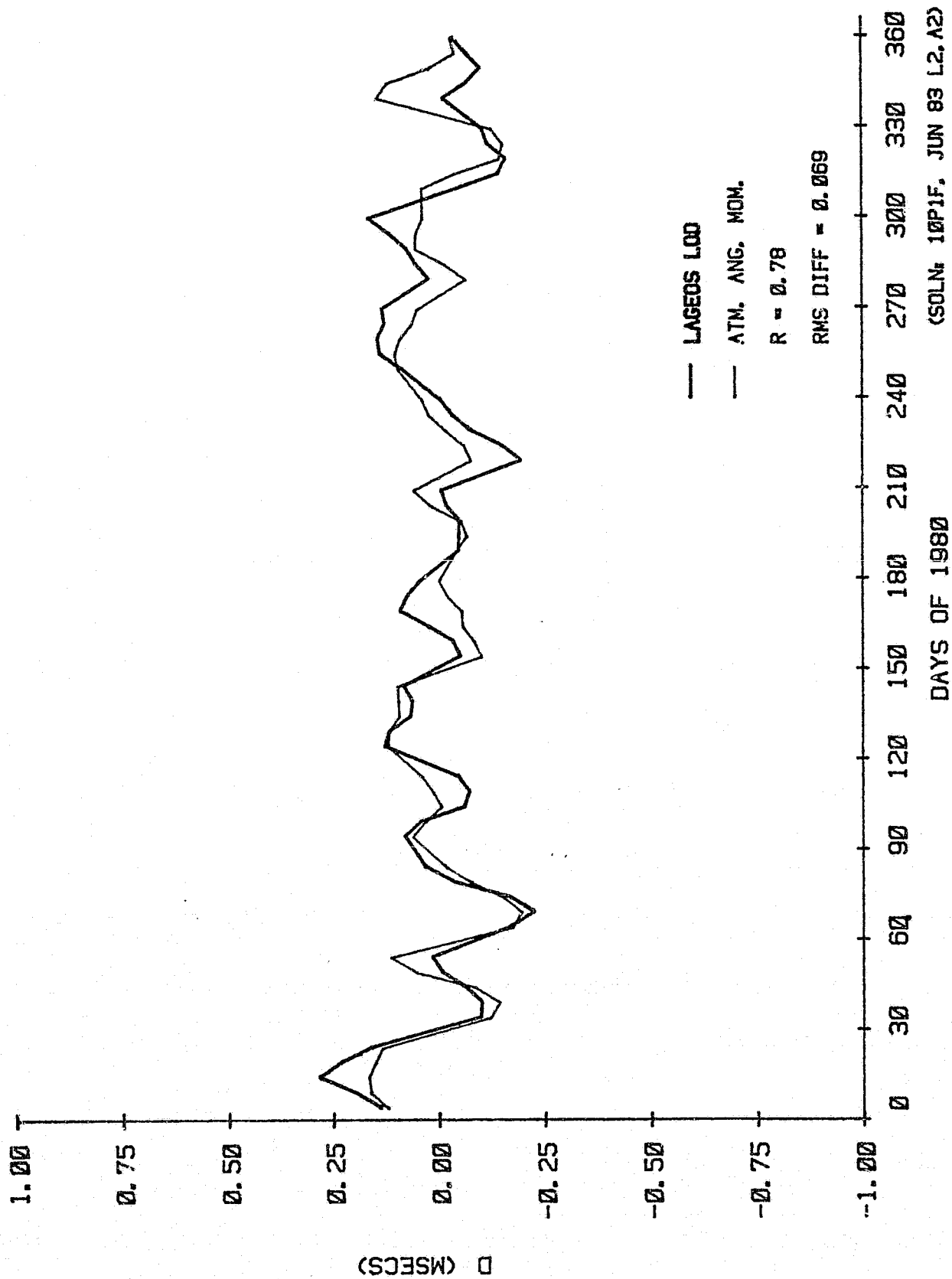Figure 1. Comparison of Atmospheric Angular Momentum with Lageos Variations in LOD.

Figure 2. Comparison of Atmospheric Angular Momentum with Lageos Variations in LOD (Annual, Semi-Annual Terms Removed).

LAGEOS LOD

ATM. ANG. MOM.

R = 0.78

RMS DIFF = 0.069

(SOLN: 10P1F, JUN 83 L2, A2)

DAYS OF 1980

D (MSECS)

CHAPTER 3

GRAVITY FIELD MODEL DEVELOPMENT

OVERVIEW

Knowledge of the earth's gravity field is fundamental to understanding the dynamics of the earth. For solid earth physics, knowledge of the variations in the gravity field provides information on the earth's physical properties and geodynamic processes and places constraints on the internal structure of the earth. In oceanography, knowledge of departure of the actual sea surface from a unique equipotential surface of the earth's gravity field (the geoid) can reveal information on oceanic circulation. In addition, other areas which benefit from knowledge of the earth's gravity field are satellite orbit determination and classical geodesy.

This chapter describes: (1) the development of a refined gravity field model for LAGEOS in order to obtain more accurate orbits that will provide better baseline measurements for the analysis of tectonic plate motion; (2) the study of the evolution of the orbit of LAGEOS for the purpose of improving our knowledge of the force model for the satellite's motion; (3) the development of specialized earth gravity field model of the STARLETTE satellite to improve the precision of that satellite's orbit, and (4) current and future geodynamic computational systems development.

Contributors to this chaper include D.C. Christodoulidis, F.J. Lerch, J.G. Marsh, B.H. Putney and D.E. Smith

GRAVITY MODEL REFINEMENT FROM LAGEOS

Francis J. Lerch

OBJECTIVE

The objective is to improve the gravity field model for Lageos in order to obtain more accurate orbits that will provide better baselines for plate tectonics, improved polar motion and earth rotation. Also the purpose is to improve the low degree and order geopotential which will provide for refinement of our knowledge of the broad features of ocean circulation.

BACKGROUND

The development of the gravity field for Lageos is a principal investigation in the Crustal Dynamics Project. Based upon the previous Goddard Earth Model, GEM 9, baselines from Lageos orbits gave an rms of approximately ±5 cm from a global set of laser tracking sites. Statistical error analysis based upon the GEM 9 accuracy of the coefficients confirms that the baseline error (±5 cm) from Lageos can be attributed significantly to the gravity field model. From the accuracy of the Lageos laser data (down to ±10 cm) error analysis shows that the gravity model can be improved on Lageos to the extent that baseline errors should reduce by at least 50 percent of previous values when considering errors only due to the gravity field.

RECENT ACCOMPLISHMENTS

A refined gravity field model, Goddard Earth Model GEM-L2 (Lerch, et al.), has been derived using the Lageos orbital data yielding better baseline measurements for the analysis of tectonic plate motion. This field also contributes to a better understanding of the broad features of ocean circulation through its improvement of the long wavelength geoid (terms through degree and order 4) with an accuracy estimated at ±8 cm. In GEM-L2 two and a half years of Lageos laser data acquired from over 20 well-distributed stations were combined with the existing data from the best satellite-derived model, GEM-9 (Lerch, et al.). Testing shows that the Lageos gravity field error at long wavelengths is less than half that for GEM 9. A comparison of global laser "base" stations from independent data sets of alternating 15-day data segments over the 2 1/2 years of Lageos show total interstation position to ±1.8 cm (Table 1) when using this new model. The same comparison using the 1979 versus the 1980 Lageos data yields ±5.2 cm; this difference in agreement reflects the change in data distrbituion and other systematic errors along with the tectonic motion which has occurred between these chronologically distinct data sets. Polar motion values were adjusted in GEM-L2 to a precision of 10 cm, which is shown to be necessary to achieve the accurate baseline and geopotential results.

SIGNIFICANCE

The accuracy of the GEM-L2 long wavelength geoid of ±8 cm should provide improved accuracy in the broad features of ocean circulation from application of Seasat altimetry.

Results based upon the gravity model GEM-L2 including adjustments of BIH polar motion and earth rotation from Lageos laser data have shown that laser tracking systems yield an intrinsic accuracy of 1.8 cm for a global set of baselines (Table 1). Tests in this table clearly show that it is equally important to adjust the polar motion and earth rotation as well as the gravity field with the Lageos data in order to achieve the 1.8 cm baseline agreement.

FUTURE EMPHASIS

Future work is continuing with use of more recent and accurate laser data from Lageos.

REFERENCES

Lerch, F.J., S.M. Klosko, R.E. Laubscher, C.A. Wagner, "Gravity Model Improvement Using GEOS-3 (GEM 9 and 10)," GSFC X-921-77-246, September 1977; also, J. Geophys. Res., Vol. 84, 3897-3916, July 31, 1979.

Lerch, F.J., S.M. Klosko, R.E. Laubscher, C.A. Wagner, "Gravity Model Improvement Using GEOS-3 Altimetry (GEM 10A and 10B)," EOS, Vol. 59, No. 4, 260, April 1978.

Lerch, F.J., B.H. Putney, C.A. Wagner and S.M. Klosko, "Goddard Earth Models for Oceanographic Applications (GEM 10B and 10C)," Marine Geodesy, Vol. 6, No. 2, 1981.

Table 1
Baseline Comparison from Two Independent Lageos Data Sets
Spanning 1979 Through 1980*

	GEM-9		GEM-L2		
	w/BIH** Polar Motion and A1-UT1	w/LAGEOS Polar Motion and A1-UT1	w/BIH Polar Motion and A1-UT1	w/LAGEOS Polar Motion & BIH A1-UT1	w/LAGEOS Polar Motion and A1-UT1
Baseline Agreement for Eight "Base" Stations (All 28 Baselines)	7.2 cm	6.0 cm	6.9 cm	4.7 cm	1.8 cm

"Base" Stations are:

7063 GSFC, MD
7086 Ft. Davis, Texas
7090 Yarragadee, Australia
7091 Westford, MA
7115 Goldstone, CA
7114 Owens Valley, CA
7907 Arequipa, Peru
7943 Orroral, Australia

*The data has been divided into alternating 15 day segments and therefore both solutions have similar and uniform data distribution from these sites.

**BIH circular D 90-day smoothed values.

LAGEOS ORBIT EVOLUTION

Demosthenes C. Christodoulidis
and
David E. Smith

OBJECTIVE

Analysis of the evolution of the orbit of the Lageos satellite can improve our knowledge of the force model for the satellite's motion. More accurate representations of the earth, ocean and atmospheric tides and of the gravity model are of general geophysical interest. Improvements in the perturbation model for drag or radiation pressure will allow better determination of the geodynamic measurements which are the main goals of the Lageos analysis.

BACKGROUND

Rubincam (1980) has suggested charged particle drag as the cause of an observed downward trend in the satellite's semimajor axis. Anselmo, et al. (1983) have proposed a model for the variations about this trend based on the effect of reflected radiation from an earth whose albedo exhibits hemispherical assymetry.

The procedure employed to determine a set of locations for the network of stations over the total time period for which laser observations of the Lageos satellite are available has been described by Smith, et al. (1978). It includes the adjustment of Lageos elements at the epoch of each 30-day time span over which a dynamically consistent orbit is determined, and which is the subject of the orbit evolution studies.

RECENT ACCOMPLISHMENTS

The estimated values of along-track acceleration at 30-day intervals obtained in a recent solution are shown in Figure 1. Their average effect of -3.3×10^{-12} m/sec^2 corresponds to a semimajor axis decrement of approxiamtely 1.1 mm/day. The semimajor axis time history due to this unmodeled force is shown in Figure 2 as two time spans during which the semimajor axis decrement was about 1.1 mm/day separated by a period in 1979 when it was somewhat larger in magnitude.

The inclincation and node residual signatures shown in Figures 3a and 3b include the effects of errors in the adopted tidal model on the estimated orbit parameters. The variations can be reduced by correcting the inclination and node values with sinusoidal functions at the three tidal frequencies of 1051, 521, and 280 days corresponding respectively to the K1, K2 and S2 tides. If we assume that the earth tidal model (Wahr, 1979) is correct, these functions can be used to correct the second and fourth degree terms of the ocean tidal model (due to Schwiderski). The values derived in the Lageos analysis are shown in Figure 4 together with those corresponding to the Schwiderski ocean tidal model and that due to Yoder (JPL E.M. 335-30).

SIGNIFICANCE

The relatively low amplitude in the second degree S2 tide observed by Lageos could be caused by the atmospheric tide to be expected at this frequency. The only other serious disagreement with the ocean tidal models is in the phase of the fourth degree term at the K1 frequency. This is a manifestation of the long period variation observed in the nodal signature of Figure 3b. An error in our model of the 18.6 year tide could provide an alternative reason for this error. Although the effect of the neglected ocean tide at this frequency is too small by a factor of 10, an increase in the effective Earth tidal Love number k_2 from 0.299 to 0.6 could produce a nodal variation similar to that observed.

The amplitude of a quadratic function of time which can be used to describe an observed curvature in the nodal signature corresponds to a variation in the second zonal harmonic J_2 amounting to $-.35 \times 10^{-10}$/yr. Rubincam (1983) has proposed post-glacial rebound as the cause of this variation, which when removed leaves us with a signature dominated by errors in the adopted time reference system of the BIH Circular D.

FUTURE EMPHASIS

Numerical models of the earth's albedo will be calibrated and employed to help explain the observed variations in the semimajor axis and eccentricity of Lageos. As the time history of the inclination and node signature extends, better separation of the tidal frequencies will be possible. Improved definition of the quadratic nodal signature which can be described by a variation in the earth's second zonal harmonic can also be expected.

REFERENCES

Rubincam, D.P., "Atmospheric Drag as the Cause of the Secular Decrease in the Semi-Major Axis of LAGEOS' Orbit," Geophys. Res. Lett. 7, No. 6, 1980.

Anselmo, L., P. Farinella, A. Milani, A.M. Nobili, "Effects of Earth-Reflected Sunlight on the Orbit of the LAGEOS Satellite," Astronomy and Astrophysics, in press, 1983.

Smith, D.E., R. Kolenkiewicz, P.J. Dunn and M. Torrence, "Determination of Polar Motion and Earth Rotation from Laser Tracking of Satellites," Proc. IAU Symp., No. 82, 1978.

Wahr, J.M., "The Tidal Motions of a Rotating, Elliptical, Elastic and Oceanless Earth," Ph.D. Thesis, University of Colorado, 1979.

Yoder, C.F., "Spherical Harmonic Decomposition of M.E. Parke's Ocean Tidal Models," J.P.L. Eng. Memorandum 335-30.

Rubincam, D.P., "Postglacial Rebound Observed by LAGEOS and the Effective Viscosity of the Lower Mantle," NASA Technical Memorandum 84982, 1983.
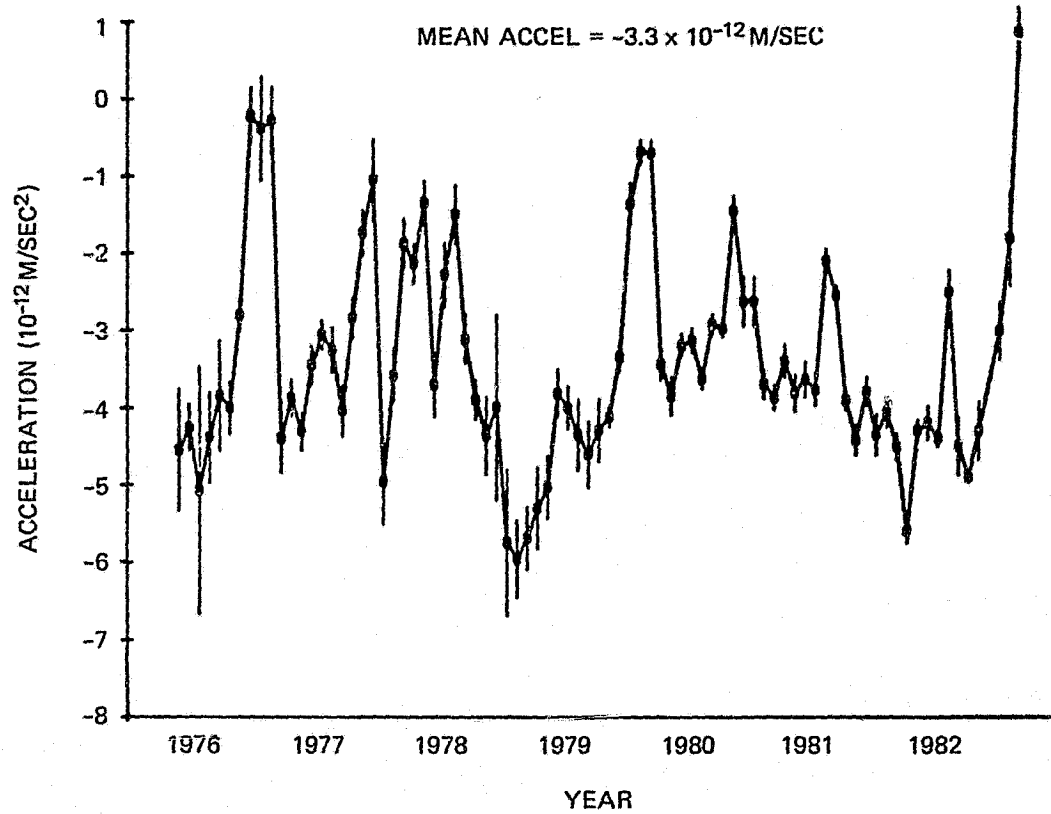
Figure 1. Along-Track Acceleration Estimates
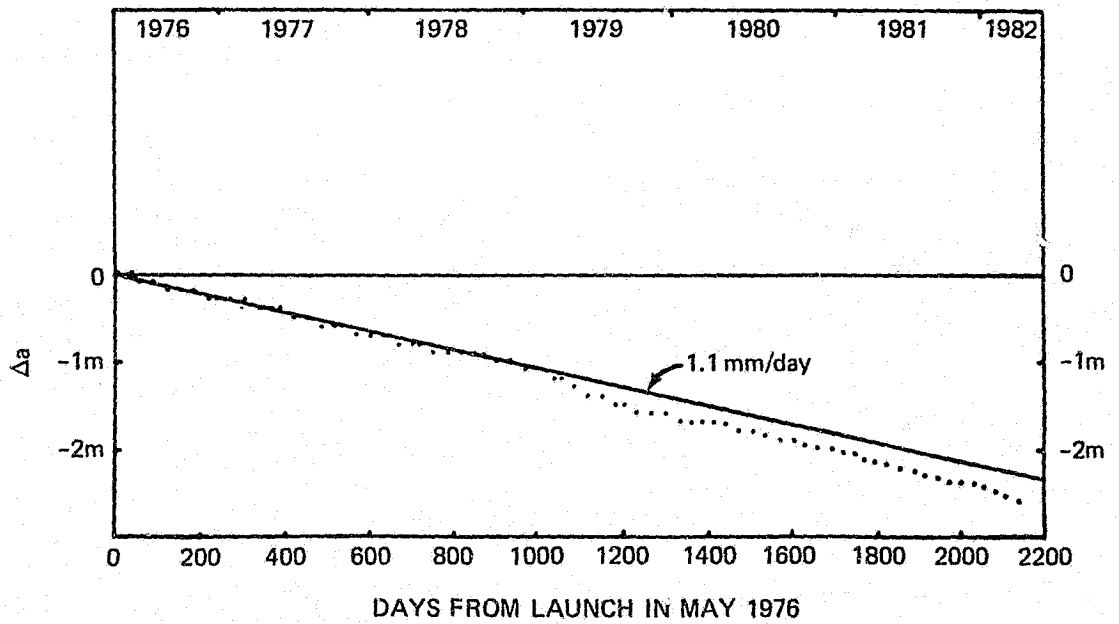
Figure 2. Evolution of the LAGEOS Semi-Major Axis
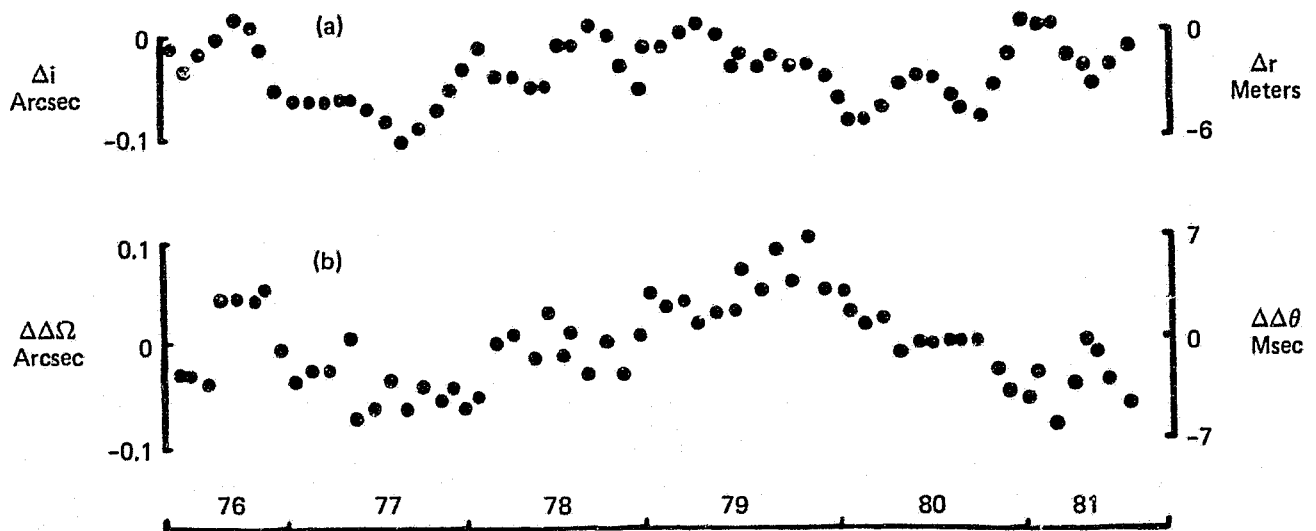
Figure 3. Evolution of Inclination and Node Errors

		SECOND DEGREE		FOURTH DEGREE	
		AMP (cm)	PHASE (deg)	AMP (cm)	PHASE (deg)
K1	LAGEOS	3.03 ±.12	322 ± 2	1.93 ±.36	150 ±11
	SCHWIDERSKI	2.82	315	1.92	254
	PARKE/YODER	2.46	312	1.72	241
K2	LAGEOS	0.10 ±.02	340 ±12	0.23 ±.07	245 ±19
	SCHWIDERSKI	0.27	316	0.11	105
	PARKE/YODER	———	———	———	———
S2	LAGEOS	0.74 ±.04	309 ± 3	1.01 ±.16	85 ± 9
	SCHWIDERSKI	0.93	314	0.37	103
	PARKE/YODER	0.88	301	0.39	85

Figure 4. Comparison of Ocean Tidal Models

3-9

GEODYNAMICS AND GEODETIC PARAMETER ESTIMATION
FROM STARLETTE LASER TRACKING DATA

James G. Marsh

OBJECTIVES

Laser tracking data covering a 4-year period (1975-1978) have been ana-
lyzed for the development of a specialized earth gravity model for
STARLETTE precision orbit computations. Subsequent to this development,
a detailed analysis of the STARLETTE laser data recorded during 1980 has
been performed for the estimation of tracking station coordinates, polar
motion, GM, and ocean tidal constituents. This solution is a simul-
taneous least squares solution based upon normal equations for 65 5-day
arcs of laser tracking data.

BACKGROUND

The Starlette satellite launched in February 1975 (CNES/GRGS, 1975) by
the French Centre National d'Etudes Spatiales (CNES) was designed to
minimize the effects of non-gravitational forces and to obtain the highest
possible accuracy for laser range measurements. The satellite is a sphere
with a radius of 12 cm. It is a passive satellite constructed of a core
which is largely Uranium 238 covered by an aluminum alloy shell which
contains 60 laser corner reflectors. The mass of the satellite is 47.295
kg. The orbit has perigee and apogee heights of 810 km and 1105 km
respectively and an inclination of 49.8 degrees.

Laser tracking data recorded during the time span from 1975 to 1981 have
been used in these analyses. The data analyzed have been contributed by
the CNES, Smithsonian Astrophysical Observatory (SAO), Goddard Space
Flight Center (GSFC) and the Technische Hogeschool Delft in the
Netherlands.

Initial orbit computations using 5-day arc lengths of the laser data
produced rms fits for a typical set of orbits in 1979 which ranged from
1.5 to 3 meters. In these reductions the GEM 10B gravity model was used.
Analyses of these solutions indicated that the primary error source was
the earth gravity model, and thus a comprehensive effort was undertaken
to adjust all gravity model coefficients which would have an effect of 1
cm or larger on the STARLETTE orbit. The final set of coefficients
adjusted consisted of a complete (36,36) model plus selected higher order
coefficients to degree (48).

The high level of orbital accuracy provided by this gravity model solution has provided a basis for the adjustment of a global set of tracking station coordinates, polar motion, GM, and ocean tidal coefficients. Laser tracking data recorded during 1980 have been used in these analyses.

RECENT ACCOMPLISHMENTS

The new STARLETTE gravity model designated PGS-1331 reduced the rms orbital fits for the laser data (5-day arcs) from several meters to a few decimeters.

The analyses of the more precise globally distributed laser tracking data recorded during 1980 have provided a highly accurate set of tracking station coordinates. This independently derived solution has provided a means of independently verifying the Lageos derived values and has thus placed bounds on the overall precision relative to the center-of-mass of the coordinate system.

Comparisons of the STARLETTE derived tracking station coordinates with those derived from LAGEOS at GSFC (GSFC SL5) and at the University of Texas (UT8081 A-M) are presented in Table 1. In these comparisons, translation and rotation parameters have been adjusted in order to removed any systematic differences in the coordinate system definitions. The ΔX and ΔY translation parameters were small (<10 cm) however an unexplained ΔZ shift of about 70 cm is noted between the LAGEOS solutions. The rms agreement of the Starlette derived values with the LAGEOS solutions is generally better than 20 cm.

The recovered value for GM is $398600.43 \pm .01$ km^3/sec^2 which is in good accord with the value of 398600.436 recovered by Smith, et al. (1983) from 1980 LAGEOS data. This indicates the overall scale control in the solution is good and that the potential model is reasonably complete.

From our previous work on STARLETTE presented in Marsh and Williamson (1978) and in Felsentreger, et al. (1979), we were aware of the fact that STARLETTE is significantly perturbed by tides. The earth and ocean tidal effects on satellite position in a typical 5-day arc of STARLETTE are substantially over a meter. Given a sparse data set, there is little hope of attaining 10 cm station positions or baseline determinations without appropriately modeling this effect. At the time we designed this current solution, our software system at GSFC, GEODYN, had recently been enhanced with the capability to model the tides as individual constituents. This modeling, developed by D. Christodoulidis, provides for linear responses at each specific frequency in the tide generating potential and is expressed in terms of the osculating ecliptic elements of the disturbing body and the equatorial position of the desired point on the earth's surface.

The approach we were able to use in this study is to recover tidal parameters directly in the simultaneous least squares data reduction along with the other geodetic parameters--tracking station locations, geopotential coefficients, and the like. This technique is possible only because of the improvement in the quality of the laser tracking data, in our knowledge of the geopotential, and in our other improved modeling related to centimeter satellite geodesy and geodynamics.

Table 2 presents the STARLETTE recovered tides. These tides are the full tidal effect relative to the Wahr free space potential, and the Woolard nutation series coordinate system. Where significant sideband terms existed (typically those differing by the period of the lunar node from the dominant central term), the analytic theory of Cartwright and Taylor (1971) and the later Cartwright and Edden (1973) have been used to determine the appropriate value at the central frequency. The basic assumption in this projection is that the earth's response function (admittance) should be approximately the same at nearby frequencies. Otherwise, the values are as recovered. Note that the diurnal tides are appropriate to the coordinate system definitions described which incorporate the Woolard series nutations. The uncertainties in these values range from about 0.5 cm in C_{20} to about 0.2 cm in C_{22}.

SIGNIFICANCE

Analyses of the 1980 Starlette tracking data have:

o   independently confirmed the relative positioning of the LAGEOS recovered tracking station locations to an accuracy in each coordinate of 20 cm.

o   illustrated a sub-meter bias in the ΔZ network center of origin in the satellite laser systems.

o   demonstrated that the tidal response of the earth has been mapped to better than .01 in effective k_2 for the entire tidal frequency range from the direct analyses of the laser tracking data. This includes the determination of long period tides which are fundamental to UT1 variations. This mapping substantially agrees with a combination of the Schwiderski ocean tides and the Wahr body tide.

o   demonstrated that the precision laser tracked satellites are quite sensitive to nutation error and in fact may be a good way to measure it.

o   demonstrated that STARLETTE can be used to recover reasonable polar motion values after suitable corrections are made for nutation errors.

FUTURE EMPHASIS

Additional analyses using more recent laser tracking data recorded during 1981 to 1983 are in progress. Techniques to better account for the effect of using the Woolard nutation series as versus using the modern Wahr series are also in progress. These analyses are expected to provide a further refinement of the present parameters and further insight into precision orbit determination at the decimeter level.

ACKNOWLEDGEMENT

REFERENCES

Cartwright, D.E. and A.C. Edden, 1973, "Corrected Tables of Tidal Harmonics," Geophys. J.R. Astr. Soc., 33, 253-264.

Cartwright, D.E., and R.J. Taylor, 1971, "New Computations of the Tide Generating Potential," Geophys. J.R. Astr. Soc., 23, 45-74.

Centre National d'Etudes Spatiales, Groupe de Recherches de Geodesie Spatiale, STARLETTE, Toulouse, France, February 1975.

Felsentreger, T.L., J.G. Marsh and R.G. Williamson, 1979, "M_2 Ocean Tide Parameters and the Deceleration of the Moon's Mean Longitude from Satellite Orbit Data," J. Geophys. Res., 84, No. b9 4675-4679.

Marsh. J.G., R.G. Williamson, "Precision Orbit Computations for STARLETTE," Bulletin Geodesique, Vol. 52, No. 1, 1978.

Marsh, J.G., F.J. Lerch, and R.G. Williamson, "Geodynamics and Geodetic Parameter Estimation from STARLETTE Laser Tracking Data," Bulletin Geodesique, submitted, 1983.

Smith, D.E., D.C. Christodoulidis, P.J. Dunn, and M.H. Torrence, 1983, "Geodetic Parameters Estimated from LAGEOS Laser Data, SL-5," presented at the Fifth Annual NASA Geodynamics Program Conference and Crustal Dynamics Project Review, Washington, D.C.

Table 1.   Tracking Station Coordinate Comparison
8 Stations

	Translation Parameters			Rms of Fit		
	ΔX	ΔY	ΔZ	X	Y	Z
Starlette vs. UT8081 A-M	-9 cm.	-4 cm.	-43 cm.	19 cm.	25 cm.	19 cm.
Starlette vs. GSFC SL5	8	4	29	17	20	14
GSFC SL5 vs. UT8081 A-M	2	-8	-72	6	10	14

7063	Greenbelt, Maryland
7086	McDonald Observatory, Texas
7090	Yarragadee, Australia
7091	Haystack Massachusetts
7114	Owens Valley, California
7115	Goldstone, California
7907	Arequipa, Peru
7943	Orroral Valley, Australia

Table 2
Tidal Coefficients from 1980 Starlette Data Analyses
Relative to Wahr Earth Potential and Woolard Nutation

		Second Degree		Fourth Degree	
		Amplitude — C_{2m}^+ (cm)	Phase* — ϵ_{2m}^+ (deg)	Amplitude — C_{4m}^+ (cm)	Phase* — ϵ_{4m}^+ (deg)
M_m	065.455	1.99	42.7		
M_f	075.555	1.70	175.4		
	085.455	1.47	149.6		
Q_1	135.655	2.14	282.1	1.63	227.6
O_1	145.555	3.32	255.5	1.44	214.5
M_1	155.655	.37	284.6	.66	41.7
	162.556	1.14	35.7	1.03	33.0
P_1	163.555	.92	106.1	.74	174.9
K_1	165.555	3.28	32.2	3.40	3..4.4
J_1	175.455	1.34	75.9	1.00	292.5
OO_1	185.555	4.56	109.9	.19	252.9
$2N_2$	235.755	.05	159.9	.06	103.5
N_2	245.655	.76	232.9	.24	102.7
M_2	255.555	2.57	229.2	1.70	28.5
T_2	272.556	.27	13.4	.15	34.4
S_2	273.555	.78	302.4	.42	4.8
K_2	275.555	.83	293.4	.53	6.0

*Doodson (1921) convention used for Phase Definition

GEODYN PROGRAM SYSTEMS DEVELOPMENT

B.H. Putney

OBJECTIVES

The purpose of the Geodyn Orbit Determination and Parameter Estimation, the SOLVE and ERODYN Programs is to recover geodetic and geophysical parameters from satellite and other data in a state-of-the-art manner.

BACKGROUND

In 1971 the NONAME and GEOSTAR programs were combined to create the GEODYN program. The SOLVE program was created at the same time. A few years later the ERODYN, error analysis program was written. The philosophy of the development of the software system has been maintenace of computer efficient, well-structured software, with appropriate orbit, earth and numerical models, using precise satellite measurement modeling and efficient numerical models, and performing careful benchmark procedures. This care has paid off in the production of several GEM's (Goddard Earth Models), precision station locations, improved tidal, GM, and polar motion and earth rotation values and consistent baselines. Careful usage, analysis, and modeling using laser, altimeter and other satellite data from LAGEOS, SEASAT, STARLETTE, GEOS and BE-C satellites as well as many others has made these accomplishments possible.

RECENT ACCOMPLISHMENTS AND SIGNIFICANCE

As part of the Crustal Dynamics Project a significantly improved gravity field, pole positions, earth rotation, GM and baselines have been determined. The new solid earth and ocean tidal model and observation normal point technique are being used and evaluated.

In support of GRM, several mission successful simulations were performed using spherical harmonics, geoid heights and gravity anomalies. Numerical experiments with block interpolation, more accurate block integration, Fourier analysis of geopotential parameters and Householder transformation techniques for least squares estimation, have been studied. In preparing for the MERIT Campaign the DE 118 JPL sun, moon and planetary ephemerides are available in GEODYN 8210 version. This provides us with improved planetary positions and the Wahr nutation series. In addition, the ocean loading displacement is modeled in that same program.

Conversion of GEODYN and SOLVE to the Control Data Corporation Cyber 205 has been accomplished this year. Both programs are being optimized for that computer. GEODYN II is a rewrite of the GEODYN program. When completed it will execute on the Cyber 205 and on IBM compatible computers. Initial timings on the sequential GEODYN program show a 20 percent improvement over the IBM 360/95 computer. Solve is running

three times faster on the Cyber than on the IBM 3081. We are pleased
with the progress on the new computer. Modifications to make this a
flexible tool, by allowing multiple satellites (GPS) to be handled in a
single arc, processing a pass of observations simultaneously, allowing
variation in numerical stepsize for high and low degree and order spheri-
cal harmonic coefficients, making easier additions of new adjusted para-
meters, restructuring of observation and input files to allow for more
information and precision, are designed into the new program. The SOLVE
program is currently being vectorized but its basic structure appears to
be appropriate for the Cyber. However, modifications of Input /Output
techniques are required for optimal use of the Cyber and these modif-
ications are underway. Several new versions of GEODYN, SOLVE and ERODYN
were released this year. Versions of the program were requested and
delivered to England, Germany, Japan, the Netherlands, Australia, JPL
and Ohio State University.

FUTURE EMPHASIS

The conversion and optimization of the GEODYN and SOLVE programs on the
Cyber 205 will be completed. It is hoped to begin the conversion of the
ERODYN program as well. At this time it is very important to thoroughly
check out the GEODYN program models, i.e., albedo, relativity, plate
motion, tidal model, coordinate system. Reexamining of approximating
assumptions for correctness and for now required accuracies, of formu-
lation and implementation is now necessary. Additional changes for the
MERIT campaign such as changing the reference year from 1950 to 2000
need to be implemented. It is desirable to model and solve for a set of
spherical harmonic coefficients for the sea surface topography and to
incorporate a range difference data type to be used with laser data.

The software will be modified to meet the needs of the Topex mission as
they are defined and required. Additional GRM modifications will be
made as defined and funded.

Every effort will be made to continue to mold the software in a timely
manner to support the needs of the scientific community determining
earth models.

CHAPTER 4

SEA SURFACE TOPOGRAPHY

OVERVIEW

The overall goal of this area of research is to apply remote sensing data to studies of dynamic ocean and earth processes. The primary data types are satellite altimetry data, orbit perturbation data and gravity data. These data are analyzed in conjunction with surface observations, for example, ocean temperature and density measurements.

Global sets of satellite altimeter data have been collected during two satellite missions: The GEOS-3 mission (1975 to 1978) and the Seasat mission (1978).

Research programs are underway in the following areas to analyze and interpret the altimeter data: (1) the computation of highly precise regional mean sea surfaces which can be used for studying the oceanic mesoscale variability and to perform detailed analyses of the earth's crustal structure; (2) the study of lithospheric flexure seaward of subduction zones to obtain a better mechanical model of oceanic lithosphere; (3) to develop and test an interpolation technique which allows accurate extrapolation of tidal height fields in the ocean basins by making use of selected satellite altimetry and conventional tidal gauge measurements.

Contributors to this chapter include J.G. Marsh, D.C. McAdoo and B.V. Sanchez.

REGIONAL MEAN SEA SURFACES BASED UPON
GEOS-3 AND SEASAT ALTIMETER DATA

James G. Marsh

OBJECTIVE

The objective of this work has been the computation of highly precise regional mean sea surfaces based upon crossing arc adjustments of the combined GEOS-3 and SEASAT altimeter data sets. These surfaces have provided a basis for studying the oceanic mesoscale variability and for detailed analyses of the earth's crustal structure.

BACKGROUND

The GEOS-3 (1975-1978) and SEASAT (1978) altimeter experiments provided very dense coverage in the N.W. Atlantic, the Gulf of Mexico and the Bering Sea. The number of available passes ranged from 558 in the Gulf of Mexico to 1284 in the N.W. Atlantic. The GEOS-3 data were smoothed over a frame to provide data at a rate of 1 point/second. Only intensive mode data were used, and gross data outliers were eliminated in the smoothing process. The SEASAT data used were the JPL distributed Geophysical Data Records (GDR) also at the rate of 1 point/second.

The precision of the GEOS-3 altimeter measurements is about 25 cm and that of the SEASAT altimeter measurements is about 3-10 cm. However, in order to achieve precision of this order in the computed sea surfaces, other sources of error, chiefly the radial orbit error of the spacecraft, which may be on the order of a few meters, must be removed. This is done in the crossing arcs least squares adjustment process.

The satellite radial orbit error is primarily due to the errors in the gravity field model. Several studies have shown that most of the radial orbit error has frequencies close to once per rev. Thus, over distances of thousands of kilometers, the radial orbit error can be well represented by a linear function of time, and can therefore be removed by the least squares adjustment process if the parameters of a linear trend are solved for. Any other long wavelength sources of error, for example errors caused by mis-modeling of the ocean tides, will also be removed in the adjustment process. The adjustment process has been extensively described elsewhere (Marsh, et al., 1980).

The large amount of data in these areas coupled with the increased constraints provided by the combination of data from two orbital inclinations has provided the basis for a detailed precision adjustment of the data. The precision of these surfaces is estimated to be on the order of 15 cm with a horizontal resolution of 25 km.

RECENT ACCOMPLISHMENTS

Figure 1 shows the sea surface contour map of the Northwest Atlantic derived from the SEASAT and GEOS-3 altimeter data. Several features of the ocean floor topography are clearly reflected in the sea surface topography. Bermuda is clearly visible, and the long minimum in the center corresponds to the Hatteras abyssal plain. To the west, the Blake Bahama Outer Ridge and the Blake Escarpment are visible.

Figure 2 shows the sea surface computed in the Bering Sea using SEASAT and GEOS-3 altimeter data. The surface clearly shows where the shallow ocean over the continental shelf (in the northeastern portion of the map) is divided from the deeper ocean over the Bering Abyssal Plain in the southwest of the sea. Also clearly visible are the ocean bottom ridge at about 170° longitude, and the feature known as Bowers Bank (the circular feature below latitude 55° and between 175° and 180° longitude).

The details of this work are presented in a report by Marsh et al. (1983).

SIGNIFICANCE

Except for mean dynamic topography, the altimetric surfaces presented in this paper are equivalent to the geoid. It should thus be possible to use these surfaces to remove the geoid signal from synoptic altimeter data in order to detect transient mesoscale features. Of course, one must proceed with caution for a quasi-permanent current such as the Gulf Stream, since both synoptic and time-averaged altimeter data contain a Gulf Stream signal. In contrast, gravimetric reference surfaces can be used to detect permanent circulation features. This is demonstrated in Figure 3 where we have differenced the Atlantic 3-year mean surface with the detailed 5' geoid model of Marsh and Chang (1978). The Gulf Stream can be clearly seen as a 1-m step running eastward from Cape Hatteras. South of the Gulf Stream is a broad area in which the two reference surfaces show agreement to within approximately 20 cm. Even though this area is populated by cold rings with sea height signatures of 50-100 cm, the transient nature of these features causes them to be considerably smoothed in the 3-year mean surface. Large differences occur in the northeast due to the New England seamounts and in the southwest due to the Bahamas. These differences are attributable principally to errors in the detailed geoid model.

FUTURE EMPHASIS

Future work in this area will be oriented toward further definition of mesoscale variability from crossover difference statistics, the detection and monitoring of individual cold and warm core rings using the mean sea surfaces as a reference and toward the orientation of these

highly precise mean sea surfaces into an absolute center-of-mass coordinate reference system.

ACKNOWLEDGEMENTS

REFERENCES

Marsh, J.G., R.E. Cheney, J. McCarthy, T.V. Martin, "Regional Mean Sea Surfaces Based Upon GEOS-3 and SEASAT Altiemter Data," submitted to Marine Geodesy, 1983.

Marsh, J.G., T.V. Martin, J.J. McCarthy, "Mean Sea Surface Computation Using GEOS-3 Altimeter Data," J. Marine Geodesy, Vol. 3, No. 1-4, 359-379, 1980.

Marsh, J.G., E.S. Chang, "5' Detailed Gravimetric Geoid in the North Western Atlantic Ocean," J. Marine Geodesy, Vol. 1, No. 3, 253-261, June 1978.
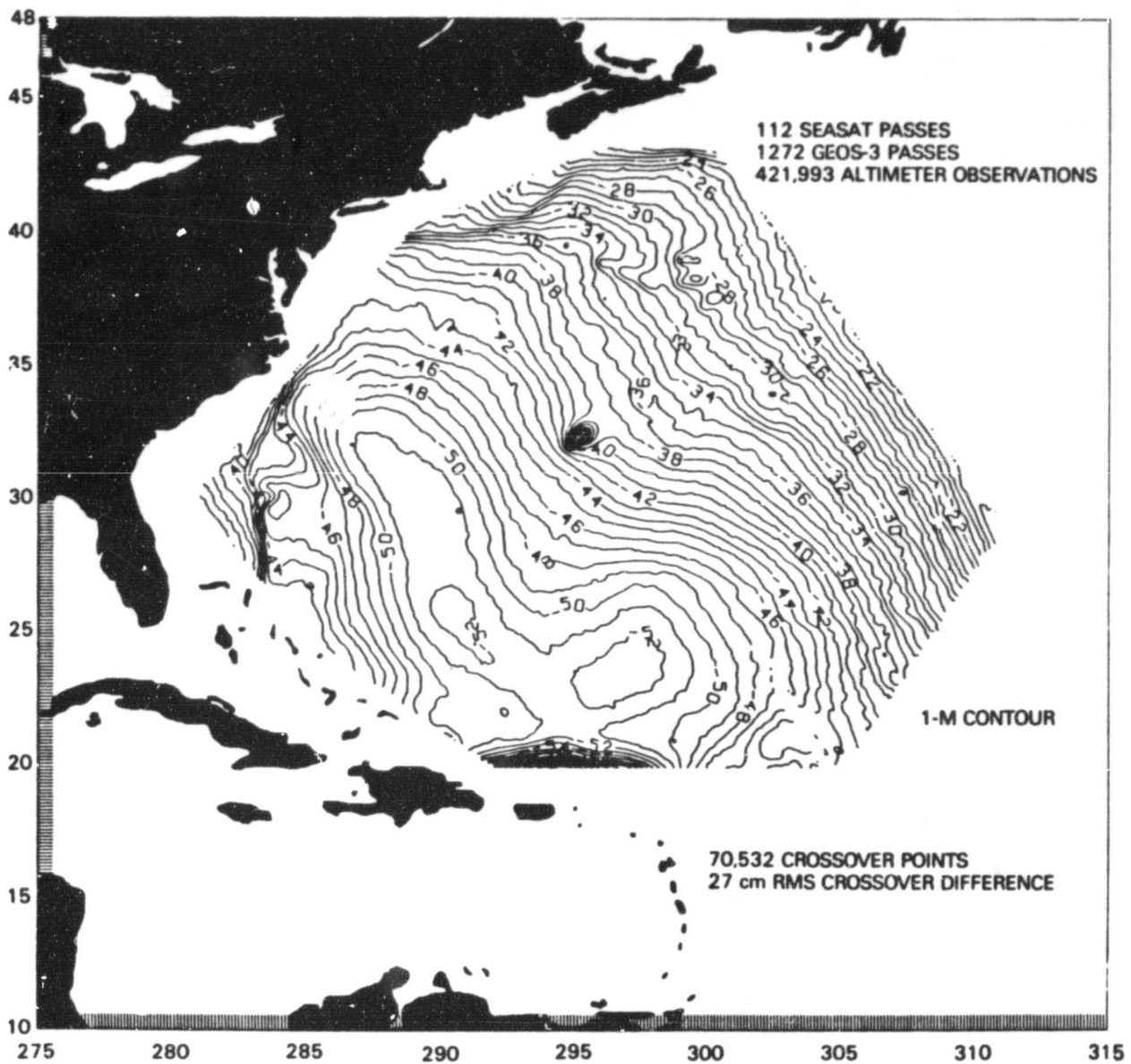
Figure 1. Mean Sea Surface Based Upon SEASAT and GEOS-3 Altimeter Data, 1975 – 1978

1-M CONTOUR

16,873 CROSSOVER POINTS
23 cm RMS CROSSOVER DIFFERENCE

185 SEASAT PASSES
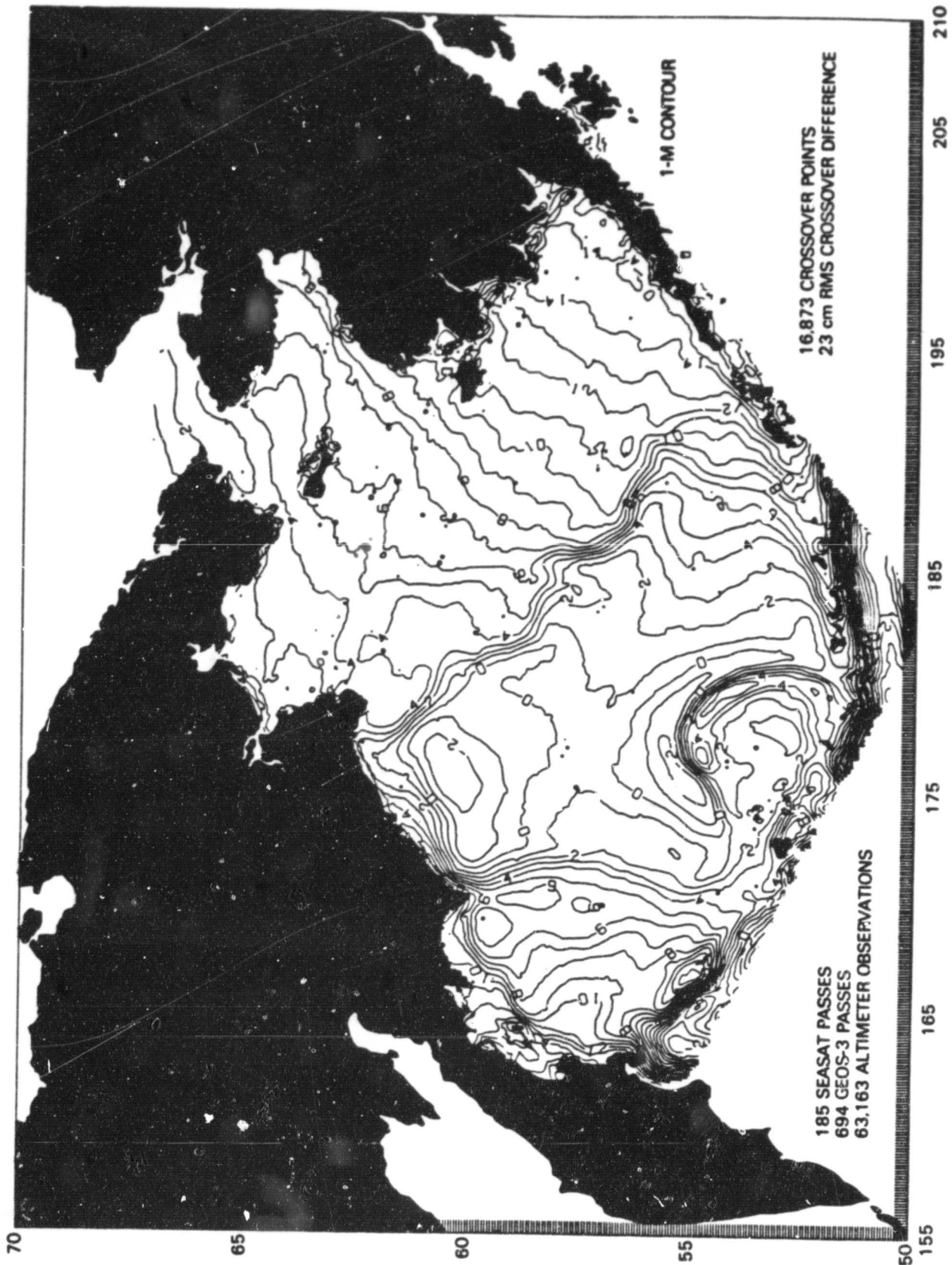694 GEOS-3 PASSES
63,163 ALTIMETER OBSERVATIONS

Figure 2. Mean Sea Surface Based Upon SEASAT and GEOS-3 Altimeter Data, 1975 – 1978
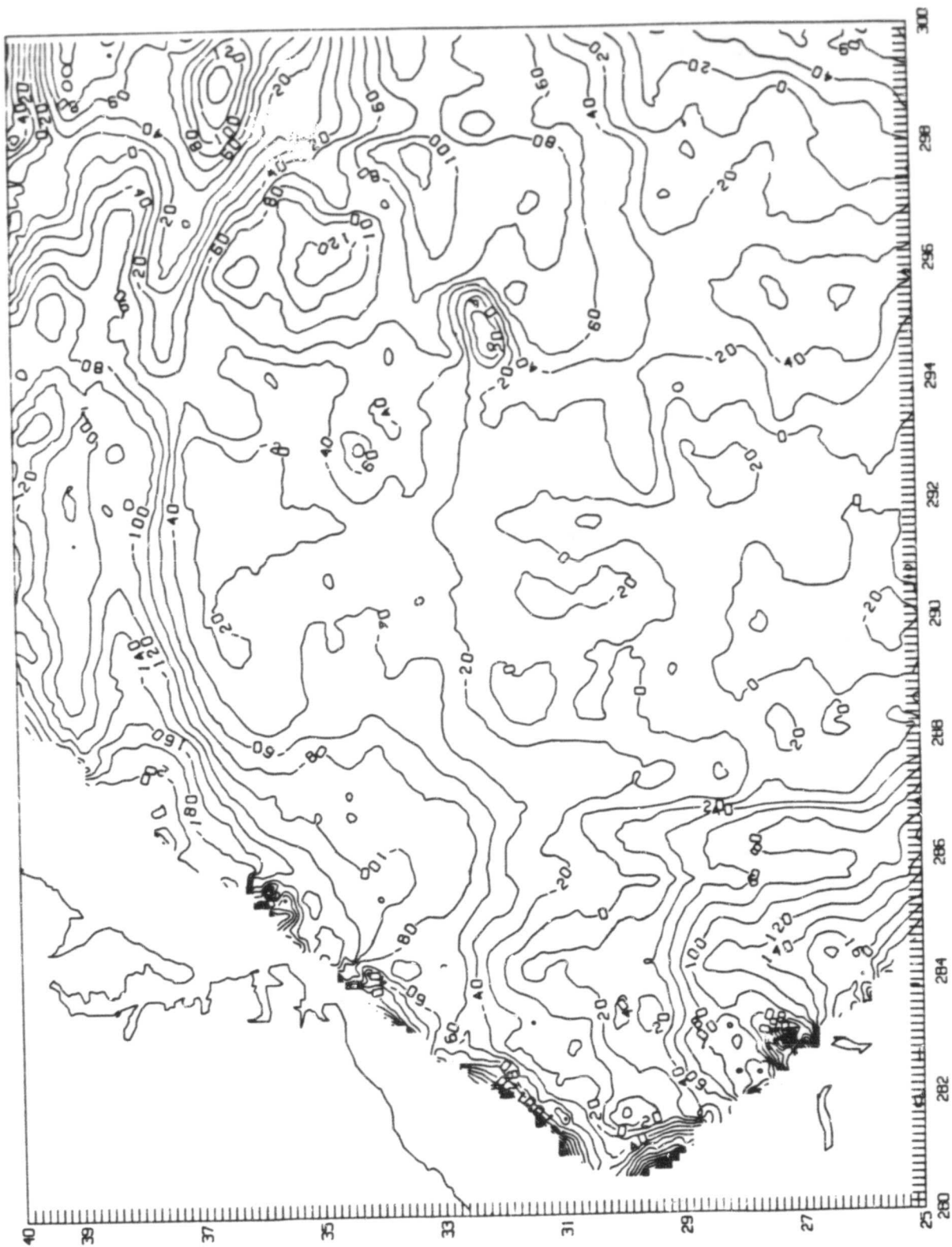
Figure 3. GEOS-3 – SEASAT Mean Sea Surface Minus 5' Gravimetric Geoid

SEASAT OBSERVATIONS OF LITHOSPHERIC FLEXURE

David C. McAdoo

OBJECTIVE

The individual lithospheric plates move about the Earth's surface as units which remain relatively rigid on geological time scales. It is of considerable importance for geophysicists to know as much as possible about the actual strength of the lithosphere including the dependence of strength on age. This study of lithospheric flexure seaward of subduction zones seeks a better mechanical model of oceanic lithosphere. The study is based primarily on SEASAT altimeter observations. An improved understanding of forces acting at subduction zones is also sought.

BACKGROUND

The Outer Rise seaward of deep ocean trenches is generally attributed to flexure of the oceanic lithosphere prior to subduction. Various models have been proposed to describe this flexure. They all include a mechanically strong lithosphere--loaded from the arcward side of the trench axis--overlying a fluid-like asthenosphere. Simplest among them is the uniform elastic plate model which was first applied to Outer Rises by Hanks (1971), and subsequently by a number of others.

More complex models which include a variable rheology with depth have also been developed. These complex models produce more realistic estimates of stress but, aside from this, the elastic model hs been shown (Bodine, et al., 1981) to be adequate for describing flexure of the oceanic lithosphere.

Quite naturally these lithospheric models have been tested almost exclusively on bathymetric profiles. However, the Outer Rise also has a clear gravitational expression. Watts and Talwani (1974) showed that gravity anomalies over the Outer Rise tend to mimic--in form--the bathymetry. It should, therefore, not be surprising that a geoidal counterpart of the Outer Rise exists and is evident in the SEASAT altimeter observations of the marine geoid. This study extends the popular elastic plate model to include a predicted geoid signal and then tests this model directly on SEASAT observations of the marine geoid. One anticipated result from this study is a clearer understanding of the dependence of the lithosphere's effective elastic thickness (EET) on age.

Using bathymetric data Bodine, et al. (1981) concluded that--in the absence of horizontal loading--the effective thickness, T_e, increases with age according to $T_e = C \cdot age^{1/2}$. Their results suggest the thickness (EET) is, in several regions, significantly less than the value predicted by this thickness-age relation; they attributed this discrepancy to horizontal compressive loads acting across these trenches.

RECENT ACCOMPLISHMENTS

A paper, McAdoo and Martin (1983) has been completed. In this paper, segments of 102 SEASAT altimeter passes over six trench/Outer Rise complexes have been analyzed. For each trench the number of passes analyzed is a follows: Middle America, 14; Philippine, 12; Aleutian, 23; Mariana, 12; Izu-Bonin, 10; Kuril, 30. Thes sea surface height profiles obtained from these passes will be treated as geoid height profiles.

After long-wavelength component of the geoid is removed, these observed geoid height profiles--i.e., the SEASAT passes are then compared to geoid profiles predicted by the elastic model. As an example, one pass over Mariana Trench is shown in Figure 1.

Using the method of least squares, model parameters are adjusted and estimated for each SEASAT pass. For each pass an estimate of flexural wavelength is obtained. A mean flexural wavelength is then obtained from the ensemble of SEASAT passes over each trench. From this mean flexural wavelength, an effective elastic thickness can be derived. The six crosses in Figure 2 represent the effective elastic thickness versus age of the subducting oceanic lithosphere for each of the six trenches studied. The solid curves represent the thickness age law predicted by Bodine, et al. (1981) from thermal and experimental constraints. The agreement between this law and effective elastic thicknesses derived from SEASAT data is good; in fact it is better than the agreement obtained in previous studies (see Bodine, et al., 1981) which use bathymetric data--not SEASAT data--to estimate thicknesses (EET). The lack of agreement obtained in these previous studies was generally attributed to unmodeled horizontal compressive forces acting across certain trenches. This work is described in McAdoo and Martin (1983); see also McAdoo, et al. (1982).

SIGNIFICANCE

SEASAT altimeter data provide important new information on the deformation of the lithosphere seaward of deep ocean trenches. These data, when compared with a mechanical model, produce estimates of the effective elastic thickness of the lithosphere which are more consistent from profile to profile in a given region than those derived from bathymetry. For the six trenches which we studied, the effective elastic thickness derived from altimetry increases with the square root of lithospheric age as predicted by Bodine, et al. (1981). Significant horizontal compression across these trenches is not indicated.

FUTURE EMPHASIS

The potential utility of SEASAT and other satellite altimeter data for studying dynamics of the lithosphere and sub-lithosphere is only beginning to be exploited. This particular study of outer rises will be extended to include all the deep ocean trenches. Mechanical structure of the lithosphere can be similarly studied in mid-plate regions. These types of studies which refine our models of the lithosphere are necessary if we are to isolate, with confidence, dynamical effects arising beneath the lithosphere such as smallscale convection in the mantle.

REFERENCES

Bodine, J.H., M.S. Steckler and A.B. Watts, "Observations of Flexure and of the Oceanic Lithosphere," J. Geophys. Res., 86, 3695-3707, 1981.

Hanks, T.C., The Kuril Trench-Hokkaido Rise System: Large Shallow Earthquakes and Simple Models of Deformation," Geophys. J.R. abstr. Soc. 23, 173-189, 1971.

McAdoo, D.C. and C.F. Martin, "SEASAT Observations of Lithospheric Flexure Seaward of Trenches," submitted for publication, 1983.

McAdoo, D.C., R. Kolenkiewicz, C.F. Martin, and S. Poulose, "The Correlation of Bathymetry with Geoid Heights Near Trenches of the North Pacific," EOS 63, No. 5, 907, 1982.

Watts, A.B. and M. Talwani, "Gravity Anomalies Seaward of Deep-Sea Trenches and Their Tectonic Implications," Geophys. J.R. Astron. Soc., 38, 119-141, 1974.
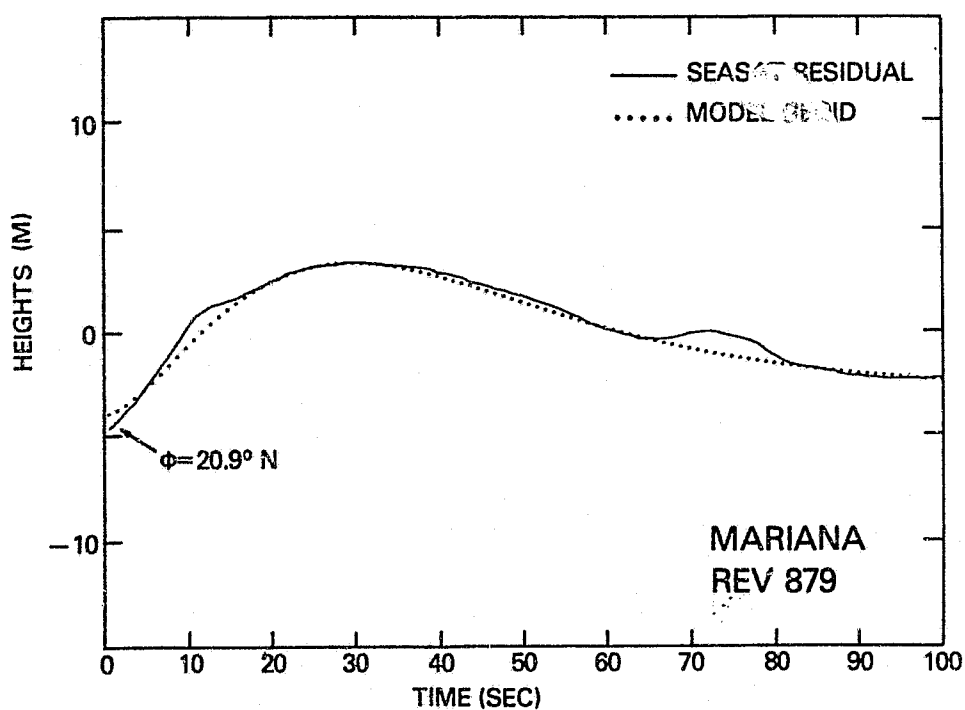
Figure 1. A residual SEASAT height profile compared with best fitting
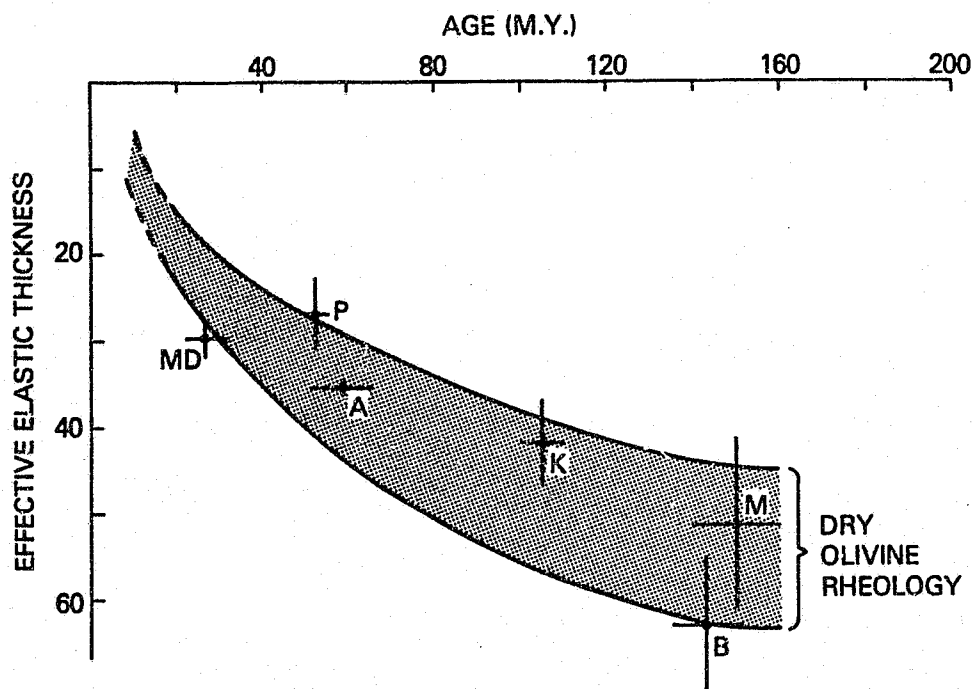result from the elastic plate model.

Figure 2. Effective elastic thickness (EET) derived from SEASAT data (crosses)
over six trenches (Middle America (MD), Aleutian (A), Philippine (P), Kuril (K),
Mariana (M) and Bonin (B). EET's are plotted versus age. Bodine, et al.'s (1981)
age-thickness relation is shown as curves.

AN OBJECTIVE ANALYSIS TECHNIQUE FOR EXTRAPOLATING TIDAL FIELDS

Braulio V. Sanchez

OBJECTIVES

1. To develop and test an interpolation technique which allows accurate extrapolation of tidal height fields in the ocean basins by making use of selected satellite altimetry measurements and/or conventional gauge measurements.

2. To develop a dynamical model of the ocean tides.

3. To test the technique initially for the M2 tide in a small water body such as Lake Superior by theoretically computing the tide and to compare the results with available tidal data.

4. To test the interpolation technique in Lake Superior in order to ascertain its capabilities for further application in the ocean basins.

BACKGROUND

The theoretical foundation of the method used in the calculations is based on Proudman's theory (1918) as reformulated by D.B. Rao (1966). The theory provides a formulation for calculation of gravitational normal modes and rotational normal modes of irregularly shaped basins with realistic bathymetry. The method has been extended to compute the forced solution (M2 tide) in Lake Superior to serve as a test to evaluate the objective analysis procedure. The objective analysis uses orthogonal functions that formed the basis to represent the water level fluctuation field in the free and forced calculations. The available tidal amplitudes and phases are expressed as a linear combination of these functions. Since data points are usually available only at irregularly spaced points, instead of using the orthogonality property of these functions to determine the expansion coefficients, they are determined through a least squares procedure. In the computation of the forced solution we include the effects of the yielding of the solid earth to tide generating forces.

RECENT ACCOMPLISHMENTS

a.   The M2 tide solution

Figure 1 shows the amplitude and phase fields for the M2 tide in Lake Superior. The maximum amplitudes, which are close to 20 mm, occur at the western end of the basin. The phase values obtained by Mortimer and Fee (1976) from analysis of records of water levels are given in parentheses. The amplitudes values were provided by C.H. Mortimer (personal communication) from the original calculations on the water level data. Also given are the phase and amplitude values obtained in this investigation. The latter are the values obtained at the grid points closest to the stations in Mortimer and Fee's analysis. The contours of equal amplitude and phase are given by the solid and dotted lines respectively. The solution was obtained by including the first 80 eigenfunctions from the velocity potential and stream function solutions. The forced solution then contains 80 coefficients, the magnitudes of the coefficients indicate the relative importance of the different characteristic functions in accounting for the variance of the total solution. Most of the power is contained in the first coefficient. The results for the first 12 coefficients are given in Table 1. An examination of Figure 1 shows excellent agreement between the theoretically computed tidal response and observed amplitudes and phases. The theoretical simulation also serves as a guide in choosing the most energetic modes to be used in the objective analysis at any order of truncation of the representation.

b.   Interpolation Technique Evaluation

The data locations selected for the analysis are the ten water level stations analyzed by Mortimer and Fee. The tidal amplitudes and phases at these ten locations were extracted from the theoretical simulation. An objective extrapolation of the tidal field is carried out with these 10 data points using 2,4,5,8, and 10 most energetic modes listed in Table 1. A comparison of the objectively analyzed amplitudes and phases with the "true" values at all grid points is shown in Table 2. The table lists the percentage of total grid points where the analyzed and true values of amplitude and phase agree with each other within the limits indicated and for the number modes chosen in the objective analysis. There are a total of 227 points within the basin. Also given in the table are the rms errors of the amplitude over the entire basin and only at the data points, as well as the ratio of the potential energy of the analyzed and true fields. It is seen from Table 2 that the method of analysis yields a tidal height field that is within 3% of the "true" potential energy with just 2 basis functions. As the number of functions are increased to 5, the energy difference is within 5%. For the ten selected data points, the fit with 5 functions appears to be the best. The tidal pattern using 5 coefficients is shown in

Fig. 2. Comparison with Fig. 1, the theoretical solution obtained with 80 coefficients, shows excellent agreement between the two fields. As the expansion coefficients are increased to 10, which represents an exact determination of the values of the coefficients, the overall fit at the tidal pattern deteriorates. Obviously, the maximum number of coefficients that would result in a best fit over the entire basin depends on the number and distribution (in space) of the available data points. The combination of theoretical simulation and objective analysis also helps in choosing locations for additional observations that would contribute most to the resolution of the tidal field in an ocean basin.

SIGNIFICANCE AND FUTURE EMPHASIS

A method has been described to objectively analyze available tidal amplitudes and phases to map the tidal constituent over an entire basin. The method consists of constructing a set of orthogonal functions that are determined by the geometry and topography of the basin. These functions are linearly combined and the expansion coefficients are determined from available data in such a way as to minimize the mean-squared error by a simple matrix inversion. Since the orthogonal functions used are characteristic of the given basin, they would reflect the basin properties in a sense and hence would be capable of giving the best fit for the overall tidal field in the basin. Using Lake Superior as a test case, a theoretical simulation was done for the M2 tidal amplitudes and phases in the basin. This theoretically simulated field has been used as a "true" solution to evaluate the recovery of the total tidal field in the basin from application of the analysis procedure to data taken at selected points. The agreement between the analyzed and the "true" fields is found to be excellent. The theoretically calculated M2 tidal heights and phases also agree very well with those obtained from analysis of water level data by Mortimer and Fee. The method is now being extended to ocean basins. The results of the Lake Superior investigation have been submitted for publication by Sanchez, Rao and Wolfson.

REFERENCES

Mortimer, C.H., and E.J. Fee, 1976. Free surface oscillations and tides of Lakes Michigan and Superior. Phil. Trans. R. Soc. of Lon. Ser. A, 281, 1-61.

Proudman, J., 1918. On the dynamical equations of the tides. Proc. of the Lon. Math. Soc. 18, 1-68.

Rao, D.B., 1966. Free gravitational oscillations in rotating rectangular basins. J. Fluid Mechanics, 25, 523-555.

Sanchez, B.V., D.B. Rao and P.G. Wolfson, 1983. An objective analysis technique for extrapolating tidal fields in a closed basin. Submitted to Marine Geodesy.
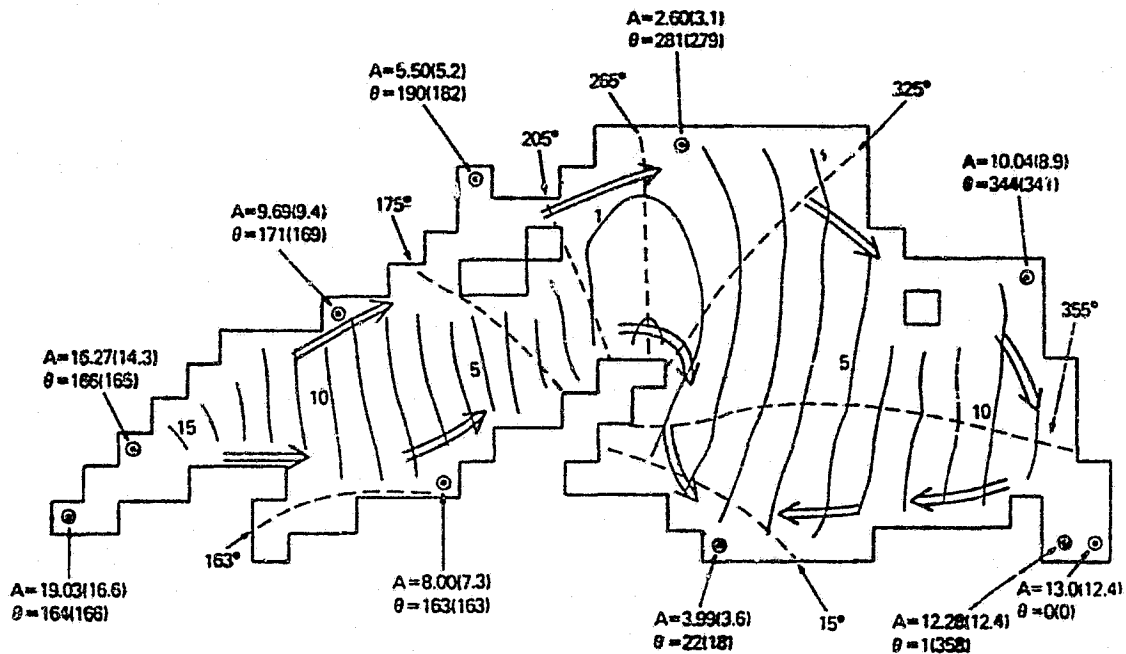
Figure 1. Theoretical solution for the M2 tide in Lake Superior (80 coefficients). Contours of equal amplitude (mm) and equal phase (degrees) are given by the solid and dotted lines respectively. The values from Mortimer and Fee's data reduction are given in parentheses.
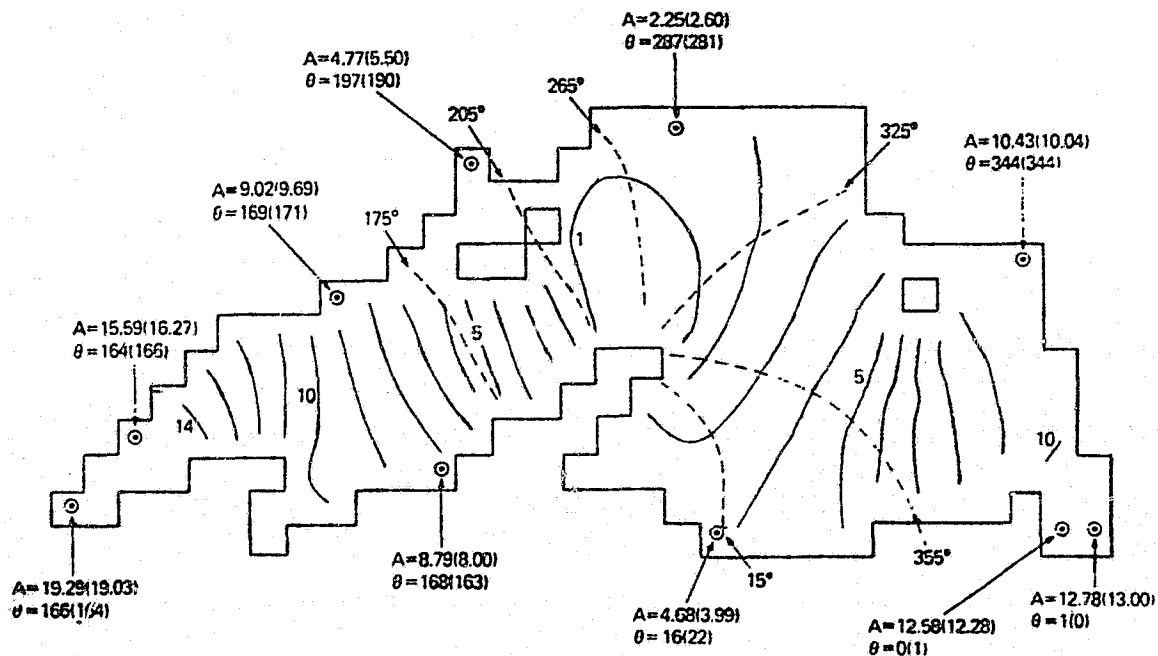

Figure 2. Solution for the M2 tide based on objective analysis using 5 coefficients corresponding to the five most powerful modes. Contours of equal amplitude (mm) and equal phase (degrees) are given by the solid and dotted lines respectively. The values from the theoretical solution (80 coefficients) used as data are given in parentheses.

4-15

Table 1
Power Spectrum for the M2 Tide

Mode	Power (%)	Period (hours)
1	94.62	7.83
2	1.74	4.42
3	0.79	3.75
4	0.95	3.16
5	0.96	2.96
6	0.05	2.57
7	0.03	2.40
8	0.35	2.32
9	0.05	2.20
10	0.15	1.91
11	0.09	1.82
12	0.10	1.65

Table 2
Comparison between Objectively Analyzed and Theoretical Fields

Coefficients	Amplitude			Phase			$\frac{P_A}{P_T}$	RMS Error (mm)	RMS (Data PTS)
	<5%	<10%	<20%	<5°	<10°	<20°			
2	23.8%	43.6%	64.8%	46.7%	68.7%	83.3%	1.0295	1.2006	1.18
4	26.9%	51.5%	76.7%	64.8%	85.0%	96.0%	1.0749	1.2059	1.11
5	42.3%	67.8%	87.2%	61.2%	86.8%	93.4%	0.9521	0.8838	0.54
8	25.1%	41.0%	55.5%	59.9%	87.2%	96.5%	1.0872	3.1046	0.31
10	14.1%	22.9%	36.1%	24.7%	39.6%	58.6%	3.9678	12.185	0

CHAPTER 5

ADVANCED STUDIES

OVERVIEW

The advanced studies activities considered by the Geodynamics Branch provide a sound basis for the planning, design, and development of sensor and space mission concepts. Studies have been conducted based on extensive current research experience and simulations. The utility of the data expected from these systems is evaluated in terms of predicted contributions to program objectives and user applications.

Currently, the horizontal resolution of satellite-determined gravity field models is of the order of 500 km. This level of resolution must be increased to meet requirements for solid-earth and ocean studies. A gravity field mapping mission, namely The Geopotential Research Mission (GRM) is planned for the latter part of this decade to map the earth's gravity and magnetic fields. GRM consists of two spacecraft in the same circular/polar orbit with a separation distance varying from 1° to 6° and a nominal orbit altitude of 160 km. From Doppler measurements made between the two satellites with a precision of 1 micrometer per second it is the goal for GRM to map the earth's gravity field to an accuracy of 1 milligal and the geoid to an accuracy of 5 cm with a horizontal resolution of 100 km.

Two GRM simulation studies are presented in this chapter. The studies describe (1) the gravity field signal characteristics of the GRM Doppler sensor and (2) the computer simulations which were performed to assess the capability of GRM to map the gravity field of the earth for geophysical and oceanographic applictions. Another new sensor is discussed in this chapter which provides a method of precise positioning of a large number of points on the earth's surface in a short period of time. That is, a measure of the relative location of geodetic markers from an aircraft. Such a system, "The Airborne Laser Ranging System (ALRS) is a potential sensor for performing rapid (few days) mapping of local crustal motion in seimsically active areas.

In a somewhat different vein, an analysis of soil moisture based on measurements of the earth surface temperature has also been under study. Although this study is most applicable to problems in non-renewable resources, the coupling of soil moisture and atmospheric conditions to geodynamic processes is also under investigation.

Contributors to this section are: T.L. Felsentreger, F.J. Lerch, W.D. Kahn, and J.E. Welker.

GRAVITY FIELD SIGNAL ANALYSIS STUDY FOR A GEOPOTENTIAL RESEARCH MISSION (GRM)

Theodore L. Felsentreger

OBJECTIVE

The objective of this report is to discuss the gravity field signal characteristics of the SST Doppler sensor to be flown on GRM.

BACKGROUND AND RECENT ACCOMPLISHMENTS

The Geopotential Research Mission (GRM), formerly known as GRAVSAT/MAGSAT, has been proposed for the mapping of the Earth's gravity field. It is a candidate for a NASA new start in the near future. GRM is to be composed of a pair of surface-force compensated satellites in identical polar orbits, spaced approximately 3° apart at a nominal altitude of 160 km with a system precision of 1 μm/sec.

The perturbation by the gravity field induced on the intersatellite Doppler signal is given by the following relationship:

$$\delta(r\dot{\psi}) = \int_{t_0+\delta t}^{t_1+\delta t} \frac{1}{r}\frac{\partial T}{\partial \psi}\,dt - \int_{t_0}^{t_1}\frac{1}{r}\frac{\partial T}{\partial \psi}\,dt \tag{1}$$

where

$T \equiv$ disturbing potential
$a \equiv$ Earth's mean equatorial radius
$h \equiv$ satellite orbit altitude
$r \equiv a+h$
$\psi \equiv$ true anomaly
$\delta t \equiv$ time separation of two satellites in identical orbits.

The form of the disturbing potential most useful for formulating (1) is given by the formula

$$T(r,\psi) = \frac{a}{4\pi}\iint_\sigma \Delta\bar{g}\ S(r,\psi)\,d\sigma \tag{2}$$

where

$$S(r,\psi) = \frac{2a}{\ell} + \frac{a}{r} - \frac{3a\ell}{r^2} - \frac{a^2}{r^2}\cos\psi\left[5 + 3\ln\left(\frac{r-a\cos\psi+\ell}{2r}\right)\right]$$

$$\ell = [r^2 + a^2 - 2ra\cos\psi]^{\frac{1}{2}}$$

$\Delta\bar{g} \equiv$ mean gravity anomaly
$d\sigma \equiv$ element of area.

Using (1) and (2), velocity profiles resulting from the perturbation produced by a (1° x1°) 1 mgal gravity anomaly as sensed by the two satellites are shown in Figure 1.--results are shown for 160 km and 200 km satellite altitudes. The amplitude of the gravity signal drops off by a factor of 1.5 when the altitude increases from 160 km to 200 km. By extrapolation the amplitude is further decreased by about a factor of 3 when the orbital altitude is increased to 250 km. Thus, the amplitude of the measurement drops off as the altitude increases, to the point where the measurement amplitude is insignificant at the 1 mgal level for altitudes above 200 km. By way of contrast, Figure 2 shows the SST signal generated by GRM for one full orbit, under the influence of a full (36,36) spherical harmonic gravity field (GEM 10B).

The ability to resolve the signal from a (1° x 1°) 1 mgal gravity anomaly for two spacecraft whose orbits are displaced from the anomaly by 1° and 5° is shown in Figure 3. For a 1° displacement, better than 60% of the gravity signal is sensed; however, for a 5° displacement, only 10% of the gravity signal is sensed. This implies that the gravity anomaly signals from adjacent blocks drop off drastically with increased distance from the satellite ground track. Nevertheless, it is significant that remote gravity anomalies do contribute appreciably to the overall gravity signal.

FUTURE EMPHASIS

Studies of this type will be continued, along with rapid error analysis and full-scale simulation studies.

REFERENCES

Kahn, W.D. and T.L. Felsentreger, "Signal Analysis and Error Analysis Studies for a Geopotential Research Mission (GRM)," NASA TM 83970, July 1982.

Jekeli, C., and R.H. Rapp, "Accuracy of the Determination of Mean Anomalies and Mean Geoid Undulations from a Satellite Gravity Field Mapping Mission," The Ohio State University Department of Geodetic Science Report 307, August 1980.

Heiskanen, W. and H. Moritz, 1967, "Physical Geodesy," W.H. Freeman.

Lambeck, K., "Methods and Geophysical Applications of Satellite Geodesy," Reports on Progress in Physics 1972, Vol. 42, 547-628.

Kaula, W.M., "The Appropriate Representation of the Gravity Field for Satellite Geodesy," Proceedings of the IV Symposium of Mathematical Geodesy; Trieste, 1969.

Lerch, F.J., et al., "Gravity Model Improvement Using GEOS-3 (GEM-9 and GEM-10)," GSFC X-921-77-246, 1978.
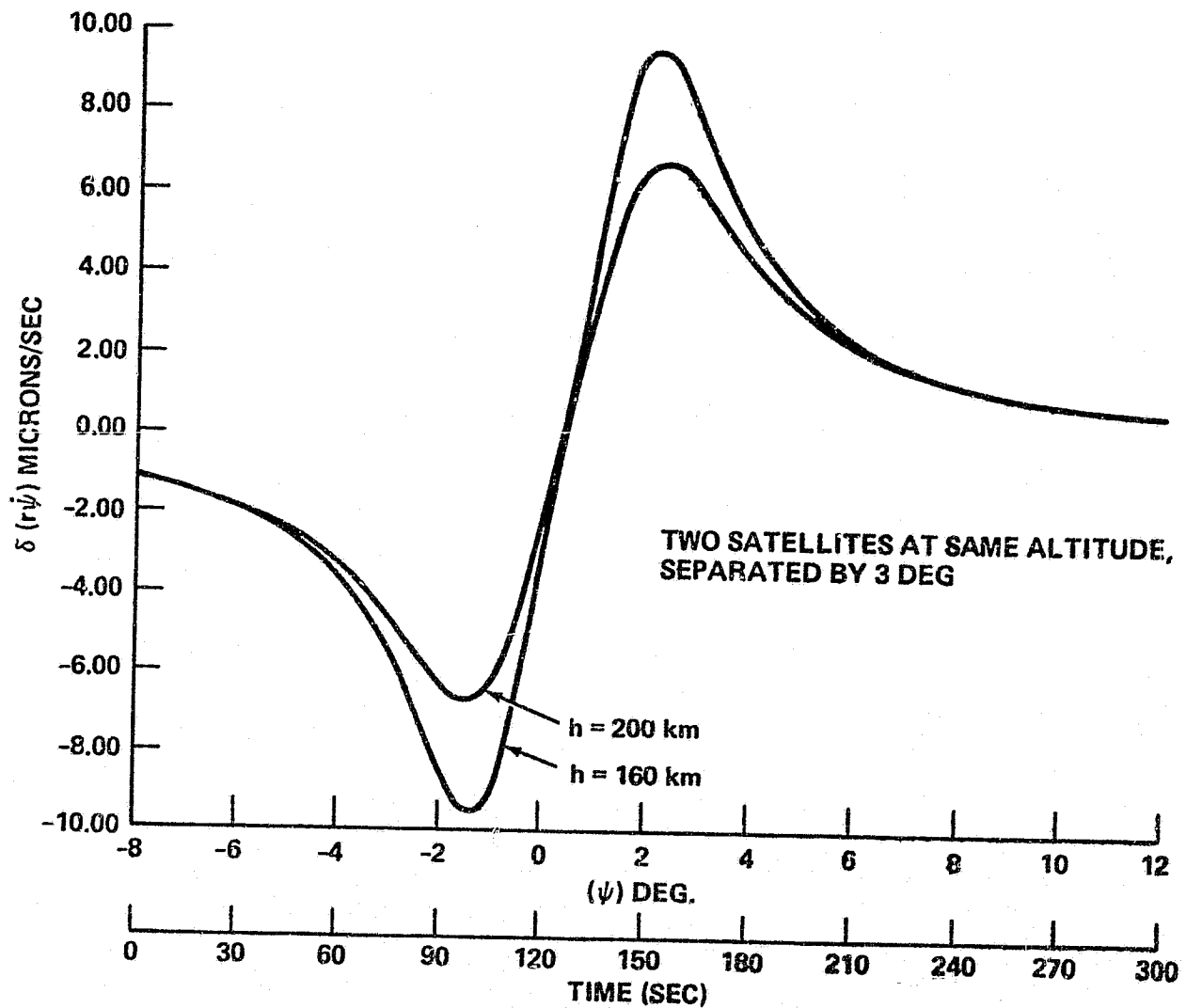
RANGE RATE SIGNAL PRODUCED AT TWO ORBIT ALTITUDES
BY A SINGLE 1 DEG. X 1 DEG., 1 MGAL GRAVITY ANOMALY
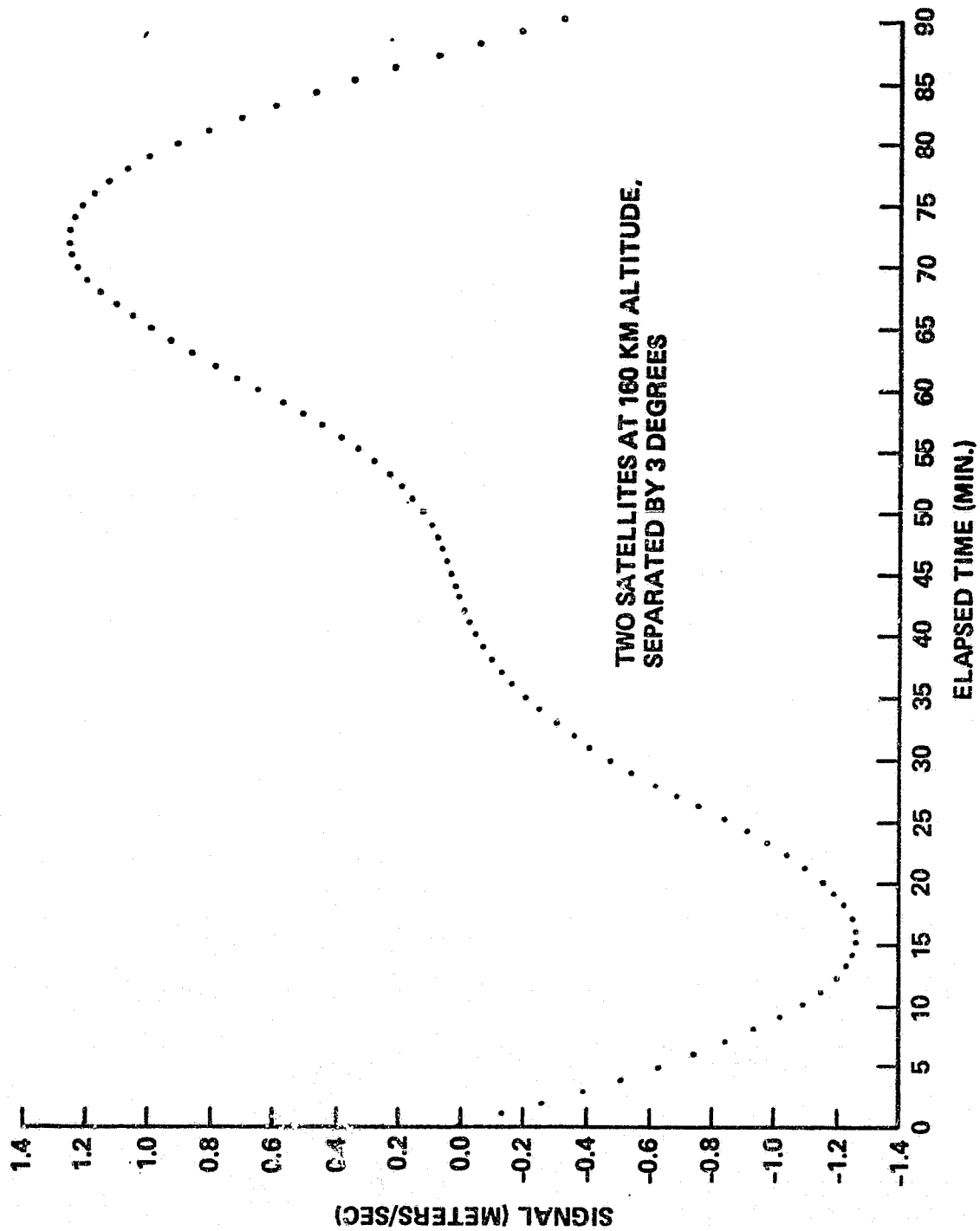
Figure 1. GRM Anomaly Sensing at Two Altitudes.

TWO SATELLITES AT 160 KM ALTITUDE,
SEPARATED BY 3 DEGREES

ELAPSED TIME (MIN.)

SIGNAL (METERS/SEC)

Figure 2. GRM Full (36, 36) Gravity Field Sensing

TWO SATELLITES AT 160 KM ALTITUDE,
SEPARATED BY 3 DEGREES (SIMULATED)

$\delta(r\dot\phi)$ MICRONS/SEC

(DEG)

TIME (SEC)

B) RANGE RATE SIGNAL WHEN ORBIT IS
DISPLACED 5 DEGREES FROM A SINGLE
1 DEG x 1 DEG, 1 MGAL GRAVITY
ANOMALY

TWO SATELLITES AT 160 KM ALTITUDE,
SEPARATED BY 3 DEGREES (SIMULATED)

$\delta(r\dot\phi)$ MICRONS/SEC

(DEG)

TIME (SEC)

A) RANGE RATE SIGNAL WHEN ORBIT IS
DISPLACED 1 DEGREE FROM A SINGLE
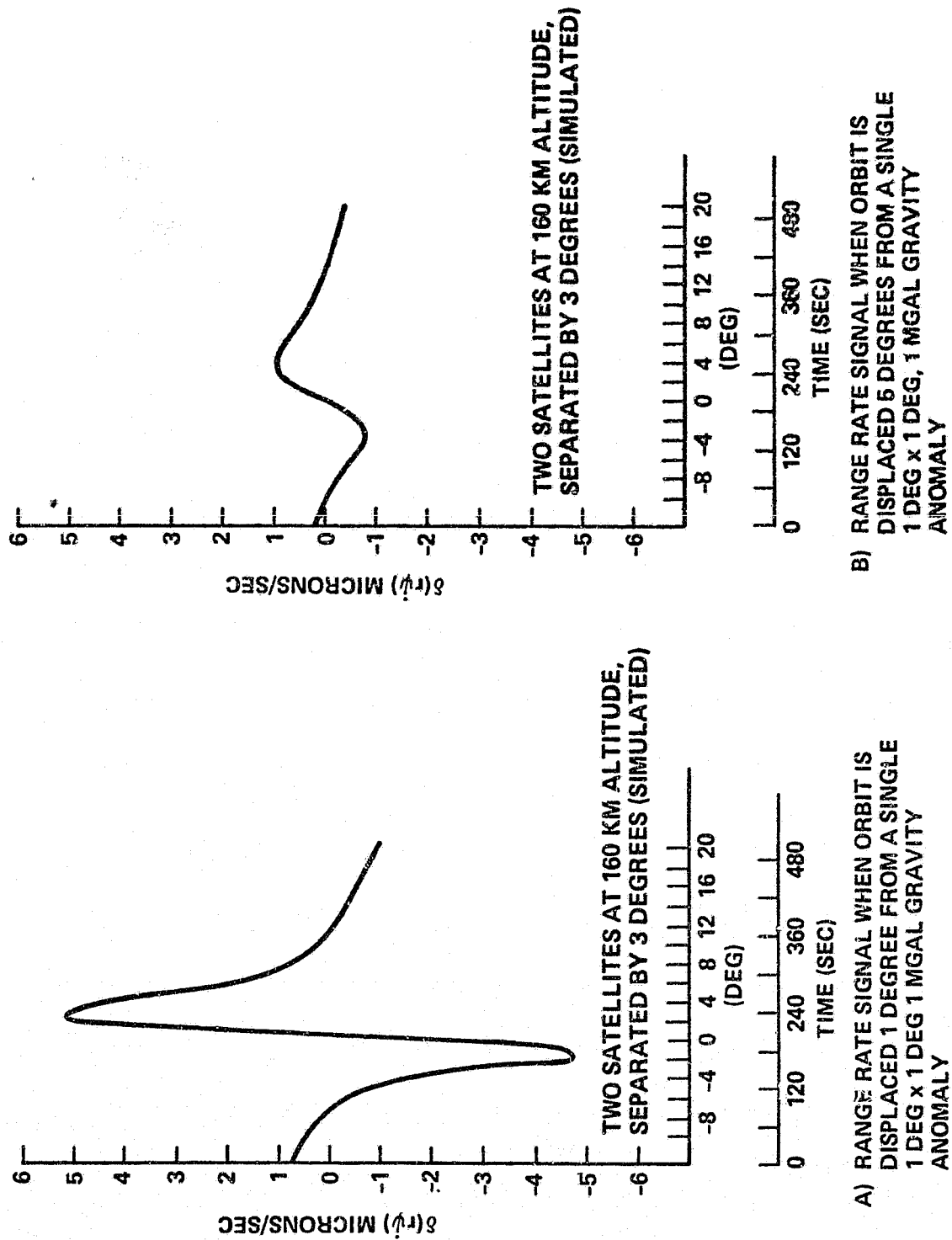1 DEG x 1 DEG 1 MGAL GRAVITY
ANOMALY

Figure 3. GRM Anomaly Sensing at Two Lateral Separation Distances.

GRAVSAT SIMULATIONS FOR GEOPOTENTIAL ANALYSIS

Francis J. Lerch

OBJECTIVES

The objective of this work is to assess through computer simulations the capability of the Geopotential Research Mission (formerly Gravsat for improving the gravity field of the earth for geophysical and oceanographic applications. Objectives of the mission are 3 mgal for gravity anomaly for geophysical analysis and 10 cm for the geoid for ocean circulation with resolution down to 1° half-wavelength.

BACKGROUND

The Geoptential Research Mission (GRM) through use of a dedicated satellite will map the gravity field fine structure over the earth and thus provide knowledge and understanding of (1) the origin and structure of geological features on the earth's surface; (2) the mechanical properties of the earth's lithospheric plates and the forces which drive their motion; and (3) the large-scale circulation of the oceans and major current systems by the determination of an improved ocean geoid.

The mission configuration for the GRM spacecraft consisted of two low-altitude satellites at 160 km in a drag free system separated by 300 km (used for simulations) with satellite-to-satellite doppler tracking (±1 micron/sec) surveying the globe in polar orbits. Error analysis studies have been made for GRM (see references). However, the main benefit of the present technique is that a simulation is performed from numerical integration of the force equations where a set of exact GRM observations are computed from an assumed gravity model (ground truth) which is to be recovered from the study. This method is free of a number of different approximations made in other studies but is generally costly in computer time and hence must be limited in scope.

RECENT ACCOMPLISHMENTS

Computer simulation results for the Geopotential Research Mission (formerly Gravsat) have been obtained which support accuracy objectives of the mission, namely 3 mgals for gravity anomaly and 10 cm for geoid height with a half-wavelength resolution of 1 degree. The computer simulations were performed with satellite-to-satellite doppler tracking (+ 1 micron/sec) between two low altitude satellites at 160 km in polar orbits and separated by 300 km in a drag-free environment for a 6-month mission lifetime. Results from studies have been obtained as follows: (1) the recovery of spherical harmonics with potential coefficients complete through degree and order 36 gave an accuracy of 2 to 3 orders of magnitude better than current knowledge; (2) recovery of geoid height and gravity anomaly in a local region (50° LAT x 20° LONG) in the presence of unmodeled errors external to the region gave an accuracy of 7 cm for geoid height and 4 mgal for the gravity anomaly for 1° x 1° blocks within the interior of the region; (3) the recovery of 1/2° x 1/2° blocks of geoid height and gravity anomaly ;in a local area containing a trench region gave, with use of eigenvalue analysis, commission errors of 5 cm for geoid height and 3 mgal

for gravity anomaly for 1° x 1° block sizes; and (4) a Fourier analysis over the trench region in (3) confirmed the results of this study which satisfy accuracy goals of GRM. Table 1 gives a further summary of these results.

SIGNIFICANCE AND FUTURE EMPHASIS

Results obtained so far are encouraging in that they satisfy mission goals but they are not complete and need to be extended. Future analysis should be conducted to extend the spherical harmonics to high degree (70 to 100) to reduce the aliasing effect on the solution due to the truncation of the harmonics. Because of computer time limitations it is necessary to truncate the spherical harmonic series. The residual potential including the smaller wavelengths of the truncated harmonics will then be recovered from localized functions by combining steps (2) and (3) above to cover a considerably broader region than the 50° x 20° area used in the present analysis. Also, because of computer time efficiency, the technique of deriving the potential first at satellite altitude and then downward continuing the result to the surface of the earth is being investigated.

TABLE 1. SUMMARY OF GRAVSAT SST SIMULATIONS

1. Recovery of Spherical Harmonics to 36 x 36

    o   20 days of SST data only employed
    o   2 to 3 orders of magnitude improvement over GEM 9
    o   Iteration will give another order of magnitude improvement
    o   Aliasing error is significant so a high degree solution is required
    o   Orbit parameters modeled with a priori constraints of 30 m in position
        3 cm/sec in velocity
    o   Combined SST+NWL dopper tracking gave similar solution as above.

2. Geoid Solution in a Local Region

    o   Local solution of 1° x 1° geoid heights in a 20° x 50° region gave
        7 cm accuracy for the interior region
    o   Error mostly due to aliasing effects of unmodeled residual potential
        exterior to the region
    o   A buffer zone of a priori constraints between the interior and exterior
        regions was necessary to control the aliasing error

3. Short-Wavelength Resolution in Trench Area (Tonga Tr.)

    o   1/2° x 1/2° geoid heights and gravity anomalies simulated over a
        5° x 5° trench area

    o   The recovery gave errors for 1° x 1° blocks of 5.0 cm for geoid
        height and 3.0 mgal for gravity anomaly by eigenvalue analysis.

REFERENCES

Bender, P.L., "Spherical Harmonic Fitting to GRAVSAT Data," paper presented at Fall Meeting of the AGU, 1982.

Breakwell, J.V., "Satellite Determinations of Short Wavelength Gravity Variations," J. Astronaut. Sci., 27 (4), 1979.

Colombo, O.L., "Global Geopotential Modeling from Satellite-to-Satellite Tracking," Ohio State University Department Geological Science, Columbus, Rep. 317, 1981.

Douglas, B.C., C.C. Goad, and F.F. Morrison, "Determination of Geopotential from Satellite-to-Satellite Tracking Data," J. Geophys. Res. 85, 5471-5480, 1980.

Jekeli, C. and R.H. Rapp, "Accuracy of the Determination of Mean Anomalies and Mean Geoid Undulations from a Satellite Gravity Field Mapping Mission," Ohio State Univesity Department of Geodetic Science, Columbus, Rep. 307, 22 pp, 1980.

Kahn, W.D. and T.L. Felsentreger, "Signal Analysis and Error Analysis Studies for a Geopotential Research Mission (GRM)," NASA TM 83970, GSFC, Greenbelt, MD, July 1982.

Kaula, W.M., "Inference of Variations in the Gravity Field from Satellite-to-Satellite Range-Rate," J. Geophys. Res., in press, 1983.

Kaula, W.M., "The Next Development in Satellite Determintion of the Earth's Gravity Field," Proc. USA-Hungarian 1981 Workshop on Dynamics, Eötvös University, Budapest, 127-134, 1982.

NAS (National Academy of Sciences) Committee on Geodesy of the National Research Council, "Applications of a Dedicated Gravitational Satellite Mission," Washington, DC, 1979.

Pisacane, V.L. and S.M. Yionoulis, "Recovery of Gravity Variations from Satellite-to-Satellite Tracking," Johns Hopkins University, Applied Physicsl Lab, Baltimore, Rep. SDO-5583, 1980.

Pisacane, V.L., J.L. MacArthur, J.C. Ray, and S.E. Bergson-Willis, "Description of the Dedicated Gravitational Satellite Mission (GRAVSAT)," Proc. Symp. Inst. Geosci. and Remote Sensing, Washington, in press, 1981.

Rummel R., "Geoid Heights, Geoid Height Differences, and Mean Gravity Anomalies from 'low-low' Satellite-to-Satellite Tracking--an Error Analysis," Ohio State University Dept. Geod. Sci., Columbus, Rep. 306, 44 pp, 1980.

Wagner, C.A. and C.C. Goad, "Direct Determination of Gravitational Harmonics from Low-Low GRAVSAT Data," J. Geophys. Res., submitted, 1983.

THE AIRBORNE LASER RANGING SYSTEM

Werner D. Kahn

OBJECTIVES

The Airborne Laser Ranging System (ALRS) is a potential sensor for performing rapid (few days) mapping of local crustal motion in seismically active areas. Through the use of covariance error analysis techniques, studies are performed to determine measurement precision, measurement rate accuracy, and geometry requirements for the ALRS to detect and monitor small earth surface motions.

BACKGROUND

The Airborne Laser Ranging Sytem is a proposed multibeam short pulse laser ranging system on board an aircraft. It simultaneously measures the distances betweeen the aircraft and six laser retroreflectors (targets) deployed on the earth's surface. Depending on the host aircraft and terrain characteristics, the system can interrogate hundreds of targets distributed over an area as large as 6×10^4 sq. kilometers in a matter of hours. Potentially, a total of 1.3 million individual range measurements can be made in a six hour flight. The precision of these range measurements is approximately ± 1 cm. These measurements are then used in a procedure which is basically an extension of trilateration techniques to derive the intersite vector between the laser ground targets. By repeating the estimation of the intersite vector, strain and strain rate errors can be estimated. These quantities are essential for crustal dynamics studies which include determination and monitoring of regional strain in the vicinity of active fault zones, land subsidence, and edifice building preceding volcanic eruptions.

RECENT ACCOMPLISHMENTS

Simulations have shown that range measurements must be taken at two widely separated altitudes in order to strengthen the geometry sufficiently to recover baselines at the centimeter level in agreement with earlier results (1). Thus, in a typical mission, the aircraft (i.e., NASA's NP3A Orion) approaches the target grid at an altitude of 3.9 km as in Figure 1. After acquiring the first few targets, the instrument shifts to the tracking mode for the remainder of the mission. After overflying the rows of targets at 3.9 km, the aircraft climbs to its maximum cruise altitude (say 6 km) for a second set of passes over the target grid.

The spacing between targets will depend on several factors including the scientific objectives of the mission, the aircaft altitude and the terrain limitations. For the NP3A aircraft, the spacing is nominally taken to be 7 km. At typical cruise velocities (i.e., 200 knots), laser range data to a given target is taken for approximately 130 seconds before the pointing system is commanded to acquire a new target. For a laser repetition rate of 10 pps, this corresponds to 1300 range measurements per target. Since a given target is common to a number of six target sets, and data are collected at two altitudes, approximately 7800 measurements are typically made to each target.

Figure 2 shows the important of refraction errors and also illustrates that an extensive network of meteorological sensors is not required. Atmospheric measurements made at a single site collocated with a laser target within the ALRS grid, will significantly reduce the effects of atmospheric refraction upon ALRS baseline precision. In the estimation process, if the information from that single "met sensor" is used and the atmospheric parameters for the other ALRS targets are made part of the set of estimated parameters, a factor of about 7 improvement in baseline precision is achieved. The figure also shows that the inclusion of additional meteorological sensors within the ALRS target area does not signficantly improve baseline precision. In the simulation it was assumed that the surface measurements of pressure and temperature were accurate to 1 mbar and 1.4°C respectively. The vertical variation in pressure was assumed to be determined by the hydrostatic equation.

In Figure 3 the evolution of baseline precision is given for a series of randomly deployed laser targets. These targets are distributed (as shown in the inset) in a potential ALRS flight test region in the vicinity of Shenandoah, VA. The targets were located at approximately 17 first order survey monuments currently maintained by the U.S. Geological Survey. The simulation indicates that the random pattern does not significantly affect baseline precision as can be seen by comparing the results with those in Figure 2. The baseline error typically grows at the rate of 0.05 cm/km. For the simulation one meteorological sensor was located in the middle of the gap and the meteorological parameter at other sites were determined in the estimation process.

The ALRS System has the potential capability to measure the relative horizontal and vertical locations of targets spaced tens to hundreds of kilometers apart to precisions of a few centimeters, it is thus an attractive candidate for use in a number of fundamental and applied crustal geodynamics measurements. Among these measurements are relative motions of tectonic plates across the plate boundaries and crustal determinations prior to and after major earthquakes.

Baseline rate accuracies can be obtained from the baseline precision by using the covariance matrix from a least squares fit to a linear regression line. S.C. Cohen in (2) analyzed the level of precision with which crustal strain rates can be determined. The method used for the results given here follow his analysis. By assuming that the baselines are surveyed during a one-day period every 90 days, then as shown in Figure 4, baseline rate accuracies at the end of a ten-year observation period under the assumption of constant baseline motion can be determined for 5 km baselines to better than 0.02 cm/yr and for 100 km baselines to about 0.1 cm/yr. By repeated measurements of the grid area within the seismically active region to the baseline rate accuracy level indicated, the ALRS could observe the deformation of plates at their boundaries, as well as general plate motion and attempt to "capture" a moderate sized earthquake, i.e., one of approximately magnitude 7 through repeated and densified monitoring of the grid area once changes in the baseline rate are observed.

FUTURE EMPHASIS

Rigorous covariance error analysis studies for ALRS have been completed. Approval is sought for an ALRS demonstration experiment. Upon approval, computer software must be developed in order to perform simulations which are to verify the covariance analysis performed to date, also to test the closed loop data processing capability and to develop the experiment plan encompassing the operational aspects of the ALRS demonstration test.

REFERENCES

Mueller, I.I., B.H.W. Van Gelder and M. Kumar, "Error Analysis for the Proposed Closed Grid Geodynamics Satellite Measurement System (CLOGEOS)," Department of Geodetic Science Report No. 230, The Ohio State Univesity, September 1975.

Cohen, S.C. and G.R. Cook, "Determining Crustal Strain Rates with a Spaceborne Geodynamics Ranging System Data," Manuscripta Geodetica, Vol. 4 (1979), 245-260.

Kahn, W.D., J.J. Degnan and T.S. Englar, "The Airborne Laser Ranging System, Its Capabilities and Applications," NASA TM 83984, September 1982.
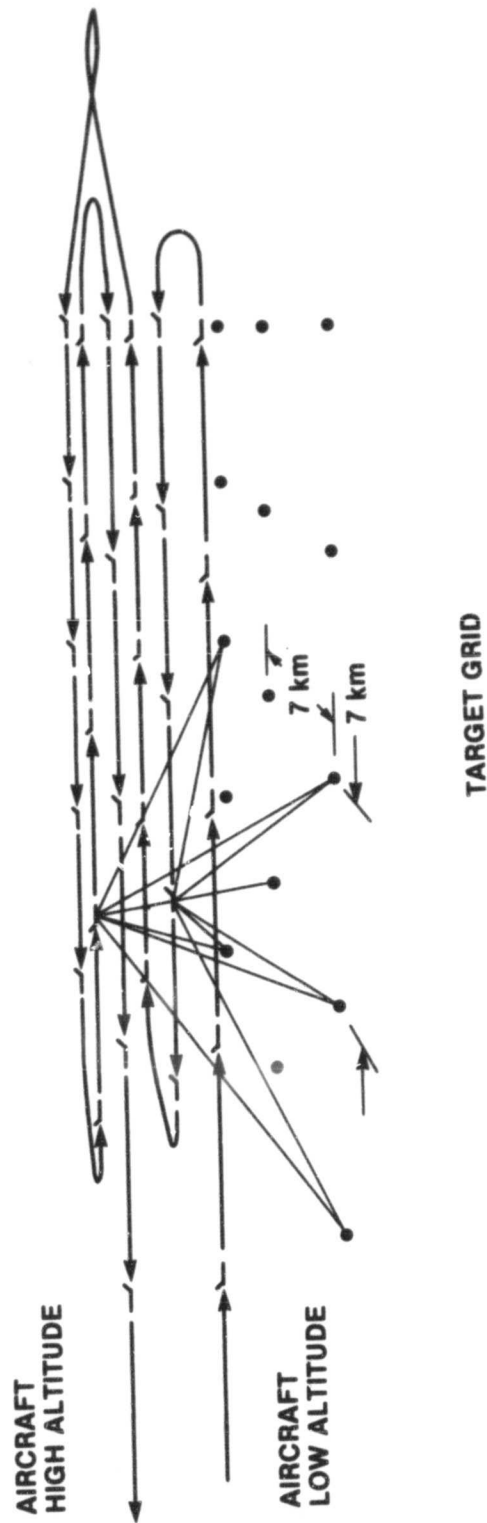
Figure 1. Typical ALRS Mission Scenario Perspective Showing Ranging from Two Different Altitudes.
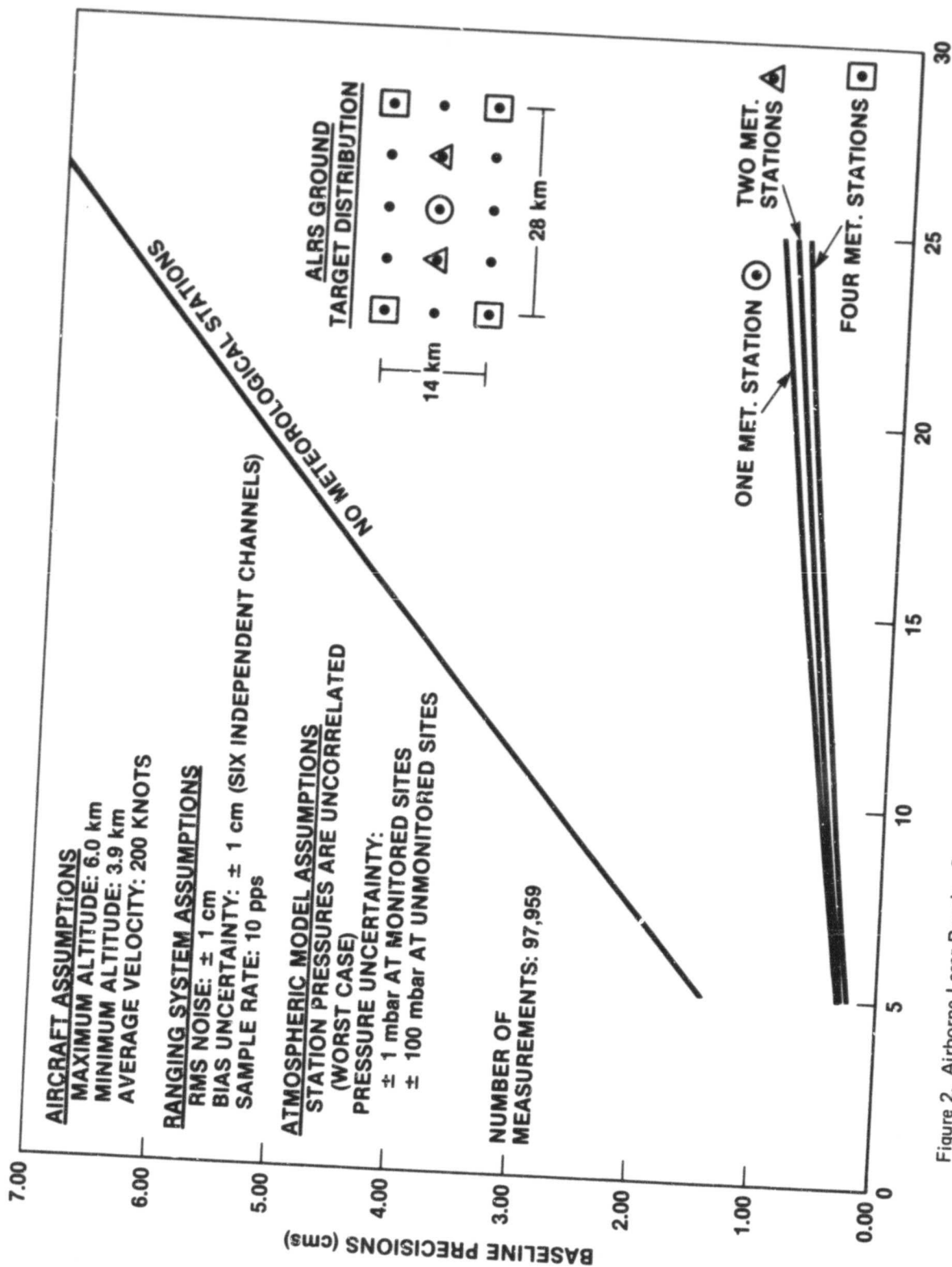
Figure 2. Airborne Laser Ranging System Baseline Precision as a Function of the Number of Meteorological Stations.
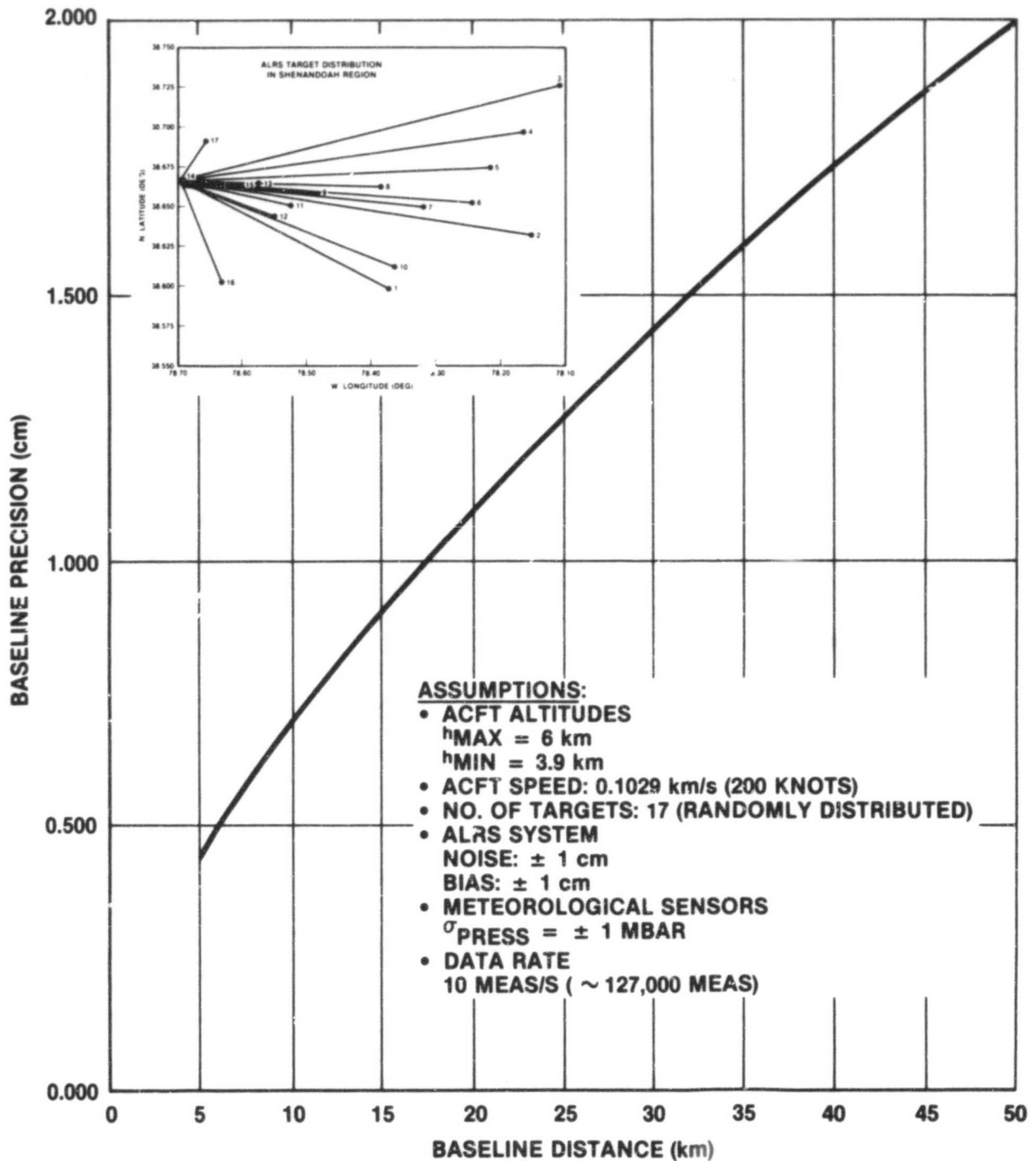
Figure 3. Airborne Laser Ranging System Baseline Precision for Random Laser Target Distribution.
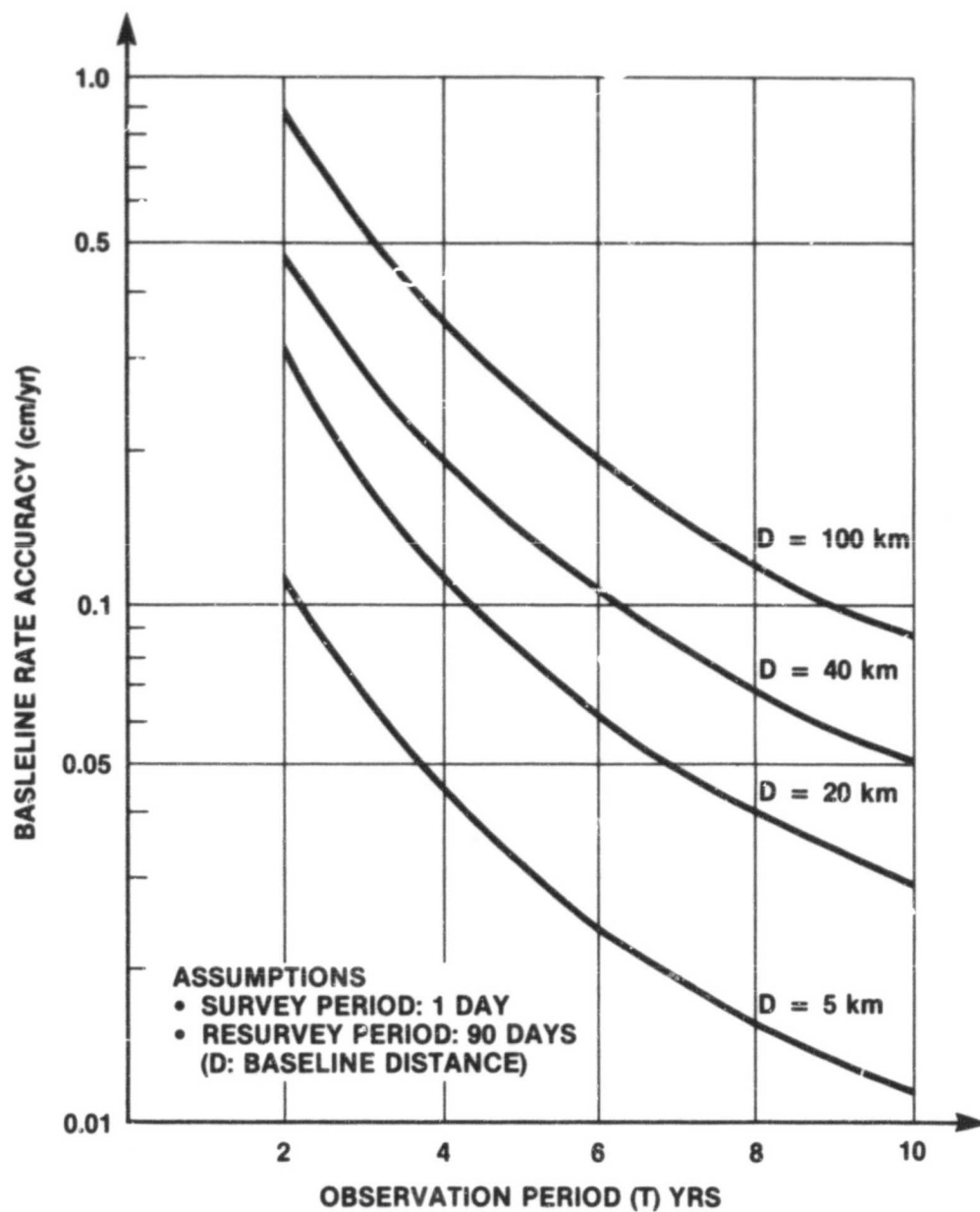
Figure 4. Baseline Rate Accuracy vs. Total Observation Period.

SOIL MOISTURE FROM TEMPERATURE MEASUREMENTS AT THE EARTH'S SURFACE

Jean E. Welker

OBJECTIVE

To determine soil moisture budgets at the earth's surface from soil and atmospheric temperature variations.

BACKGROUND

The soil surface and atmospheric interface can be considered a boundary between two dynamic systems. On the one hand, the atmospheric strata immediately above the earth's surface can be viewed as a number of layers, each responding individually and collectively to air flows and currents, to irradiation both from incoming solar radiation as well as reflected and emitted radiations from the ground surface below, and to rapid changes of moisture content in its various states and accompanying heat transfers. The soil immediately below the earth's surface can also be treated as layers undergoing heat transfers, temperature changes, and moisture flows. Both sides of the earth's interface, the 1 to 2 meter layer at either atmosphere above or soil below, are coupled in a complex manner to this surface interface by a variety of effects.

From a one-dimensional view of temperature alone, variations at the earth's surface manifest themselves in two cyclic patterns of diurnal and annual periods, due principally to the effects of diurnal and seasonal changes in solar heating as well as gains and losses of available moisture. Beside these two well known cyclic patterns, a third cycle has been identified which occurs over a mesoscale period of roughly 3 to 10 days. This cycle, which occurs in diurnal maxima and minima extrema, is the subject of this current research.

RECENT ACCOMPLISHMENTS

A number of data sets were plotted and statistically analyzed in order to accentuate the existence and the characteristics of this mesoscale soil temperature extrema variations and its relations to other parameters. The cycle is initiated by a preciptation event, which bathes the soil and causes an immediate drop in the temperature extrema. This is followed by a temperature recovery period of roughly a week in the absence of any more precipitation. In a 5-month, March through July period in northern mid-latitudes with no elongated periods of drought, the cycle can be expected to occur approximately one to three times a month. This temperature loss and recovery can be seen in Figure 1, in which drops in maximum soil temperatures at depths of 5, 10 and 20 cm for the Tifton Meteorological Station in the State of Georgia for the period of March through July of 1979 are plotted. Other data plotted with maximum diurnal soil temperatures are maximum air and evaporation pan (4' in diameter) temperatures, recorded precipitation and pan evaporation.

This study was initiated using data from the State of Georgia, because of the contrasting severe drought and non-drought years which occurred in the late seventies-early eighties in that region. In contrast to the non-drought data in Figure 1, Figure 2 contains 1980 data which is characterized by a severe 27-day drought period in May and June with only a trace of rainfall on 1 day in this period. To eliminate soils as a critical factor in this study, Iowa station data with completely different soil characteristics were used in comparison with Georgian data. In order to broaden the contrast further, Soviet data was used in a good year/bad year comparison for the years 1971 and 1972, respectively. Other earlier data sets form Eastern Europe were also included.

All data sets are being analyzed in order to determine regional characterization of drought conditions. A number of broad drought descriptions were considered additionally in conjunction with the station temperature extrema data described above.

Analyses of the data sets have been directed toward the behavior of temperature extrema before and immediately after a precipitation event. With or without a drought condition, the diurnal minimum soil temperatures at 10 cm depth are highly correlated for 153 values, March through July diurnal values, with both the diurnal minimum air and evaporation pan temperatures. This is not to say that the 10 cm minimum soil temperatures and minimum air and evaporation pan temperatures have the same values without some offset, but only that they are highly correlated statistically, with a value greater than 0.85, for those cases tested for both drought and non-drought conditions. The presence of drought is manifested in a high correlation of diurnal maximum values rather than diurnal minimum values, for the data sets of the 10 cm soil temperatures, air temperatures, and evaporation pan temperatures. The 10 cm maximum soil temperatures and air temperatures move together under drought conditions because solar radiation at the ground during the hottest part of the day heats the soil and air together, with no energy loss to the evaporation of soil moisture. After a precipitation event, in the period when the soil is hindered in regaining its original temperature because of heat absorption by the evaporation process, it is again the diurnal maximum rather than minimum soil temperatures that appear most sensitive. For all maximum and minimum temperature data sets tested so far, the temperature recovery law is:

$$T = 8t^x$$

where

    T - extremum temperature minimum after a precipitation event
    t - recovery time in days
    x - exponent ranging between $0.62 < x < 0.92$

SIGNIFICANCE

The correlations between diurnal temperature extrema for air and soil in drought and non-drought periods appear to follow different characteristic patterns, allowing an inference of soil moisture content from temperature data. The recovery of temperature extrema after a precipitation event also follows a characteristic exponential rise between two limiting values which is an indicator of evaporation rates. If these indicators can be applied universally to regional temperature data, soil moisture content or drought conditions can be inferred directly from temperature measurements.

FUTURE EMPHASIS

An adequate statistical correlation testing of the 26 annual station data sets which have been assembled and plotted will be completed. All 26 data sets have already shown a similar characteristic temperature recovery after a precipitation event. HCMM data will be used for regional temperature data comparisons. An attempt will be made to incorporate this technique in estimates of ground water excesses related to seasonal variations of earth's rotation/L.O.D. estimates. This work will continue to be developed in consultation with Professor Helmut Landsberg of the University of Maryland.

REFERENCES

Brooks, F.A. and D.G. Rhoades, "Daytime Partition of Irradiation and the Evaporation Chilling of the Ground," Trans. Amer. Geophys. Un., 35, No. 1, February 1954, 145-152.

Landsberg, Helmut E., "Drought, A Recurring Element of Climate," World Meteorological Organization Special Environmental Report No. 5 Drought WMO No. 403 Geneva, Switzerland, Secretariat of the World Meteorological Organization 1975, 40-61.

Lettau, Heinz, "Improved Models of Thermal Diffusion in the Soil," Trans. Amer. Geophys. Un., 35, No. 1, February 1954, 121-132.

Palmer, W.C., "Meteorological Drought," Washington, DC, U.S. Department of Commerce, Weather Bureau Research Paper No. 45, February 1965, 55pp.

Schmugge, T.J., T.J. Jackson and H.L. Kim, "Survey of In-Situ and Remote Sensing Methods for Soil Mosture Determinations," in Deutsch, M., Wiesnet, D.R., and Rango, A., eds. Satellite Hydrology American Water Resources Association, June 1979.

Vehrencamp, John E., "Experimental Investigations of Heat Transfer at an Air-Earth Interface," Trans. Amer. Geophys. Un., 34, No. 1, February 1953, 22-30.

Welker, J.E., "Thermal Infrared Remote Sensing of Surface Features for Renewable Resource Applications," NASA TM 82106, Greenbelt, MD, Goddard Space Flight Center, January 1981, 26 pp.
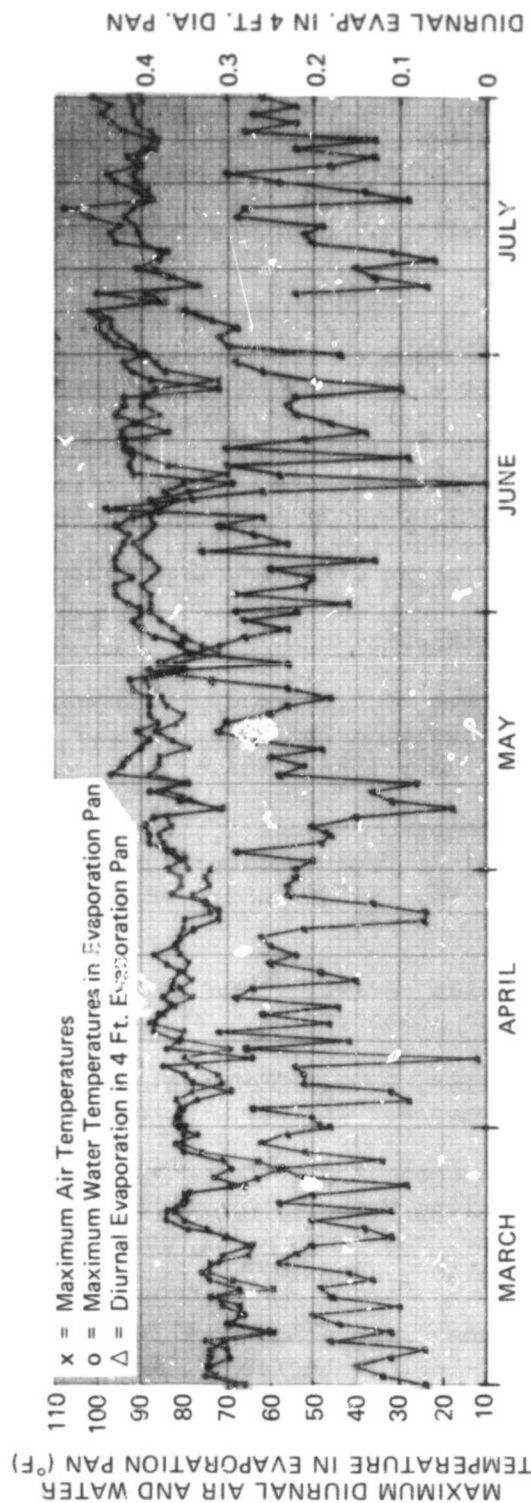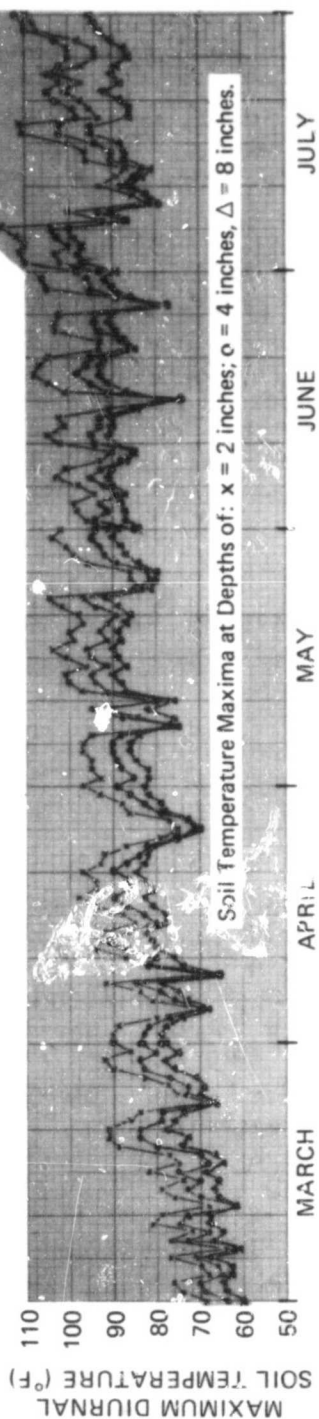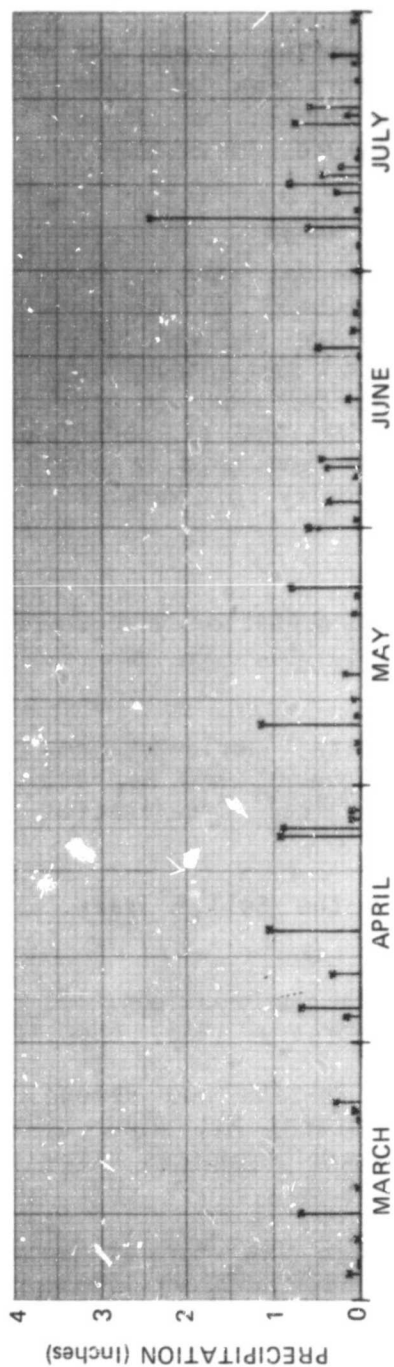
Figure 1. Soil, Pan, and Air Temperature with Precipitation and Evaporation for Tifton, Georgia, 1979
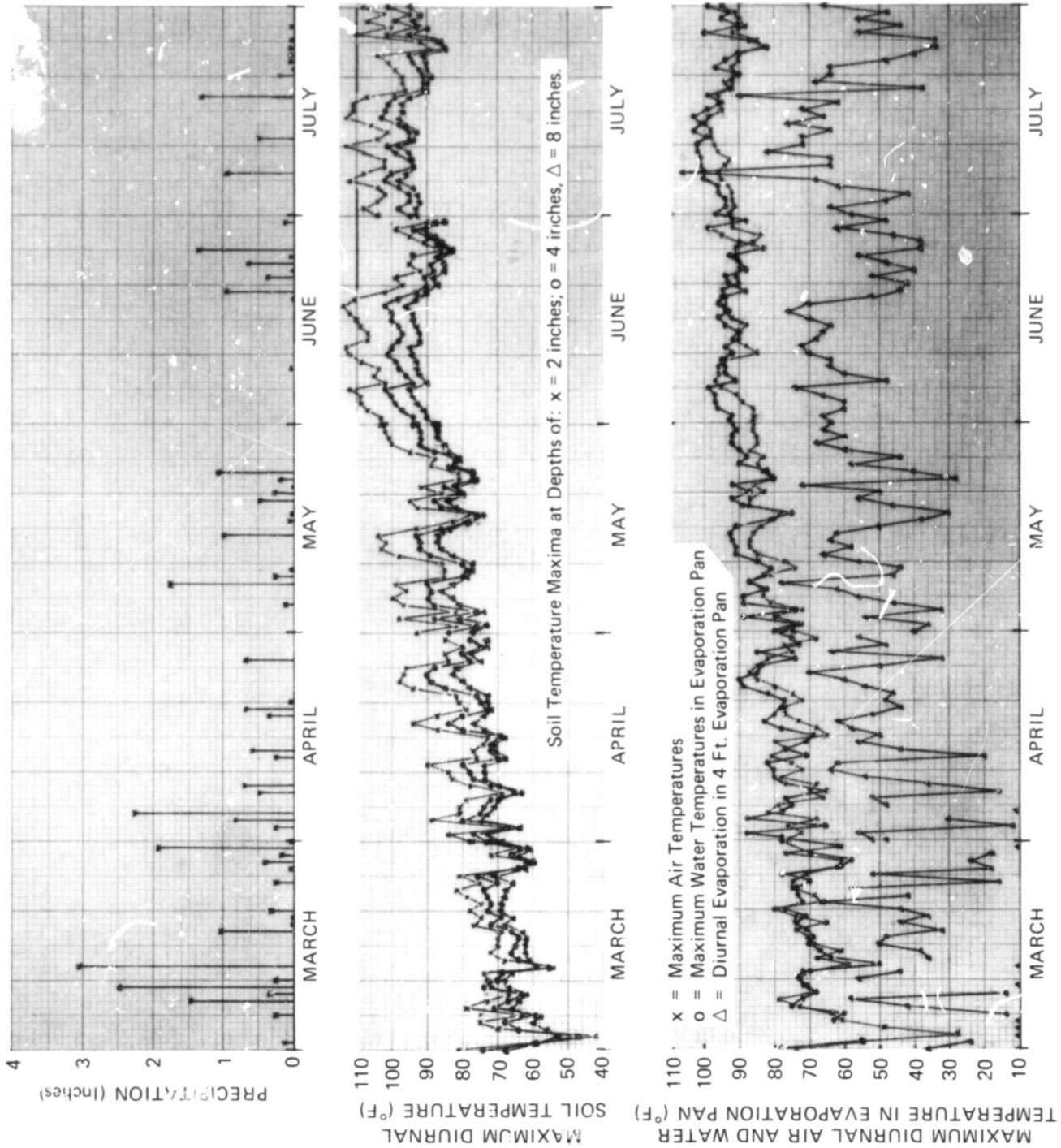
Figure 2. Soil, Pan, and Air Temperature with Precipitation and Evaporation for Tifton, Georgia, 1980

PUBLICATIONS AND PRESENTATIONS - 1982

1. Chao, B.F., "Excitation of Normal Modes on Non-Rotating and Rotating Earth Models," Geophys. J. Royal Astr. Soc., 68, 295-315.

2. Chao, B.F., "A Fine Structure Analysis of the Earth's Polar Motion Using ILS Data," EOS, 63, 903. (Presented at the Fall 1982 AGU Meeting).

3. Cheney, R.E., J.G. Marsh, and B.D. Beckley, "Global Mesoscale Variability from Repeat Tracks of Seasat Altimeter Data," J. Geophys. Res., in press.

4. Cheney, R.E. and J.G. Marsh, "Ocean Current Detection by Satellite Altimetry," Proceedings of the Marine Technology Society, Oceans.

5. Christodoulidis, D.C., D.E. Smith, P.J. Dunn, M.H..Torrence, S. Knode, and S. Anders, "The SL5 Geodetic Parameter Solution," Proceedings of Third International Symposium on the Use of Artificial Satellites for Geodesy and Geodynamics, National Technical University, Athens, Greece.

6. Cohen, S.C., "A Multilayer Model of Time Dependent Deformation Following an Earthquake on a Strike-Slip Fault," J. Geophys. Res., 87, 5409-5421.

7. Cohen, S.C., "Postseismic Deformation Due to Subcrustal Viscoelastic Relaxation Follwing Dip Slip Earthquakes," NASA TM 84005. 5421.

8. Cohen, S.C., "Discussion of Models of Postseismic Rebounds," EOS Trans. Am. Geophy. Un. (abstract), 63, 429.

9. Cohen, S.C., "Crustal Deformation During the Earthquake Cycle Temporal and Spatial Dependence, "Fifth Annual NASA Geodynamics Program Conference (abstract), p. 59.

10. Dunn, P.J., M.H. Torrence, D.C. Christodoulidis and D.E. Smith, "Earth Scale and Orientation from Lageos," EOS Trans. Amer. Geophys. Union, 63, 45.

11. Gross, R.S., 1982, "A Matched Filter for the Chandler Wobble," EOS Trans. Amer. Geophys. Union, 63, p. 903.

12. Kahn, W.D., et al., "Mean Gravity Anomalies from a Combination of Apollo/ATS and GEOS-3/ATS-6 SST Tracking Campaigns," J. Geophys. Res., Vol. 87, No. B4, pp 2904-2918, April 10.

13. Kahn, W.D., and T.L. Felsentreger, "Signal Analysis and Error Analysis Studies for a Geopotential Research Mission (GRM)," NASA TM 83970, July.

14. Kahn, W.D., et al., "The Airborne Laser Ranging System, Its Capabilities and Applications," NASA TM 83984, September.

15. Kahn, W.D., "ALRS Simulation Studies," Fourth Annual Conference on the NASA Geodynamics Program, Greenbelt, MD 1982.

16. Kolenkiewicz, R., D.E. Smith, M.H. Torrence, P.J. Dunn and D.C. Christodoulidis, "Satellite Laser Ranging Techniques in Geophysical Research," European Geophysical Society and European Seismological Commission, the University of Leeds, England.

17. Krabill W., C.F. Martin and F.E. Hoge, "Baseline Monitoring Using Aircraft Laser Ranging--Spaceborne Laser Simulation and Aircraft Laser Tracking," NASA TM 73298, June.

18. Krabill, W., L.E. Link and R.N. Swift, "A Prospectus on Airborne Laser Mapping Systems," 1982 COSPAR, May.

19. Krabill, W. and R.N. Swift, "Preliminary Results of Shoreline Mapping Investigations Conducted at Wrightsville Beach, North Carolina," Proceedings of Corps of Engineers Hydrographic Survey Meeting, Jacksonville, Florida, February 1982.

20. Lerch, F.J., J.G. Marsh, S.M. Klosko and R.G. Williamson, "Gravity Model Improvement for Seasat," J. Geophys. Res., Vol. 87, 3281-3296, April 30, 1982.

21. Lerch, F.J., S.M. Klosko and G.B. Patel, "A Refined Gravity Model from Lageos (GEM-L2)," Geophys. Res. Lett., Vol. 9, 1236-1266, November 1982.

22. Lerch, F.J., "Gravity Model Errors in SLR," Crustal Dynamics Conference, Greenbelt, MD, 1982 (presentation).

23. Lerch, F.J., "A Refined Gravity Model for Lageos (GEM L2)," Fall 1982 AGU Meeting, San Francisco, 1982 (presentation).

24. Lerch, F.J., "Gravsat Simulations at GSFC," Fourth Annual Conference on the NASA Geodynamics Program, Greenbelt, MD 1982.

25. Liu, Han-Shou, "Geodynamics of the Baikal-Stanovoy Seismic Belt," Physics of the Earth and Planetary Interiors, Vol. 31, 77-82, 1982.

26. Liu, Han-Shou, "A Dynamical Basis for Crustal Deformation and Seismo-tectonic Block Movements in Central Europe," NASA TM 84933, 1982.

27. Marsh, J.G. and T.V. Martin, "The Seasat Altimeter Mean Sea Surface Model," J. Geophys. Res., Vol. 87, No. C5, 3269-3280.

28. Marsh, J.G. and R.G. Williamson, "Seasat Altimeter Timing Bias Esti-mation," J. Geophys. Res., Vol. 87, No. C5, 3232-3238.

29. Marsh, J.G., R.E. Cheney, T.V. Martin and J. McCarthy, "Computation of a Precise Mean Sea Surface in the Eastern North Pacific Using Seasat Altimetry," EOS Trans. Amer. Geophys. U., Vol. 63, No. 9, 178-179.

30. Marsh, J.G., R.E. Cheney, T.V. Martin and J.J. McCarthy, "Mean Sea Surface Computations in the Northwest Pacific Based Upon Satellite Altimeter Data," Proceedings of the General Meeting of the IAG, Tokyo, May 7-15, 1982; J. of the Geodetic Society of Japan, 454-465.

31. Marsh, J.G., T.V. Martin, and J.J. McCarthy, "Global Mean Sea Surface Computation Using GEOS-3 Altimeter Data," J. Geophys. Res., Vol. 87, No. B13, 10955-10964.

32. McAdoo, D.C., R. Kolenkiewicz, C.F. Martin and S. Poulose, "The Correlation of Bathymetry with Geoid Heights Near Trenches of the North Pacific," EOS 63, No. 5, 907, (abstract).

33. McAdoo, D.C., "Ithaca Chasma: A Product of Tidal Stress on Tethys," EOS 63, No. 18, 365, 1982 (abstract).

34. Mognard, N.M., W. Campbell, R.E. Cheney, J.G. Marsh and S. Ross, "South Ocean Waves and Winds Derived from Seasat Altimeter Measurements," Wave Dynamics and Radio Probing of the Ocean Surface, in press.

35. Mognard, N.M., W.J. Campbell, R.E. Cheney and J.G. Marsh, "Southern Ocean Mean Monthly Waves and Surface Winds for Winter 1978 by Seasat Radar Altimeter," J. Geophys. Res., in press.

36. Rubincam, D.P., "On the Secular Decrease in the Semimajor Axis of Lageos's Orbit," Celestial Mechanics, 26, 361-382 (1982).

37. Rubincam, D.P., "Information Theory Lateral Density Distribution for Earth Inferred from Global Gravity Field," J. Geophys. Res., 87, 5541-5552 (1982).

38. Smith, D.E., P.J. Dunn, D.C. Christodoulidis and M.H. Torrence, "Global Baselines from Laser Ranging," Fourth Annual Conference on NASA Geodynamics Program, Greenbelt, MD 1982.

39.
Torrence, M.H., D.C. Christodoulidis, P.J. Dunn, S. Knode, S. Anders, R. Kolenkiewicz, G. Wyatt and D.E. Smith, "Geodetic Parameters from Laser Tracking of the Lageos Spacecraft," <u>EOS Trans. Amer. Geophys. Union</u>, 63, 18.

ACKNOWLEDGMENTS

We would like to acknowledge the support provided by the following: